Effects of Dissolved Organic Matter (DOM) on Metal Release from Solid Phases Typical for Corrosion Processes and Characterization of Interactions between DOM and Metal Cations by In Situ Spectroscopic Methods

Yuan Gao

A dissertation submitted in partial fulfillment of the requirements for the degree of

Doctor of Philosophy

University of Washington
2015

Reading Committee: Gregory V. Korshin, Chair
Mark M. Benjamin
Michael C. Dodd
Drew Gorman-Lewis

Program Authorized to Offer Degree:
Department of Civil and Environmental Engineering

University of Washington

Abstract

Effects of Dissolved Organic Matter (DOM) on Metal Release from Solid Phases Typical for Corrosion Processes and Characterization of Interactions between DOM and Metal Cations by In Situ Spectroscopic Methods

Yuan Gao

Chair of the Supervisory Committee:
Professor Gregory V. Korshin
Department of Civil and Environmental Engineering

This study examined impacts of dissolved organic matter (DOM) on copper release from copper solid model phases (tenorite and malachite) characteristic for copper corrosion in drinking water as well as characterizing interactions between DOM and metal cations (e.g., calcium, copper) by *in situ* spectroscopic approaches. The study focused on the role of DOM in determining metal release caused by corrosion and showed that DOM molecules with higher apparent molecular weight (AMW), higher aromaticities and contributions of protonation-active phenolic and carboxylic groups played a key role in adsorption and colloidal dispersion of the model solids. Results also showed that metal release from model phases was well correlated with a number of spectroscopic parameters characterizing DOM properties, notably $SUVA_{254}$, spectral slopes of DOM absorbance, and differential

absorbance at wavelength of 280 nm and 350 nm that was indicative of the contributions of carboxylic and phenolic functional groups. Treatment approaches (e.g., chlorination, ozonation) on DOM were shown to suppress the colloidal dispersion effects due to a decreased surface activity of copper solids with DOM adsorbed.

Properties of DOM as well as its interactions with major cations that are typical for drinking water and affect metal release in it were also studied by *in situ* spectroscopic approaches. To quantify ionic strength (IS) effects on DOM and its interactions, standard DOMs of allochthonous and autochthonous origins were used. This study showed that the increase of IS from 0.001 to 0.3 mol/L was accompanied by increases of the absorbance of DOM. The absolute values of the spectral slopes of the log-processed absorbance spectra of DOM calculated for a 350 to 400 nm wavelength range decreased proportionally to the logarithm of IS values. This result was hypothesized to be indicative of the deprotonation of the DOM chromophores at increasing IS. The contribution of the latter mechanisms was supported by model calculations showing that values of the spectral slopes were nearly-linearly correlated with the extent of IS-induced deprotonation of the operationally defined phenolic groups in DOM. This *in situ* approach was further applied to the investigation of DOM binding of cations highly important for corrosion processes, notably copper and calcium, as well as competitive binding of calcium and copper to DOM. The competition between calcium and copper for the binding sites in DOM was tracked by examining the intensity and shapes of the differential spectra generated for the Ca^{2+}/Cu^{2+}/DOM system. The extent of metal binding by

DOM was quantified by calculating the slopes of log-transformed absorbance spectra in the range of wavelength 350 to 400 nm and by comparing the data with predictions made using the NICA-Donnan Model. The observed effects were interpreted based on the assumption that the binding of Ca^{2+} and Cu^{2+} by DOM was accompanied by the replacement of protons bound by carboxylic and phenolic functional groups.

List of Figures

List of Tables

ACKNOWLEDGEMENTS

During these highly rewarding Ph.D. years, I have obtained enormous help and support from my professors, family and friends. Many of them deserve the length of one chapter in my thesis to describe those memorable stories, so one page of this acknowledgement is only a short list.

In the first place, I would like to show my greatest gratitude to my advisor, Dr. Gregory Korshin, who has always been highly supportive of me during these years, and beyond. I just realize that I have known him for ten years (amazing!) since I joined his research group in my undergraduate years for exchange study here. He is a role model for me and shows me how to be a passionate researcher and a wonderful professor, as well as a person with good taste in art. I would also like to thank him for all the advice and help in my career pursuit.

My deep gratitude also goes to Dr. Mark Benjamin, Dr. Michael Dodd, and Dr. Drew Gorman-Lewis. They are my committee members and provide valuable insights and suggestions in my defense and final thesis. Also, I thank Dr. David Stensel and Dr. Michael Brett for their great classes which expand my knowledge in environmental engineering.

Many thanks to my dear friends and colleagues in our lab, especially Sean Yeung, Christina Urbanzcyk, Rupal Pandya, Raji Elza, Ching-Yu Peng, I-Chieh Chieh, Haizhou Liu, Nicolette Zhou, Peiran Zhou, Bo Li, Songlin Wang and Siamak Modarresi for their friendship that we can share the joys and tears.

And, my hearty thanks go to James Liu, who gives me generous love, understanding and

comfort. When I finished work late and walked along the dark trail, with him, I did not feel lonely but contented.

Lastly, I have always been blessed by the unconditional love, care and encouragement from my parents and many other family members. I would like to express my utmost gratitude to them, and the honor that I receive should go to them.

Dedication

To my parents

1 Background and Literature Review

1.1 Dissolved Organic Matter (DOM)

Dissolved Organic Matter (DOM) is ubiquitously present in almost all water bodies and is considered to be one of the most important factors controlling water quality and properties in many biogeochemical processes and engineered systems. DOM can be formed autochthonously from biological materials generated within the water body (e.g., algae) or it can be produced via allochthonous processes involving the degradation of terrestrial biota in areas adjacent to the water body [1]. More specifically, autochthonous processes cause DOM release from algal cells as a result of both the lysis of dead phytoplankton or periphyton cells or bio-excretion of biopolymers and other chemicals generated in the cells through cell membranes [2]. Allochthonous DOM generation processes are different from the authochtonous reactions because they refer to DOM that has been exogenously generated via the decay of terrestrial vegetation and other biomass. These molecules are carried to a specific water body by precipitation, infiltration and percolation through various soil horizons. In addition to the decay of terrestrially produced biomass, allochthonous DOM can be produced via root and leaf exudation and in processes generating primary and secondary metabolites and other by-products of microbially-mediated processes in soils and sediments [3]. The diversity of DOM sources and generation pathways result in a highly complex nature of DOM whose molecules have varying molecular weights, conformations, proton affinities and concentrations of carboxylic,

phenolic and other metal cation-binding functional groups, and other properties that, for engineered systems, are also affected by specifics of water treatment processes [4]. In other words, DOM properties (such as functionality and heterogeneity) depend on DOM provenance (e.g., allochthonous vs. autochthonous)[4] and processes in environmental or engineered systems that affect them. For example, DOM of microbial/algal origin (e.g., DOM collected from Pony Lake in Antarctica; this lake has very limited plant/soil-derived inputs) has lower contributions of aromatic moieties and thus lower $SUVA_{254}$ compared to typical terrestrially derived DOM [5]. Also, DOM after ozonation treatment has been observed to have decreased portion of aromatic moieties while increased portion of oxalate structure [6,7].

Although DOM is composed of highly heterogeneous molecules, the majority (~50 to >90 %) of these DOM molecules are humic substances (humic and fulvic acids), which are typically operationally defined as compounds can be isolated from the bulk aquatic sample via adsorption on to Amberlite XAD-8 resin[8,9]. Since humic substances tend be the most important portion of DOM in the majority environmental reactions, the terms *DOM* (or frequently *NOM*, natural organic matter) and *humic substances* tend to be used interchangeably[10].

Humic substances are produced via the decay and transformation of biomolecules that involved a variety of chemical reactions. In the literature, humic species are frequently described to comprise three major fractions: fulvic acid which remain soluble at all pHs, humic acid which is frequently derived from soil and precipitates out at pH <2 and humin which is the fraction always insoluble and generally the most resistant to microbial degradation [11]. There are other fractionation protocols, for instance the frequently used

fractionation procedure [12] based on the use of two column array of Amberlit XAD-8 and XAD-4 resins in series, to separate DOM into operationally defined "hydrophobic", "transphilic" and "hydrophilic" portions based on polarity. The fraction adsorbed on XAD-8 is defined as hydrophobic fraction and is composed primarily of aquatic fulvic and humic materials; the portion adsorbed on the following XAD-4 while not absorbable onto XAD-8 is defined as transphilic fraction; the last part is hydrophilic DOM which does not sorb onto XAD-8 or XAD-4 resins and generally have a lower concentration of aromatic carbon and greater heteroaliphatic, ketone and carboxyl content than their hydrophobic counterpart. In relatively early research, MacCarthy et al. [13] described humic substances to have the following loosely defined properties: 1) they have no uniquely defined characteristic skeletal structures, 2) they cannot be purified in the conventional meaning of purity, 3) they feature the combination of an extreme molecular heterogeneity and pronounced chemical reactivity, 4) they are more resistant to microbial degradation compared to other biopolymers but they are notably reactive in a various chemical reactions.

Molecular weight of DOM is difficult to determine unambiguously but it is deemed to range from a few hundred to 100,000 Daltons (Da). Recent studies show that aqueous water-borne humic species [14] comprise molecules with relatively small molecular sizes (100~2000 Da) whereas a variety of inner- or outer-sphere interactions such as hydrogen bonding, nonpolar interactions, and polyvalent cation binding result in aggregation of smaller-sized molecules that affects macromolecular characteristics in some humic materials [4,14].

In terms of molecular structures of humic species, despite the recent advances [15–19], it is still impossible to present a uniformly accepted molecular structure. The difficulty is

caused by the intrinsic complexity of humic species and also by the highly diverse generation and alterations processes as discussed in the preceding session. Despite these difficulties, several structural models as illustrated in Figure 1.1 have been proposed to demonstrate the most important properties of these compounds, for instance their typical functional groups and composition. The molecules that are included in the humic acids generally have higher aromatic content and molecular weight, and are more hydrophobic than fulvic acids. On the other hand, the fulvic acids tend to have an overall higher concentration of proton-reactive functional groups (e.g., polycarboxyl groups as shown in Figure 1.1 (b)) on mol/kg basis. The hypothetical molecular structure shown in this figure demonstrates the notion that DOM is a complex arrangement of aromatic, carboxylic and aliphatic structures with the presence of highly diverse functionalities such as amide, keto, ether, ester, carbonyl and hydroxyl groups [4]. Among these, carboxylic and phenolic groups are believed to be most important for reactions of considerable environmental importance, for instance for fouling associated with calcium/DOM bridging or complexation in membrane filtration [20], formation of disinfection by-products, corrosion and heavy metal release in water distribution system [7,21,22] as discussed in the following section.

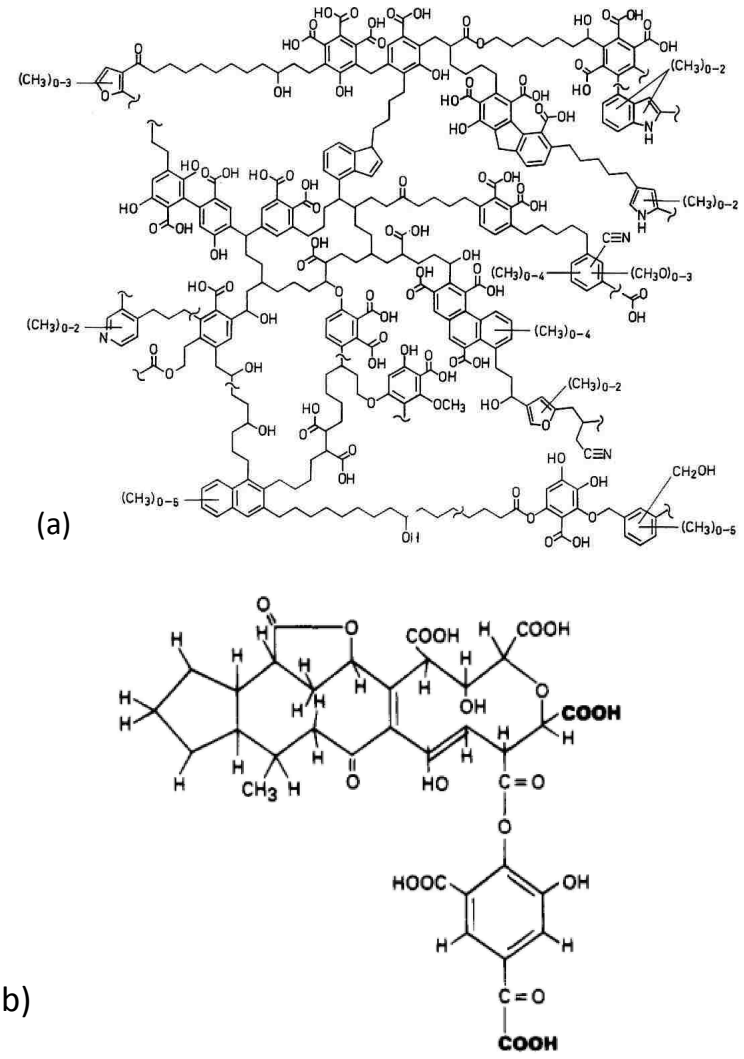

Figure 1.1 Proposed schematic structure for humic and fulvic acids: (a) model soil humic acid ("~) symbols stands for a linkage in the macromolecules to more of the same types of structure [23,24]; (b) fulvic acid molecules from the Suwannee River [25].

1.2 DOM effects on corrosion control of copper and metal release

The presence of DOM can have a significant effect on the release of metal cations from the relevant solid phases (e.g., metal oxide, metal-carbonate solids). The corrosion of metal plumbing materials and subsequent release of metal-containing corrosion by-products in

drinking water distribution system[10,26,27] is one of the examples that DOM can play an important role and therefore metal release is one of the major foci of this study. Elevated copper concentration caused by corrosion of household plumbing can negatively affect public health and require vast expenditures on corrosion control. Adverse health effects caused by short- and long-term exposure to elevated copper concentration include gastrointestinal distress and liver or kidney damage respectively (National Primary Drinking Water Regulations). The United States Environmental Protection Agency (EPA) Lead and Copper Rule (LCR) regulates that additional actions for corrosion control must be undertaken if more than 10% of customer taps sampled exceeds a copper concentration of 1.3 mg/L.

Multiple factors such as hydrodynamic conditions, temperature, pH, alkalinity, chlorine residual, concentrations of inorganic ions such as chloride, and DOM can impact copper corrosion [28–34]. Effects of DOM were specifically examined in our study due to several reasons. Specifically, copper release has been observed to exhibit a complex and sometimes inconsistent pattern of its response to the presence of DOM and its properties. While some reports indicate that DOM leads to short-term suppression of copper release [35], other investigations conclude that DOM results in prominent increases in copper concentration [26,28]. For example, Rehring and Edwards [35] found that DOM caused copper release to increase at higher pH (e.g., pH=9). Even very low levels of DOM (<0.1 mg/l) have been observed in some experiments to lead to increases of copper concentration [36].

The presence of phenolic and carboxylic groups in DOM as well as its conformational properties and charges of its molecules are likely to affect copper corrosion and release via DOM engagement in complexation, adsorption and colloidal dispersion [26,36]. Negatively

charged DOM molecules can adsorb onto corroding copper surfaces and copper solid phases (e.g., malachite) formed on them. DOM sorption on copper solids is likely to be accompanied by their colloidal dispersion similar to that observed in prior research [21,36]. DOM can also form strong complexes with Cu(II) cation via intramolecular or intermolecular bidentate chelation, depending on the functional groups available [37–39]. The scheme of copper release from Cu-containing solid phases in the presence of DOM is shown in Figure 1.2 that demonstrates the presence of potential effects of DOM sorption and complexation.

Cu(II) binding by DOM has been determined to involve the broadly defined phenolic and carboxylic moieties in DOM but effects of DOM site-specificity and alteration by water treatment processes on Cu-DOM interactions have not been studied in adequate detail. Some prior studies suggest that relatively smaller sized molecules or hydrophilic fractions of DOM bind copper preferentially [40], while others demonstrate preferential binding by DOM with higher aromaticity and apparent molecular weight [41,42]. Therefore, obtaining detailed and chemically specific information on the effects of DOM properties and its interactions with representative copper solid phases is key to understanding the role of DOM in the copper release processes.

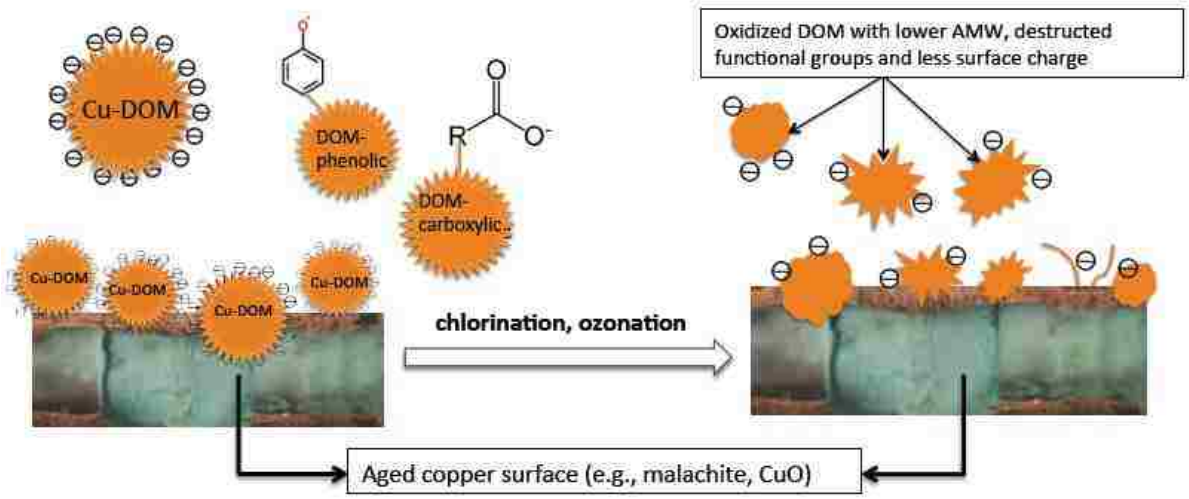

Figure 1.2 Mechanisms of copper release from associated solid phases in the presence of DOM and altered DOM

Examination of the behavior of malachite ($Cu_2(OH)_2CO_3$) and copper oxide (CuO) is especially appealing in the context of copper release control as these solid phases are typical for corroding copper surfaces. These and related compounds are be selected in our study as model phases in agreement with data of previous research indicating that copper release in drinking water is typically controlled by solid phases such as cupric hydroxide ($Cu(OH)_2$) and malachite ($Cu_2(OH)_2CO_3$) [43,44]. Cupric hydroxide is generally present on the surfaces of relatively newly exposed pipe walls but it tends to transform to copper oxide CuO in many cases [45]. The latter process can take as little as 8 hours when low silica concentration is present [46]. The absolute amount of these solid phases tends to change depending on the pipe age and water chemistry, but they are thermodynamically stable in the range of pH and dissolved inorganic carbon (DIC) concentrations typical for many drinking waters [47]. Therefore, malachite and copper oxide formed as a result of aging of cupric hydroxide are considered to be representative solid phases present on corroding copper surfaces.

1.3 Characterization of interactions between DOM and metal cations

Interactions between metal cations and DOM have been a subject of extensive studies because understanding and quantitation of these interactions provide insight into a variety of processes of high importance in environmental science and engineering. The DOM-metal interactions proceed through several mechanisms that include: 1) non-specific electrostatic interaction (e.g., DOM with Na^+ or K^+); 2) specific binding (e.g., DOM with Cu^{2+} or Pb^{2+}, etc.). In general, specific binding is stronger than its non-specific counterpart, and metal cations binding to humic substances can be mono- or poly-dentate in character, and can occur through either inner- (i.e., metal cations directly bind to the DOM ligands and form part of the first coordination sphere with no intervening water molecules) and outer-sphere (indirect binding), or can be a combination of these two types[10,48]. Consequences of DOM-metal cation interactions can be several-fold. DOM can reduce the bioavailability or toxicity of metals since metal/DOM complexes tend to have lower biotoxicity compared to the free metal ions [49]. On the other hand, the total dissolved metal concentration and the mobility of metals tend to increase in the presence of DOM due to the formation of metal-DOM complexes and also of metal/DOM colloidal particles [7]. In the case of metal corrosion in drinking water, for example, these effects have been observed for copper, lead corrosion and, in less detail, iron [22,50,51].

Prior studies have shown that the modeling of metal-DOM systems and, ultimately, in-depth understanding of its physical-chemical properties must take into account both specific interactions between Me^{n+} ions and DOM functionalities and also electrostatically

controlled interactions affected by variations of ionic strength. Prior studies have also provided evidence that concentrations of background cations such as Na^+ are important for such aspects of DOM chemistry as the supramolecular properties of DOM molecules and their aggregation [52–56], DOM adsorption on the surfaces of mineral particles and their colloidal behavior [57–59]. Because environmental concentrations of sodium and other background cations (e.g., K^+, Na^+) tend to be several orders of magnitude higher than those of trace level metals (e.g., Pb^{2+} and Cu^{2+}), this could result in a strong competition between the background and trace-level cations for binding sites in DOM [60].

The hardness cations Ca^{2+} and Mg^{2+} are ubiquitous and affect many important environmental processes [61,62]. For instance, Ca^{2+} acts as cation bridge between the dissociated functional groups on DOM and the negatively charged clay surface or other metal oxide surfaces [63,64]. Iron solid phases are also affected by the formation of complex between Ca^{2+} or Mg^{2+} and adsorbed organic matter [65]. The toxicity of trace metals such as cadmium can be increased due to the competition for the available DOM binding sites between the toxic heavy metals and hardness cations [66]. Ca^{2+} and Mg^{2+} are reported to interact with DOM mainly by weak electrostatic forces. However, both Mg^{2+} and Ca^{2+} have been also reported to form inner- and outer-sphere complex with functional DOM groups, such as its carboxylic groups at lower pH and phenolic groups at higher pH range [67,68]. Figure 1.3 provides a hypothetical scheme of the inner-sphere binding of calcium to DOM. In that scheme, calcium is coordinated with four carboxyl groups and one ether group; the latter model of coordination is meant to illustrate the importance of oxy-polycarboxylic acid structures. This model also shows the folding conformational changes in DOM that occur upon metal binding [48].

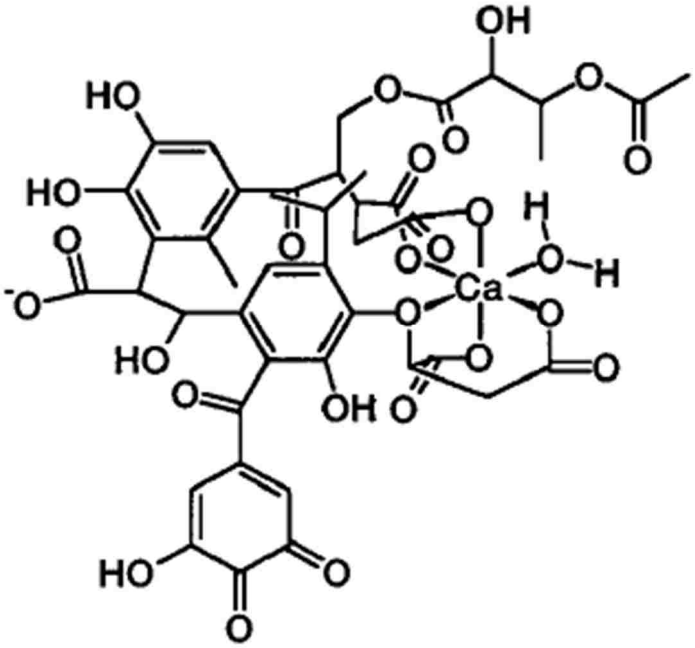

Figure 1.3 Structural model of a calcium inner-sphere complex of the metal binding fraction, adopted from Leenheer et al. (1998)[48]

Despite the importance of interaction between DOM and hardness cations for practically all natural or engineered systems, the extent and modes of interactions between Ca^{2+} and even less so Mg^{2+} have not been studied in exhaustive detail. In contrast, complexation between copper (cupric ion) and DOM have been extensively investigated, and very strong binding has been found to occur between Cu^{2+} and DOM functional groups. Data obtained using the method of Cu^{2+} ionic-selective electrode (ISE) measurements show that both in the presence of soil or surface water DOM, less than 0.2% of total Cu is present as free Cu^{2+}. Research of Cu(II) complexation by DOM indicates that Cu(II) forms inner sphere complexes that structurally are deemed to be one to two five-member chelate rings in DOM [37,69,70]. Most models suggest that these chelate structures have four oxygen or nitrogen

atoms and the atoms around the bound Cu(II) are arranged in a distorted octahedral geometry, with weaker binding to two more distant axial oxygen or nitrogen atoms (so called Jahn-Teller effect) [71,72]. These models may involve binding to oxygen atoms from carboxylate or carbonyl functionalities and emphasize the importance of oxygen-containing functional groups (e.g., carboxylate, phenolate, etc.), or nitrogen atoms of amino groups in the metal cation complexation with humic substances [10].

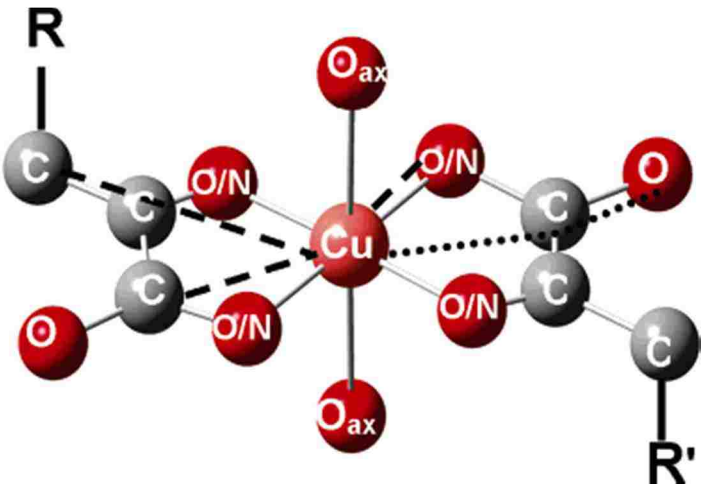

Figure 1.4 Hypothetical structural arrangement of Cu(II) binding by DOM, from Karlsson, et al. [72]

In the modeling of chemical equilibria in systems with DOM and metal ions, major features of DOM interactions with cations can be modeled assuming the presence of the moieties of operationally defined carboxylic and phenolic functional groups [49]. This approach has been used in several models, for instance in the Non-Ideal Competitive Adsorption model that accounts for ion binding by discrete functionalities operationally separated into the carboxylic and phenolic moieties, and non-specific Donnan electrostatic interactions (NICA-Donnan). In the NICA-Donnan and related models, metal-binding DOM

functionalities are separated into operationally defined carboxylic and phenolic moieties, each with a continuous distribution of pK values [73,74]. The Donnan model can be used to quantify concentrations of counter-ions (e.g., Na^+) accumulating to balance the charge of DOM molecules [75]. The Donnan approach assumes that DOM molecules behave as a gel with a uniform distribution of electric charge and potential within that gel [49,76]. Because in environmentally relevant conditions DOM molecules tend to have a net negative charge, this net charge is neutralized by the non-specific binding of counterions such as Na^+ or hardness cations that accumulate in the Donnan volume (V_D).

The NICA-Donnan model has been successfully applied to describe the binding of 23 metal ions (including, among others, Ca^{2+}, Mg^{2+}, Cu^{2+}) to DOM over a wide range of conditions [76–78]. Metal binding data used in this and other pertinent models have been typically obtained using ion-selective electrodes, ISE [79,80] that respond to changes of activities of the free ions of interest in the presence of DOM. Because a metal-specific ISE can measure the concentration of un-complexed free metal ion in solution, this allows for calculation of complexation capacities and stability constants [81,82]. The application of ISE techniques for environmental samples is in many important cases limited by the relatively high detection limits for the metal of interest (e.g., Pb^{2+}) which makes it necessary to carry out metal-DOM titrations using concentrations of metals that are significantly above the environmentally-observed level [26]. It is also necessary to utilize very high DOM concentrations (>1 g/L) in ISE experiments to obtain high-quality data for a sufficiently wide range of free metal activities. This necessitates pre-treatment or pre-concentration of environmental DOM samples, which may result in DOM with different conformations or properties than those in DOM found in real environmental condition [26]. Similarly,

potentiometric titrations that generate data necessary to quantify DOM protonation/deprotonation have been very useful for determination of stability constants and binding site capacities, but they also require very high concentrations of DOM and metal concentrations higher than typical environmentally-observed concentrations [60,83]. While these approaches can give precise data concerning activities of metal cations for which adequately sensitive probes are available, these data do not yield information about the microscopic nature of the functional groups involved in these interactions. Other advanced methods, for instance X-ray absorption spectroscopy, including X-ray Absorption Fine Structure Spectroscopy (EXAFS) and the related X-ray Absorption Near Edge Structure (XANES) techniques, [71,84–86] can provide important details concerning the number and nature (e.g., the electronic structure, bonding geometry, bonding lengths and coordination numbers) of the atoms present in the first coordination shell of the bound cations but this method requires relatively high concentrations of DOM and metals (that is, over 100 mg/L DOC and > 0.0001 mol/L Cu), and cannot be applied to many environmentally important ions. Also, its interpretation depends on the selection of representative model compounds [87–90]. Moreover, this method requires significant preparation of sample, and the data acquisition and processing require highly specialized equipment and expertise.

Other approaches, such as Nuclear Magnetic Resonance (NMR) spectroscopy can be used to examine and quantify DOM-metal interactions or elucidate details of the structural geometry of DOM-metal complexes, such as composition, segmental dynamics, domain sized, and local ordering of macromolecules. NMR uses a magnetic field to induce transitions between orientation of nuclear spins, and the frequency for these spin transitions

resonate in a particular field is dependent on the chemical environment of the nucleus [10,91]. With recent development of these techniques such as ^{13}C cross polarization-magic angle spinning (CP-MAS) technique coupled with advanced spectral editing techniques, NMR has been applied to identify specific functional groups in DOM or humic substances, determined proximities of specifically targeted groups of functionalities (e.g., lengths of aliphatic groups and their branching) and examined domains and heterogeneities of humic substances [92–95]. However, these techniques are insufficiently sensitive as to allow examining these systems in environmentally relevant conditions that are characterized by low concentrations of DOM, metal ions and resultant metal-DOM complexes. In other words, the techniques mentioned above virtually always require pre-concentration or pre-treatment of the DOM and DOM-metal complexes, which, beside constituting a difficult complication to overcome in practical terms, have a potential to alter the characteristics of DOM and its complexes [96]. This could lead to results that may not be representative of the behavior of DOM in the environment. There also remains a need to develop an effective method to characterize DOM and DOM-metal binding properties on a structural level that can be applied to unaltered DOM at the low concentrations found in environmental systems.

1.4 In situ characterization of DOM-metal interaction

Prior research indicates that among the functional groups typical in DOM, carboxylic and phenolic groups are major reactive "hot-spots" for many types of interactions [49]. These groups tend to absorb ultraviolet (UV) and visible light, or emit light upon irradiation. The

functionalities that have these properties are referred to as chromophores [97] and fluorophores, respectively. Although the overlapping contributions of the large variety of chromophores present in DOM result in DOM absorbance spectra to appear broad and featureless, important information about the properties of DOM can still be obtained from them. For instance, $SUVA_{254}$, which is calculated as the UV absorbance at wavelength 254 nm measured in inverse meters (m^{-1}) divided by the total DOC concentration (mg/L), has been shown to be a useful indicator of overall DOM character, notably its aromaticity. That is, DOM samples with higher $SUVA_{254}$ values tend to have higher contributions of hydrophobic and aromatic constituents. Similarly, the absorbance and SUVA at wavelength 280 nm correlates to the aromaticity of the DOM sample and also have been used to infer the average molecular weight of the DOM [98].

What is more important to our study, prior research has shown that numerically processed DOM absorbance spectra can be utilized to detect and interpret changes of DOM properties associated with the deprotonation of its molecules or their involvement into metal complexation. For example, the spectral slopes of log-transformed UV absorbance of DOM, vs. the wavelength in selected regions (e.g., 350~400 nm) have been found to be well correlated with the molecular weight of DOM found in various water matrixes such as wetland water and sea water, as well as for standard humic substance [97]. An *in situ* method using spectroscopic characteristics to probe the behavior of chromophores interacting with metal cations or protons is introduced as below and a more detailed description of the calculation of the important parameters will be present in the following chapter.

Differential Absorbance Spectroscopy (DAS)

The technique of differential absorbance spectroscopy (DAS) quantifies changes in DOM absorbance spectra associated with evolving reaction conditions that affect DOM chemistry, especially its aspects related to DOM chromophores [96,99,100]. Differential spectra are calculated as:

$$DAS_{i,nm} = \frac{A_j - A_{ref}}{l * DOC} \qquad \text{Equation 1-1}$$

where $DAS_{i,nm}$ is the differential absorbance at any selected wavelength. In the above formula, DOC is the concentration of organic carbon (mg/L), and l is the cell length (in cm). In studies where metal concentration is varied, A_j and A_{ref} are absorbance intensities at a particular wavelength (e.g., 390 nm) measured at a selected metal concentration (e.g., TOT_{Ca}= 0.001 M) and a relevant reference (for instance, TOT_{Ca} = 0 M), respectively. In pH variation experiments, A_j is the absorbance at any selected pH value while A_{ref} is the absorbance at an a priori selected reference pH.

DAS has been shown to be useful for precise examination of effects of pH variations on the deprotonation of DOM molecules. For example, Dryer et al. [96] described the presence in the differential spectra of several DOM types of characteristic contributing components. One of them was observed to have a prominent peak at 280 nm, which was interpreted to correspond to a spectroscopic signature of carboxylic groups undergoing deprotonation. The other important component was observed to have a broad band at >330 nm. This band was concluded to be a signature of phenolic groups in DOM (shown Figure 2.1 in the sections that follow).

The data of prior research [39] also indicate the existence of consistent and interpretable changes of DOM absorbance associated with its interactions with metal cations. For example, this approach has been used to quantify changes of DOM absorbance or fluorescence as a function of reaction coordinates, for instance, copper (II) and iron (III) concentrations [39]. Other parameters derived based on the analysis of DOM fluorescence or absorbance, for instance differential logarithms of DOM absorbance have also been found to correlate strongly with concentrations of DOM-bound metal cations [65,101].

However, such techniques have been mainly used for protons and minor or trace level metals (e.g., Cu^{2+}) rather than major hardness cations such as calcium and magnesium. As mentioned above, these ubiquitous cations affect many if not most important environmental processes [61,62]. Only a few studies have addressed intrinsic mechanisms of interactions between DOM and major hardness cations (e.g., Ca^{2+} or Mg^{2+}) [49,102], nor has the competition between these cations and other trace heavy metals (Cu^{2+}, Cd^{2+}, Pb^{2+}, etc.) been studied using in situ spectroscopic method. Kinniburgh et al. [49] reported that in the NICA-Donnan model, the relative strength of binding of metal cations has the following order for the carboxylic-type sites H^{+}» Pb^{2+} >Cu^{2+} >Cd^{2+} >Ca^{2+} and for phenolic-type sites this order is H^{+} »Cu^{2+} >Pb^{2+} »Cd^{2+} »Ca^{2+}. With the exception of Ca^{2+}, the stability constant values for the metal ions, especially those for Cu^{2+}, are considerably greater for the phenolic-type sites than for the carboxylic-type sites. Also, the models assume the occurrence of both monodentate and bidentate ligands in DOM. This results in the presence of a relatively low number of "high-affinity" sites that are favored in the case of binding of the trace heavy metals together with a larger number of weaker sites that can bind hardness cations.

1.5 Objectives of this study

This study is primarily concerned with the in-depth understanding of the nature of DOM interactions with metal solid phases and selected metal cations. Therefore three major themes are presented in this thesis: 1) the investigation of how DOM affects the release of metals from their solid phase, especially relating to corrosion process; 2) a detailed examination of ionic strength effects on DOM characterized by *in situ* spectroscopic approach; and 3) applications of the *in situ* spectroscopic approach to study DOM interaction with major hardness cation (e.g., Ca and Mg) and competition between the major cation and trace metals. Accordingly, the following specific objectives are to be addressed:

Objective 1. Investigate DOM effects on metal release from copper solid phases

Representative oxidized copper phases were selected in this study for studying DOM impacts on copper related corrosion processes. This objective is to examine mechanisms of DOM effects on copper release with a specific focus on the influence of DOM alterations resulting in changes of its aromaticity, molecular weight and surface activity. Effects of DOM altered by ozonation and chlorination are studied to provide detailed insight on how treatment processes that affect concentrations and properties of DOM impact copper release. In this section, a number of alternative parameters characterizing DOM properties

such as hydrophobicity are examined in order to evaluate the extent of DOM effects on copper release in systems controlled by representative copper-containing solid phases.

Objective 2. Characterize ionic strength effects on DOM using in situ methods

Based on the potential and advantages of *in situ* spectroscopic approach to characterize interactions between metal cations and DOM, this approach will be used to investigate the complexation behavior of functional groups in DOM with a variety of metal ions. In the first place, the effects of ionic strength (IS) on spectroscopic characters of DOM chromophores should be addressed since IS affects DOM properties and virtually all DOM-metals interactions in both pristine and engineered systems. We aimed to probe the specific spectroscopic parameters characterizing DOM microscopic properties (e.g., spectral slopes) and changes of DOM functionalities induced by IS variations, and interpreted the results based on a well-established approach (e.g., NICA-Donnan model). The ultimate goal is to provide a new level of insight into the intrinsic chemistry of DOM and its interactions with background ions that have critically important roles in the environmental reactions and fate of DOM that can be probed and ascertained at environmentally relevant DOM concentrations based on this approach.

Objective 3. Investigate DOM interactions with hardness cations and probe the competition between major and trace metal ions by in situ spectroscopic approach

Once the *in situ* spectroscopic approach developed to interpret the ionic strength effects on DOM is established, the third objective is to employed this approach to track interactions between DOM and Ca^{2+} or Mg^{2+} per se and Cu^{2+} in the presence of varying calcium

concentrations. This combination of background and heavy metal ions exists universally in the environment. The spectroscopic data are processed and compared with the data of NICA-Donnan model calculations which allow exploring the nature of the observed changes and their relationships with the engagement of DOM functional groups into the binding of the selected metal cations.

2 Research Hypothesis and Experimental Approaches

(a): Hypothesis on copper release affected by DOM and altered DOM

In the context of heavy metals control in drinking water, DOM is hypothesized to facilitate metal release by 1) the formation of Cu-DOM complexes; and 2) colloidal mobilization/dispersion with DOM adsorbed on solid phase surface (i.e., the DOM coated Cu colloids are expected to detach and disperse in solution). Both mechanisms are likely to increase copper concentrations in solution, compared to a no DOM scenario. Effects of colloidal dispersion may be very important but the hypothesis concerning the extent of this mechanism could be accepted or rejected by comparison of the experimental results with theoretical calculation of copper release with these model phase where metal-DOM complexation model is the only mechanism being taken into account. Furthermore, the presence of a colloidal dispersion mechanism assumes the occurrence of a change of surface charge on metal solids that is hypothesized to be increased by the adsorption of negatively charged DOM.

Our second hypothesis is that not all the moieties in DOM play equal roles in promoting copper release. Some DOM molecules, for example, those with higher aromaticities are

expected to preferentially adsorb onto the solid phase and contribute prominently the colloidal mobilization. In contrast, DOM fractions that have low surface activity will tend to remain in solution after the initial DOM sample has interacted with the solid phases. Therefore, applicable tests (e.g., measurements of absorbance spectra, High Pressure Size Exclusion Chromatography (HPSEC) metal concentrations before and after the introduction of DOM) will show what fractions of DOM are preferentially removed or adsorbed by metals.

Following this logic, treatment approaches targeting DOM fractions that play more important role in copper release could be used and the altered DOM with active moieties having been destructed is hypothesized to be less effective in affecting copper release or corrosion process.

(b) Hypothesis on the characterization of interactions between major cations and DOM by in situ spectroscopic methods

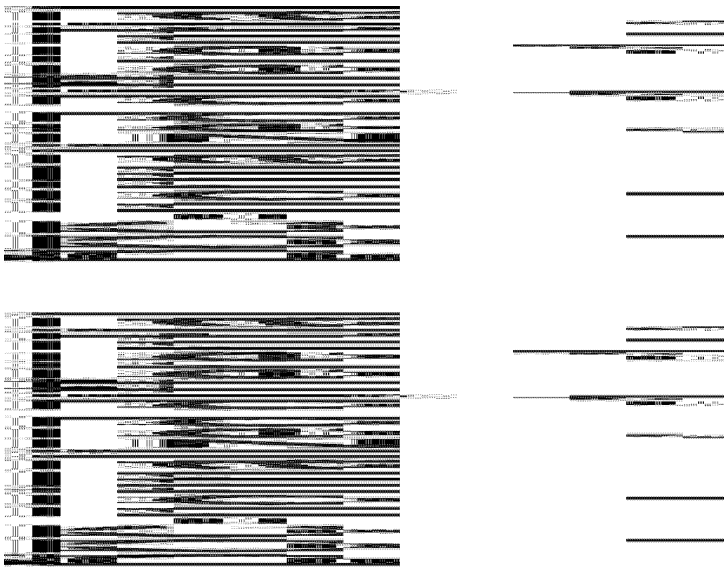

Figure 2.1 DAS profiles of the Suwannee River fulvic acid (SRFA) reflecting the engagement of carboxylic and phenolic groups at varying pHs (adopted from Dryer et al.[96])

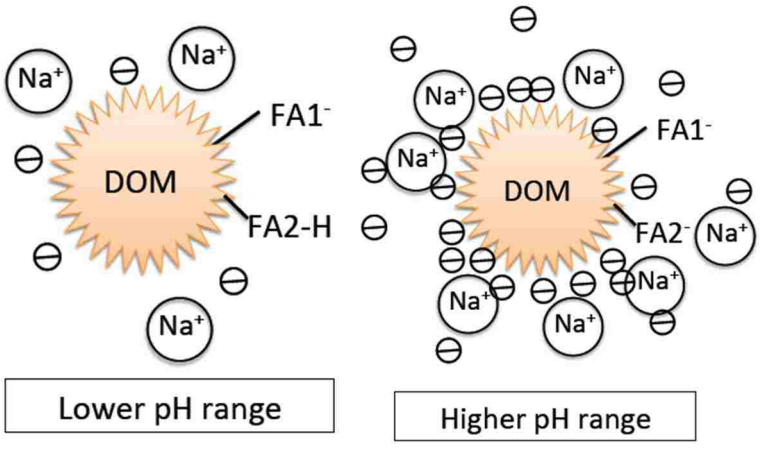

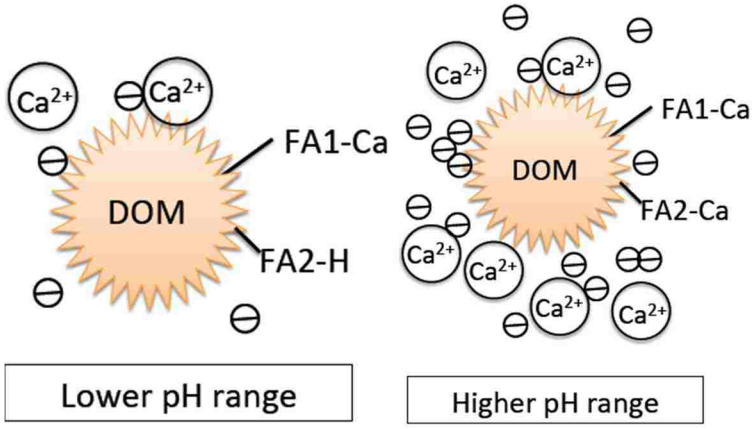

Figure 2.2 Accumulation of cations (Na^+ and Ca^{2+}) within the Donnan volume and the binding of Ca^{2+} to dissociated functional groups as cation concentration in solution increases.

Our hypothesis concerning DOM-metal interactions is based on the views on DOM chemistry that are incorporated in the NICA-Donnan model. It also reflects the previous DAS work that has been done by our group for characterization of protonation and complexation behavior of Suwannee River fulvic acid (SRFA) and other DOM types. Some important interactions relating to this hypothesis are shown in Figure 2.1. The Donnan model assumes that humic substances behave as a gel with a uniform distribution of electric charge and potential within that gel [49,76]. Because in environmentally-relevant conditions humic substances normally have a residual net negative charge after the specific binding of protons or metal cations has been taken into consideration, the net negative charge is neutralized by the non-specific binding of counterions such as Na^+ and, if present in sufficiently high concentrations, other ions such as Ca^{2+} and Mg^{2+}. The Donnan volume, which is an important parameter in the Donnan model is deemed to include a humic molecule along with the diffuse part of the electric double layer surrounding it.

Figure 2.1 shows that as the solution pH increases, the differential spectra of SRFA exhibit a number of specific features that are deemed to be signatures for carboxylic and phenolic groups. Because initial NICA-Donnan calculations predict consistent changes of the deprotonation of these groups at a constant pH but increasing ionic strengths, we expect to see changes in the DAS spectra similar to those in the case of increasing pHs. That is, we hypothesize that for monovalent cation such as Na^+ that does not form any chemical binding with the carboxylic and phenolic groups but can interact with DOM electrostatically, increases of the bulk sodium concentration result in more Na^+ ions accumulate in the Donnan volume. NICA-Donnan models shows in these conditions some of the DOM-bound protons are "squeezed out" (Figure 2.2). This means that the resultant DAS spectra should display a similar pattern to the ones undergoing deprotonation (Figure 2.1).

Importantly, the accumulation of Na^+ should depend on pH as well, since at lower pH ranges (such as below or around the pKa of carboxylic groups, as pH= 2~5), when phenolic groups with high pKa (7.2~10.9)[76] are still in protonated form while a few carboxylic groups are deprotonated, the accumulation of Na^+ in Donnan volume is limited due to the lower negative charges on DOM molecules. However, when pH is raised to higher ranges around pKa values of phenolic groups, the greater negative charge on DOM molecule will attract greater concentration of Na^+ in the Donnan volume and the impact of this process as reflected by DAS spectroscopy will be more significant than the lower pH scenarios.

On the other hand, for the divalent cations such as calcium and magnesium, interactions between these cations and DOM molecules are likely to include not only the accumulation of these cations in the Donnan volume, but, based on the data of prior research, specific

binding to carboxylic and phenolic groups also takes place (Figure 2.2). It is accordingly hypothesized that the DAS results will be different than those for sodium, due to a different binding pattern. Furthermore, some other spectroscopic parameters, such as spectral slope in the range of interest (for example, the range of 350~400 nm), the DAS absorbance value to certain wavelength (e.g., 320, 390 nm) is expected to be reflective of the amount of cations bound to functional groups or accumulated within Donnan volume.

The hypothesis presented above forms a foundation of our experiments that deal with DOM interactions with hardness cations and, ultimately, competitions between heavy metals with high binding affinity but low concentration and major hardness cations of weak binding ability while of a much higher concentration. Descriptions of the methods used in our experiments are shown in the following section.

2.1 Copper model phases and DOM preparation

Malachite $Cu_2CO_3(OH)_2$ and copper oxide CuO of analytical grade were obtained from Aldrich Chemical Company (Milwaukee, WI). The model phases were in powder form and their specific surface areas were determined by BET analysis using a Quantachrome NOVA 4200e instrument. These measurements showed that the surface areas of malachite and CuO were 44.42 and 2.02 m^2/g, respectively.

Aldrich humic acid (AHA) was obtained from Aldrich Chemical Company (Milwaukee, WI) and standard Suwannee River fulvic acid (SRFA) (standard number 1S101F) from the

International Humic Substance Society (IHSS) were used in the experiments. AHA was cleaned using the method described by Chin et al. [103] but without adding phosphate. Sodium hypochlorite solutions were obtained from Fisher Scientific Inc. (Pittsburgh, PA) and diluted to ~200 mg/L (as free chlorine) stock concentrations. The free chlorine in the stock solutions were measured by DPD method [105]. Chlorine was added to AHA stock solution to reach chlorine to dissolved organic carbon (DOC) mass ratios of 0.1, 0.5, 1.0, 2.0 and 4.0 at the original pH of DOM system (~pH 4) (we use Cl_2/DOC and Cl_2/AHA interchangeably for oxidant to DOM ratios in our following text or figures). It is to be mentioned here that experiments with unaltered AHA were carried with this organic matter from a different batch, which could result in some differences between this AHA sample and that altered by chlorine.

SRFA was chlorinated using Cl_2/DOC mass ratios of 1.0 and 2.0. SRFA ozonation was done with an ozone generator (AC2000 series) equipped with a Mini Hicon ozone analyzer. This ozonator produced a ca. 50 mg/L O_3 stock solution. The actual O_3 concentration was determined by the standard 4500-O_3 indigo colorimetric method [104]. Requisite amounts of ozone stock solution were added to SRFA solution to achieve O_3/DOC ratios of 1.0 and 2.0, at the original pH of DOM system (~pH 4). The chlorinated and ozonated DOM were kept for one week until the measured residual ozone and chlorine were below 0.1 mg/L. The DOC concentration of DOMs after chlorination and ozonation was re-determined and the mineralization of organic carbon was insignificant (5%~8%). Furthermore, the DOC concentration of chlorinated or ozonated DOM referred in the text were based on DOC measurement after chlorination/ozonation.

2.2 Metal release tests and analyses

0.1 g of malachite or copper oxide was added to pre-cleaned 200 ml polycarbonate containers (EP Scientific, Miami, Oklahoma). DOM was added to the solutions to reach DOC concentrations of 0, 1, 2, 5, and 10 mg/L. The alkalinity of solution was maintained at 200 mg/L as $CaCO_3$ by adding $NaHCO_3$. The pH was maintained at 8.3±0.1 by adding $HClO_4$ or NaOH.

The solution was agitated for 2.5 hours following which aliquots were taken from the containers, passed through 0.45 μm filters and analyzed to determine copper concentrations by a PerkinElmer ELAN ICP-MS instrument (PerkinElmer Instruments, Shelton, CT). Measurements of ζ-potential of malachite and CuO particles were performed with a ZetaPlus analyzer (Brookhaven Instruments, NY).

2.3 DOM characterization

Distributions of apparent molecular weight (AMW) of the examined DOM samples were examined using the method of high-performance size-exclusion chromatography (HPSEC), coupled with a multiple wavelength (200~445 nm) absorbance detector (ultimate 3000 diode array detector) [105]. HPSEC measurements employed a Dionex HPLC system equipped with an Agilent GPC/SEC column (PL Aquagel-OH mixed, 7.5 x 300

mm, 8 μm particle size). 90% ammonium acetate (10 mM) and 10% methanol were used as mobile phase [106] and polystyrene sulfonate (PSS) with molecular weights of 34700, 16000, 7540, 5180 and 1530 Da was used for calibration.

2.4 Ionic strength effects on DOM

Experiments were carried out with samples of Suwannee River fulvic acid (SRFA) (standard number 1S101F), Suwannee River humic acid (SRHA) (standard number 2S101H) and Pony Lake fulvic acid (PLFA) (standard number 1R109F) obtained from the International Humic Substances Society (IHSS). Ionic strength of solutions containing these DOMs was controlled by means for adding varying amounts of analytical grade sodium perchlorate $NaClO_4$ purchased from Aldrich Chemical Company (Milwaukee, WI).

In these experiments, requisite volumes of $NaClO_4$ and DOM stock solutions were added in 200 mL containers to reach a 5 mg/L dissolved organic carbon (DOC) concentration while the concentration of ionic strength was varied by adding $NaClO_4$ from 0.001 to 0.3 mol/L. pH of the solutions was controlled by adding small amounts of $HClO_4$ or NaOH. After each addition of $NaClO_4$ stock solution and a 30-minute equilibration time, aliquots were taken to record their absorbance spectra acquired with a 5-cm quartz cuvette by a Shimadzu UV-2700 spectrophotometer. pH was maintained at 6, 7, 8 and 9. In the lower end of pH range (e.g., pH 6 and 7), as the limited deprotonated DOM results in low buffering capacity of the solution, 0.01 mol/L MOPS buffer (>99.5% purity, BioXtra grade purchased from Sigma-Aldrich) was added to achieve pH stability.

Calculations of Absorbance-Based Parameters

As was mentioned above in introducing equation 1-1, differential spectra obtained in the case of variations of ionic strength were calculated as described in literature [96,99,100] and shown below:

$$DAS_{i,nm} = \frac{A_j - A_{ref}}{l * DOC} \qquad \text{Equation 2-1}$$

In the above formula, $DAS_{i,nm}$ is the differential absorbance at any given wavelength, A_j and A_{ref} are absorbance intensities measured at a selected NaClO4 concentration and a relevant reference concentration which is the lowest practically attainable concentration of background salts that can be reliably controlled (0.001 mol/L in this study). DOC is the concentration of organic carbon (mg/L), and *l* is the cell length (in cm).

Log-transformed spectra:

As discussed in more detail in the sections that follow, IS caused characteristic and consistent changes of log-transformed spectra of DOM and their slopes. Accordingly, we calculated the differentials of log-transformed spectra of DOM as defined below:

$$DlnA_{i,nm} = ln\left(\frac{A_j}{A_{ref}}\right) \qquad \text{Equation 2-2}$$

The slopes and differential slopes of log-transformed absorbance spectra of DOM were calculated and as defined below:

$$S_{350-400} = \left| \frac{d \ln A(\lambda)}{d\lambda} \right|_{350-to-400nm}$$ Equation 2-3

$$DS_{350-400} = S_{350-400,i} - S_{350-400,ref}$$ Equation 2-4

The spectral slopes in the range of wavelengths 350 to 400 nm (S350~400) were determined as the slope of the linear correlation that fits the log-transformed DOM absorbance spectra in the range between 350 and 400 nm. The differential slope is defined as the difference between $S_{350-400,i}$ and $S_{350-400,ref}$, which are the spectral slopes determined for any selected condition and an applicable reference, respectively.

2.5 Complexation of major hardness cations with DOM and competitive binding between heavy metals and hardness cations

Suwannee River humic acid (SRHA) (standard number 2S101H) obtained from the International Humic Substances Society (IHSS) was used in this study. The concentrations of SRHA were 5.0 mg L^{-1} as dissolved organic carbon (DOC) measured by a Shimadzu TOC-Vcsh carbon analyzer. Ionic strength of all solutions was controlled by adding requisite amounts of $NaClO_4$, which was the background electrolyte in all cases. Stock calcium, magnesium and copper solutions were prepared using $CaCl_2$, $MgCl_2$ and $Cu(ClO_4)_2$ of analytical grade from Aldrich Chemical Company (Milwaukee, WI).

Titrations: Ca/Mg and Cu titrations were carried out as described in detail in prior publication [107,108]. Aliquots of stock Ca/Mg and Cu solution were added by requisite

volumes into a series of 200 mL-jars. Total metal concentrations were varied from zero to levels below their respective precipitation levels determined using Visual MINTEQ for each selected metal, ionic strength and pH. DOM-metal complexation was modeled using the NICA-Donnan model [109–111] and complexation constants used in the calculations are shown in Table 2-1. pH of the solutions was controlled by adding $HClO_4$ or NaOH and buffered by 0.01 M MOPS solution (>99.5% purity, BioXtra grade purchased from Sigma-Aldrich). After the addition of metal stock solution and a 30-min equilibrium time, aliquots were taken from solutions with varied metal concentrations and then the corresponding absorbance spectra were recorded by a Shimadzu UV-2700 spectrophotometer from 200 to 600 nm.

Absorbance data processing. Processing of absorbance spectra of DOM was done as described in previous studies [107,112,113]. The linear differential absorbance spectra and differential log-transformed absorbance spectra were calculated using equation 2-1 and equation 2-2 respectively. The slopes and differential slopes of log-transformed absorbance spectra of DOM were calculated by equation 2-3 and equation 2-4:

Table 2-1 NICA-Donnan modeling parameters for DOM with major hardness ions (Ca and Mg) and Cu used in model calculations with Visual MINTEQ.

Parameters		log K_1	n_1	Q_1 (mmol g^{-1})	log K_2	n_2	Q_2 (mmol g^{-1})	b	Ratio of DOM to DOC	% active DOM that is FA
SRHA	Proton	2.93	0.81	3.15	8.00	0.63	2.55	0.49	1.904	0
	Ca	-1.37	0.78		-0.43	0.75				
	Mg	-0.6	0.77		0.6	0.77				
	Cu	2.23	0.56		6.85	0.34				

SRFA	Proton	2.34	0.66	5.88	8.60	0.76	1.86	0.57	1.904	100
	Mg	-2.1	0.77		-2.4	0.59				

3 Effects of DOM properties on copper release from model phase

3.1 Copper release in the presence of DOM

In the tests, copper released from the solid phases were found to increase with time at reaction time up to 10 hours (Figure 3.1). Despite these trends, copper concentrations measured for a 2.5- hour contact time were selected to be operationally representative of quasi-stable concentrations. This selection reflects several aspects of the experiments. Specifically, the pH of ambient solutions was observed to increase with time, especially for malachite. This appears to reflect the fact that anionic DOM molecules sorbed onto copper solids and OH^- would be released from solids into solution via surface complexation [26]. In addition, malachite dissolution per se is accompanied by the release of OH^- ions, in accord with the stoichiometry of this solid. Although pH stability could be achieved by using automatic pH-stats, for the number of the jars that were tested it was not feasible to use this apparatus in the experiments, given no buffer was introduced into the system. Therefore, a 2.5 hours contact time during which pH was continuously monitored and corrected is a feasible time frame selected based on the operational conditions. In addition, for DOM below 5 mg/L, the ratio of copper concentrations observed at 10 hours to that at 2.5 hours was on the average of 1.36 with a standard deviation of 0.21; and in most cases, the increase of copper concentration slowed down dramatically after 2.5 hours. Accordingly, we used Cu release data for a 2.5 hours exposure time as quasi-stable concentrations. Thus, in these experiments effects of DOM on copper release were

quantified for a fixed relatively short exposure time that simplified controls of pH stability and other reaction conditions.

Relevant metal release data (for a 2.5 hours contact time) presented in Figure 3.2 and Figure 3.3 show that unaltered AHA and SRFA strongly promoted metal release from the solid phase. Copper release concentrations normalized by solid surface area were also shown in Figure 3.4. This effect was affected by chlorination or ozonation on DOM and the type of model phase. In the case of malachite, unaltered AHA or AHA modified (Figure 3.3) using low chlorine concentrations (e.g., Cl_2/DOC ratios 0.1 and 0.5) significantly increased the metal release as the DOC concentration increased. For example, the copper concentrations increased from 87 to 854 μg/L as AHA concentration increased from 0 to 10 mg/L as DOC. In contrast, in the presence of AHA altered using higher Cl_2/DOC, the copper concentration only increased from 87 to 164 μg/L when DOC increased from 0 to 10 mg/L (DOC was re-measured after chlorination/ozonation).

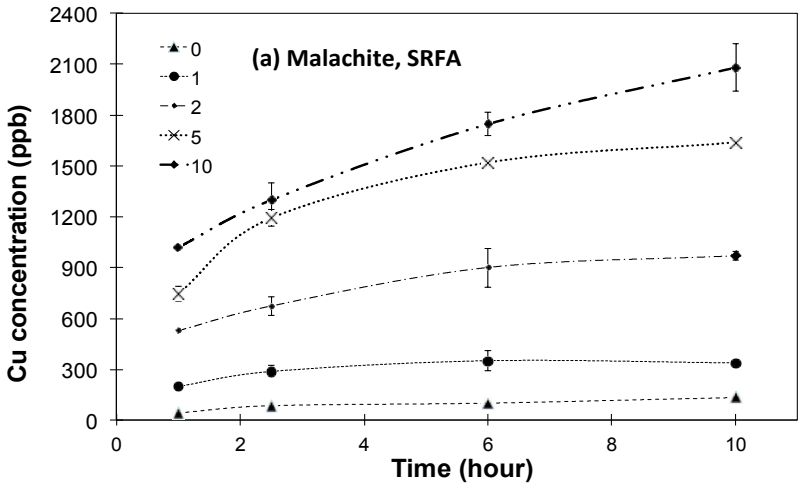

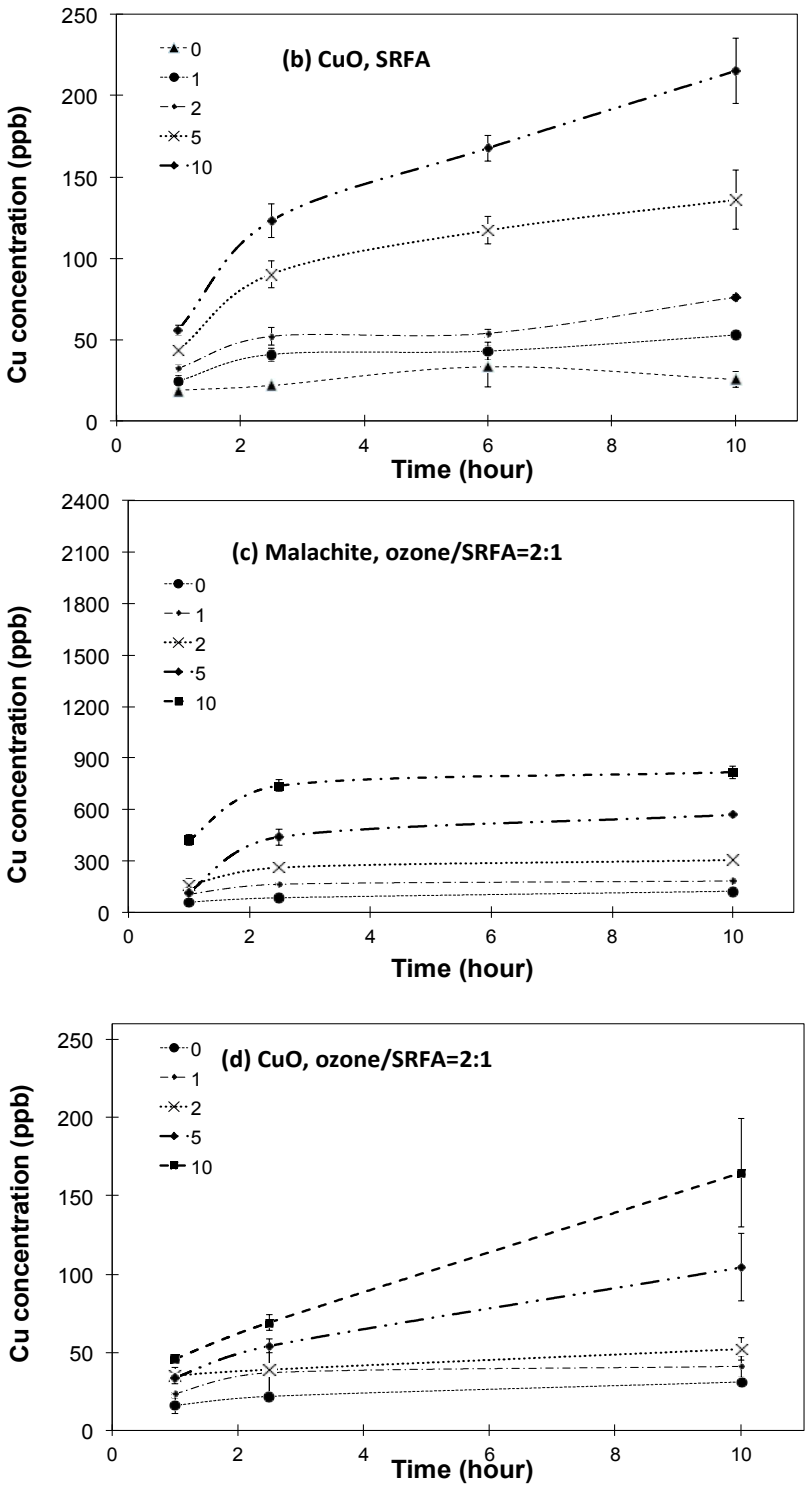

Figure 3.1 Copper release as a function of time for malachite and copper oxide (pH 8.3, alkalinity 200 mg/L).

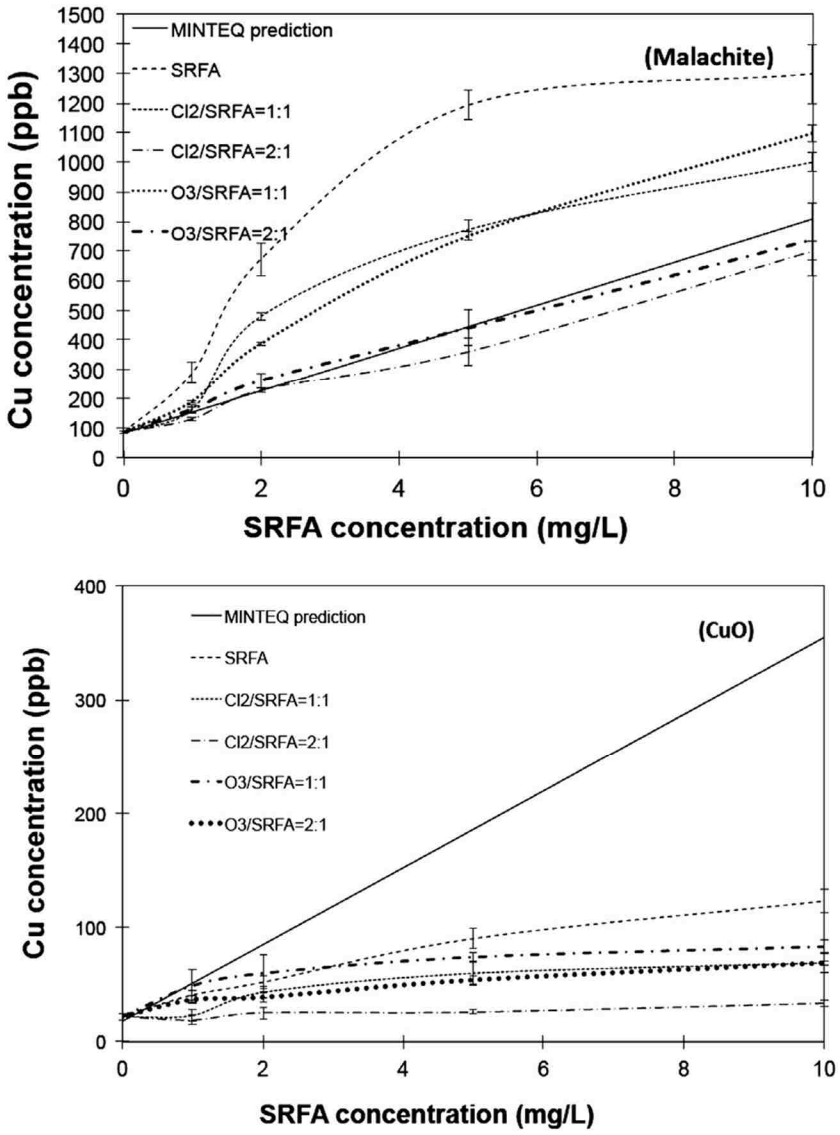

Figure 3.2 Effect of DOM (Suwannee River fulvic acid (SRFA)) on copper release from malachite and tenorite (CuO). pH 8.3, alkalinity 200 mg/L, exposure time 2.5 h.

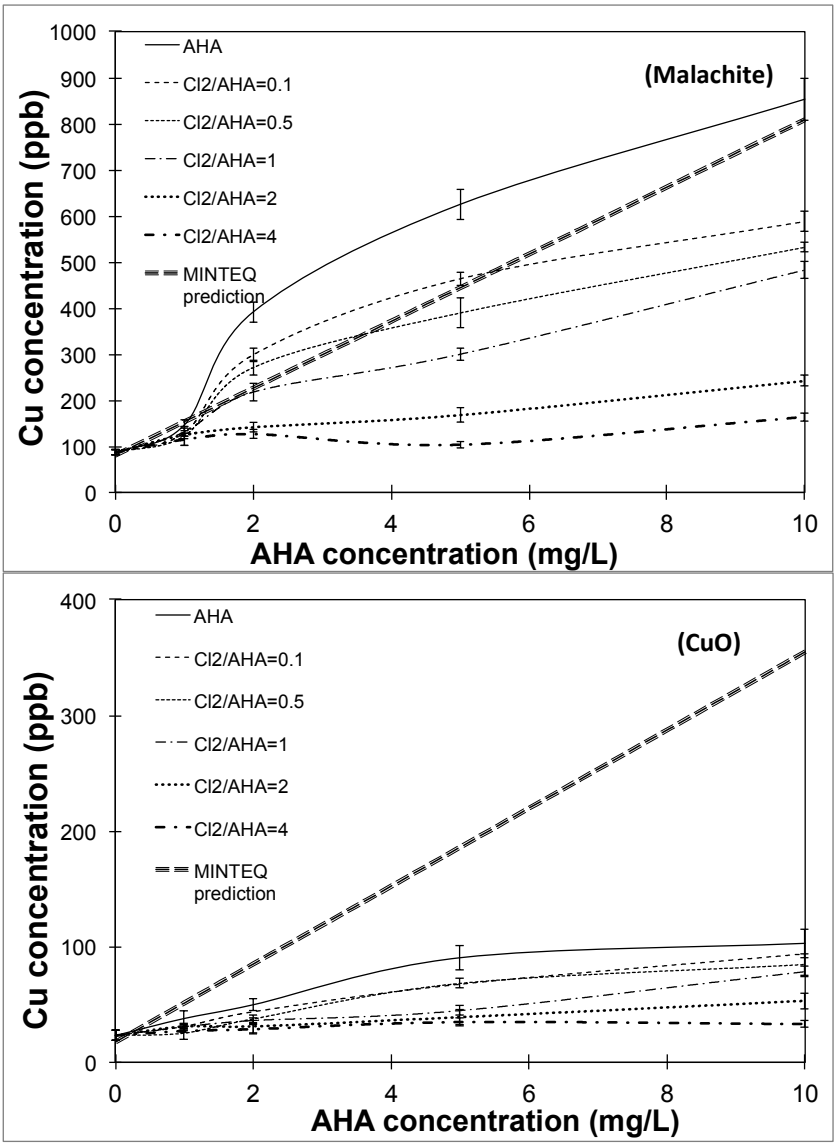

Figure 3.3 Effect of DOM (Aldrich humic acid (AHA)) on copper release from malachite and tenorite. pH 8.3, alkalinity 200 mg/L, exposure time 2.5 hours.

Experiments with SRFA (Figure 3.2) demonstrate that copper release increased at higher DOC concentrations but DOM alteration by either ozonation or chlorination reduced or eliminated this effect. The presence of SRFA led to higher copper release than AHA at the same DOC concentration, possibly due to more abundant reactive sites for binding metals in SRFA than AHA.

The suppression of DOM effects by ozone seen in this study is opposite to the trend observed in prior research for Al or Fe oxide or flocs formed by hydroxides of these metals[6]. In that study, DOM ozonation was observed to cause an increase of soluble Al or Fe concentrations compared to those in the presence of unaltered DOMs. That effect was hypothesized to be caused by the generation of ozonation by-products, notably oxalate that can strongly sorb onto both iron and aluminum oxide surface as well as by the increased acidity and complexation capacity of ozonated DOM that can lead to an increase of metal release.

The data presented above provide evidence that DOM ozonation can cause changes (other than those reported in prior research[6]) of DOM chemistry that are likely to be important in determining the role DOM in corrosion and metal release in the case of copper. Ozonation is known to cause DOM molecules to break down and form molecules with lower aromaticity, molecular weight and hydrophobicity. This has been shown to cause DOM affected by ozonation to be less active in affecting the morphology and promoting release of colloidal particles [21]. Therefore, we hypothesize that DOM molecules affected by ozonation or chlorination are less likely to exhibit surface activity at solid/solution interfaces and therefore less accumulation of negative surface charge, compared with unaltered DOM, should be expected in their presence. This point is indeed confirmed by our measurements of the ζ-potentials of malachite and CuO in the examined systems.

Visual MINTEQ software was used to determine the expected dissolved copper concentration at equilibrium with copper oxide or malachite. In these calculations, the properties of DOM and the Cu-DOM interactions were assumed to be described by the NICA-Donnan model [114,115]. Generic Cu-DOM complexation constants included in the

database of Visual MINTEQ were used and correction for solubility equilibrium constant and temperature was taken into account in these calculations. Although the measured copper concentrations in our experiments (that used a fixed 2.5 hour contact time) were not necessarily equilibrium concentration, we would use this model to evaluate the role of complexation in metal release.

Results of these calculations show that for malachite exposed to unaltered AHA and SRFA, and chlorinated/ozonated SRFA with ratio=1:1 examined in this study, the observed copper concentration exceeded the corresponding theoretically predicted values by Visual MINTEQ, indicating that not only complexation but other mechanisms such colloidal mobilization were likely involved in the promotion of copper release[22] . Copper concentrations found in solutions in contact with CuO tended to be below the levels predicted by Visual MINTEQ calculations, possibly because of much lower specific area of this solids and a relatively short contact time (2.5 hours) during which the equilibrium was yet to be reached.

However, trends in relative changes of copper concentrations released from CuO or malachite were largely identical (Figure 3.5). This figure demonstrates that relative changes (that is, those concentrations normalized by the copper concentrations observed in the absence of DOM) of copper released from CuO and malachite were prominent and significant in the presence of unaltered DOM but copper release became largely insensitive to DOM concentrations after it had been altered by chlorination or ozonation. For example, for malachite in contact with AHA, the relative change of copper release in the presence of 1 mg/L slightly chlorinated AHA (Cl_2/DOC=0.1) was around 1.5; and this ratio increased to ~6.8 when DOM concentration increased to 10 mg/L. In contrast with that, for highly

chlorinated AHA (e.g., Cl_2/DOC=4), the relative copper change did not exhibit any significant change when DOM concentration increased from 1 to 10 mg/L.

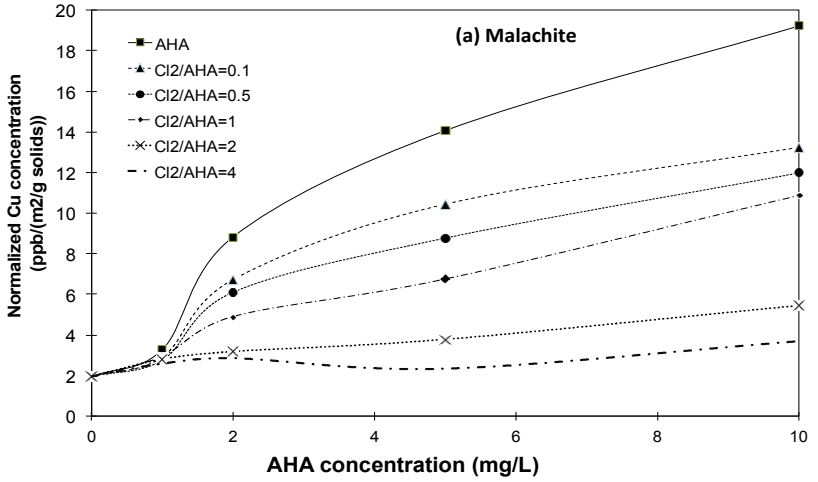

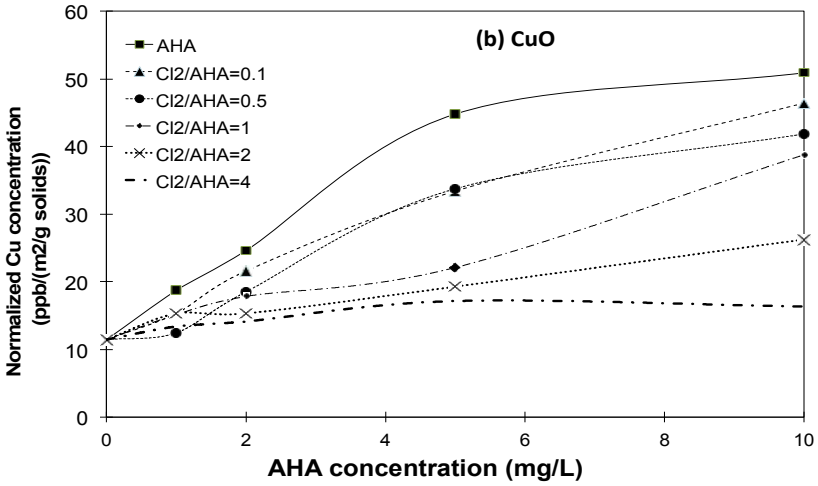

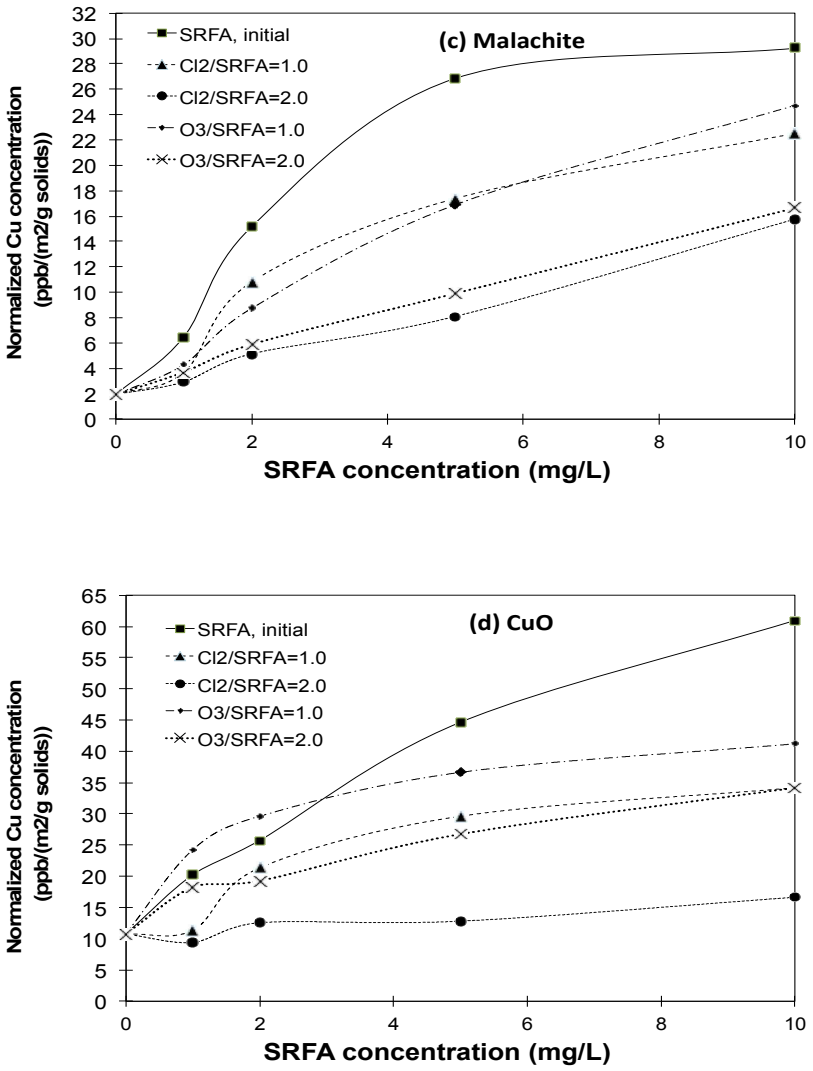

Figure 3.4 Copper release normalized by the specific surface area of the model phases.

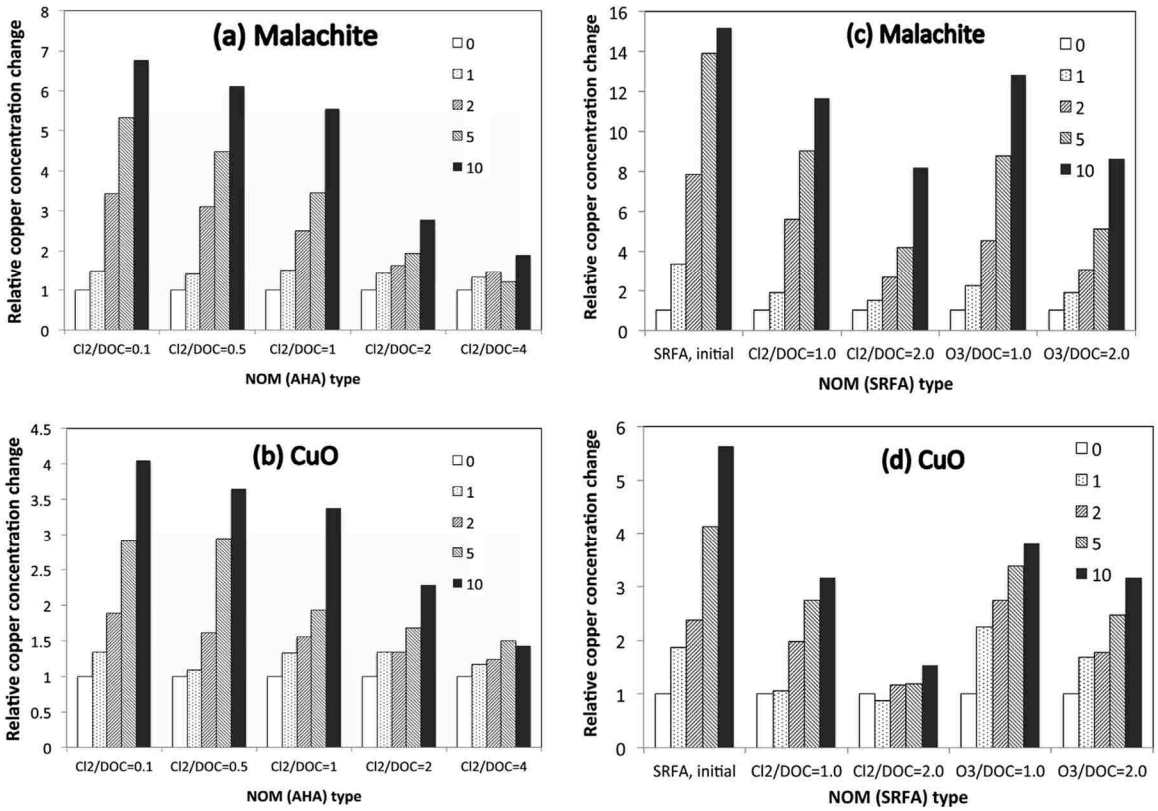

Figure 3.5 Relative changes of copper concentration in the presence of varying DOC concentrations. All concentrations were normalized by the copper concentration in the absence of DOM.

3.2 Characterization of changes of DOM properties caused by chlorination and ozonation

Given that the alteration of AHA and SRFA properties by chlorine and ozone had a prominent effect of copper release, properties of these DOM samples were examined in more detail using the methods of differential absorbance spectroscopy (DAS) and high-performance size exclusion chromatography (HPSEC). As described in earlier studies, pH-differential absorbance spectra of DOM allow detecting contributions of chromophores associated with the carboxylic and phenolic moieties. Prior research and this study

demonstrate that DAS spectra of DOM contain characteristic features whose position and intensity depend on the pH and intrinsic DOM properties [20,96,115].

In the case of unaltered SRFA, the deprotonation of carboxylic groups that took place when the pH was increased from ca. 3.0 to 7.0 resulted in a characteristic feature with a peak at 280 nm; while the deprotonation of phenolic groups taking place at pH > 8 resulted in a more intense band located in the region 330 to 380 nm, and an additional feature with a peak at 244 nm (Figure 3.6). Chlorination of SRFA diminished the spectra intensity, as well as their signature peaks. The broad structure at $\lambda > 330$ nm associated with the phenolic chromophores became much weaker after SRFA was treated with a 1.0 Cl_2/DOC dose while the band with a maximum at 280 nm remained. For SRFA chlorinated with a 2.0 Cl_2/DOC dose, the intensity of the DAS spectra became even lower and the intense feature at $\lambda > 330$ nm disappeared almost completely.

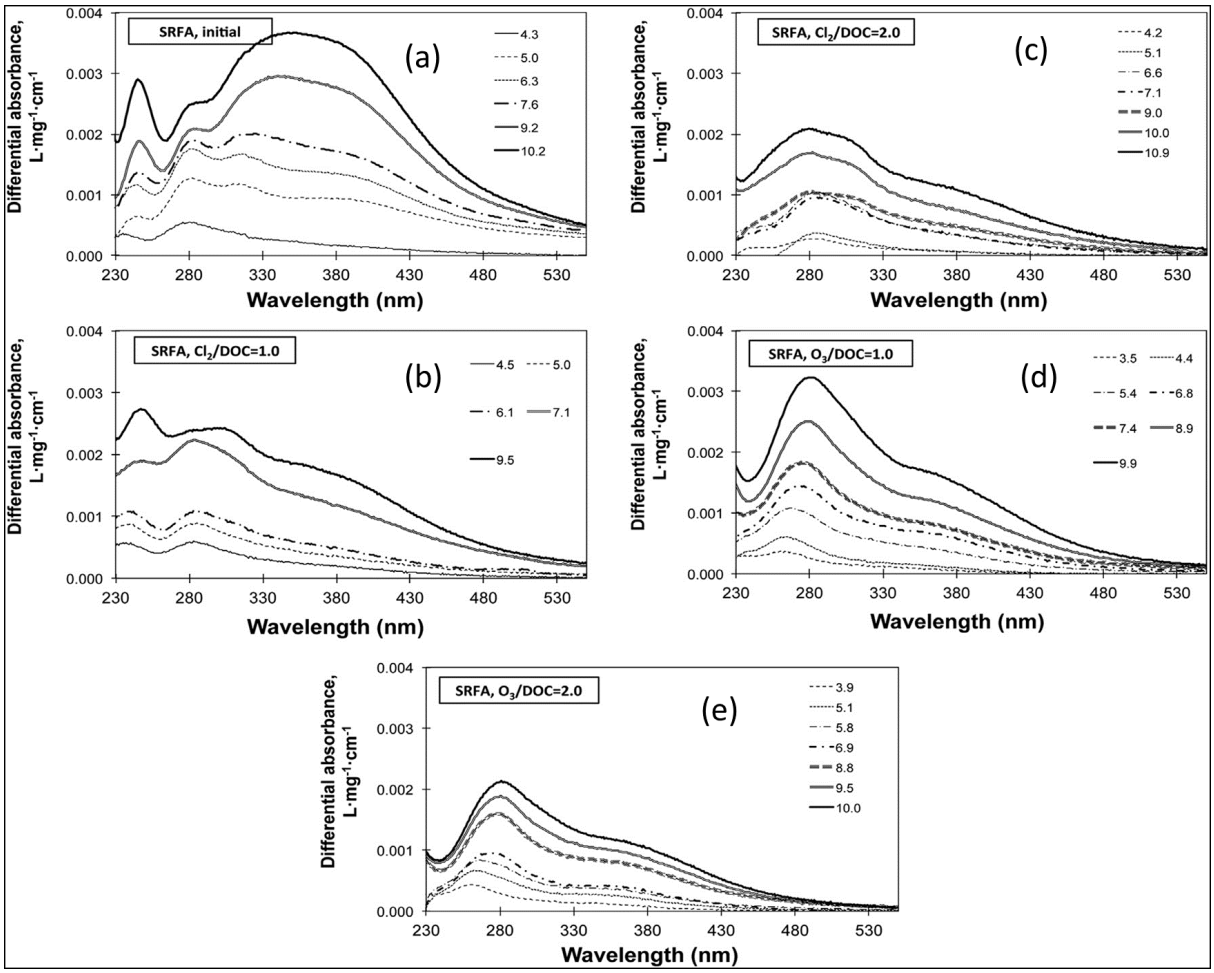

Figure 3.6 DOC-normalized differential spectra of SRFA altered by chlorination and ozonation at varying Cl_2/DOC and O_3/DOC weight ratios: (a) SRFA in its initial form without any ozonation/chlorination treatment, (b) chlorinated SRFA with Cl_2/DOC ratio of 1, (c) chlorinated SRFA with Cl_2/DOC ratio of 2, (d) ozonated SRFA with O_3/DOC ratio of 1 and (e) ozonated SRFA with O_3/DOC ratio of 2. The reference spectrum was recorded at pH 3.3.

The decrease of intensity and ultimately virtual disappearance of the later structure can be additionally demonstrated using the differential spectra normalized by the intensity of the structure located at ca. 280 nm when carboxylic DOM chromophores were deprotonated as the pH of solution increased. Figure 3.7 shows that the intensity of the feature associated with the protonation-active phenolic chromophores decreased for SRFA chlorinated with a 1.0 Cl_2/DOC dose, and for a 2.0 Cl_2/DOC dose this structure was almost absent.

Ozonation caused very similar effects in the DAS of SRFA, although the disappearance of the features associated with the phenolic chromophores was as prominent at a 1.0 O_3/DOC ratio as it was for a 2.0 ratio.

Similar trends were observed for AHA altered by chlorination, although the structure of the DAS spectra for AHA was somewhat different from that of SRFA. The deprotonation of the phenolic chromophores in AHA altered using the lowest Cl_2/DOC ratio of 0.1 causes the emergence of a band at λ> 300 nm with a maximum at 390 nm (Figure 3.8). Similarly to the data for SRFA, chlorination carried out using increasing chlorine concentrations caused this band to weaken and disappear. An additional structure with a maximum at 325 nm was also observed in the DAS of AHA but not in those of SRFA. The overall intensity of the DAS spectra decreased dramatically as the chlorine dose increased, and for the highest Cl_2/DOC ratio of 4, the intensity of DAS was an order of magnitude less than that for a 0.1 Cl_2/DOC ratio.

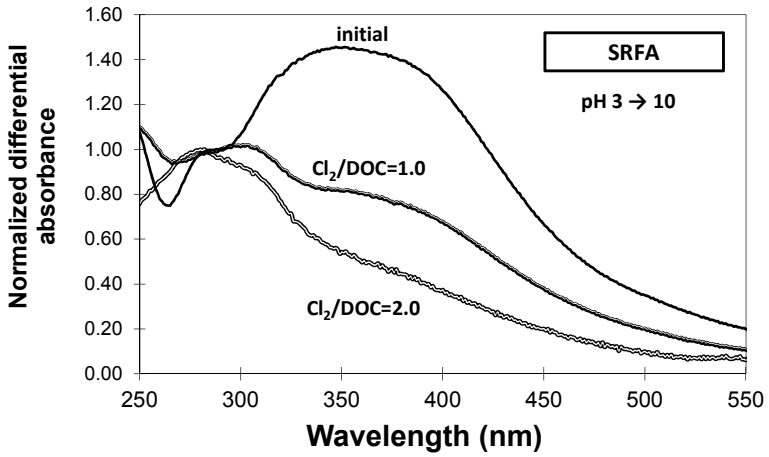

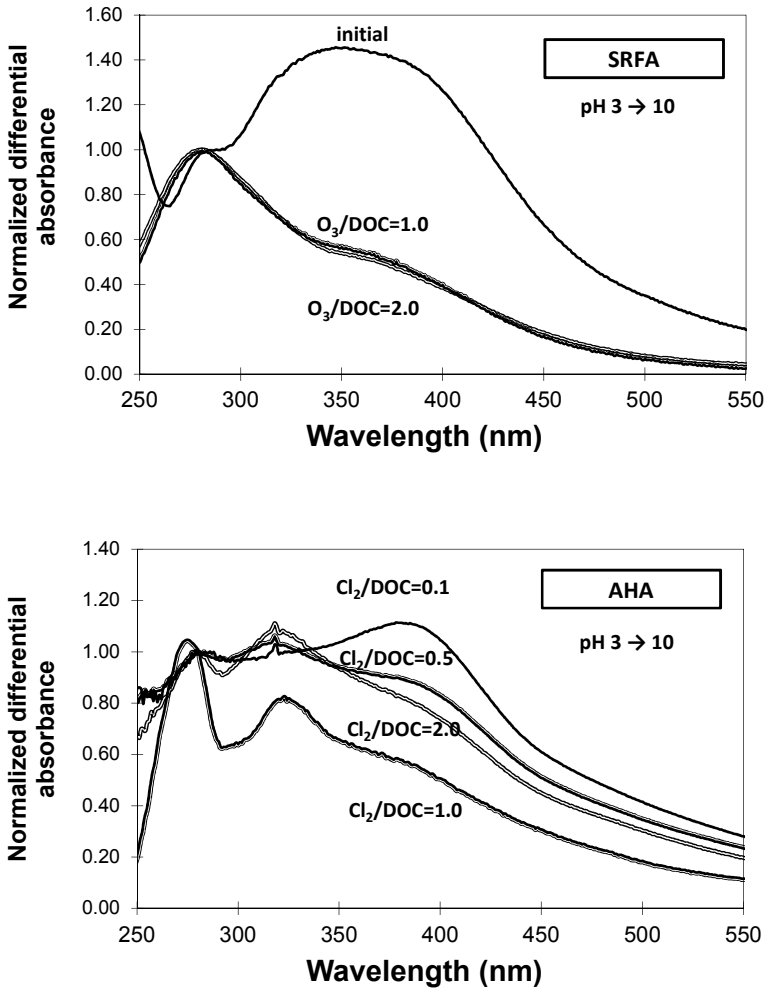

Figure 3.7 Comparison of relative intensities of the major features of pH-differential absorbance spectra of SRFA and AHA altered with chlorine and ozone. Normalization by the intensity of differential absorbance at 280 nm

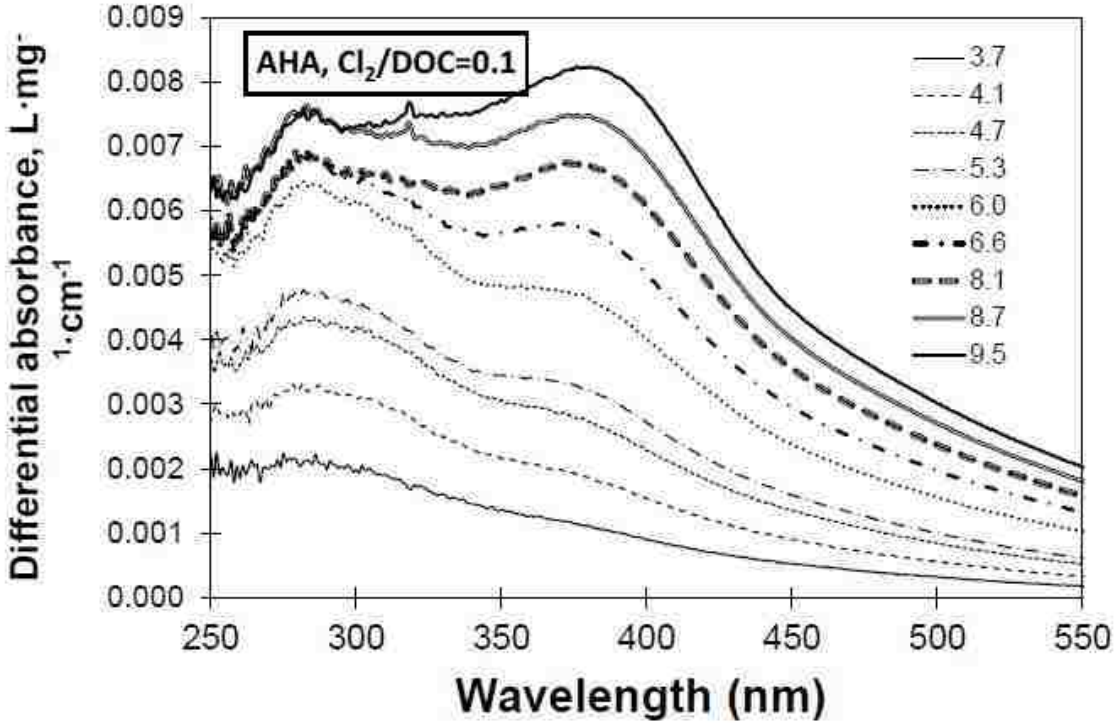
AHA, Cl2/DOC=0.1
3.7
4.1
4.7
5.3
6.0
6.6
8.1
8.7
9.5
Differential absorbance, L·mg-1·cm-1
Wavelength (nm)
0.000
0.001
0.002
0.003
0.004
0.005
0.006
0.007
0.008
0.009
250
300
350
400
450
500
550

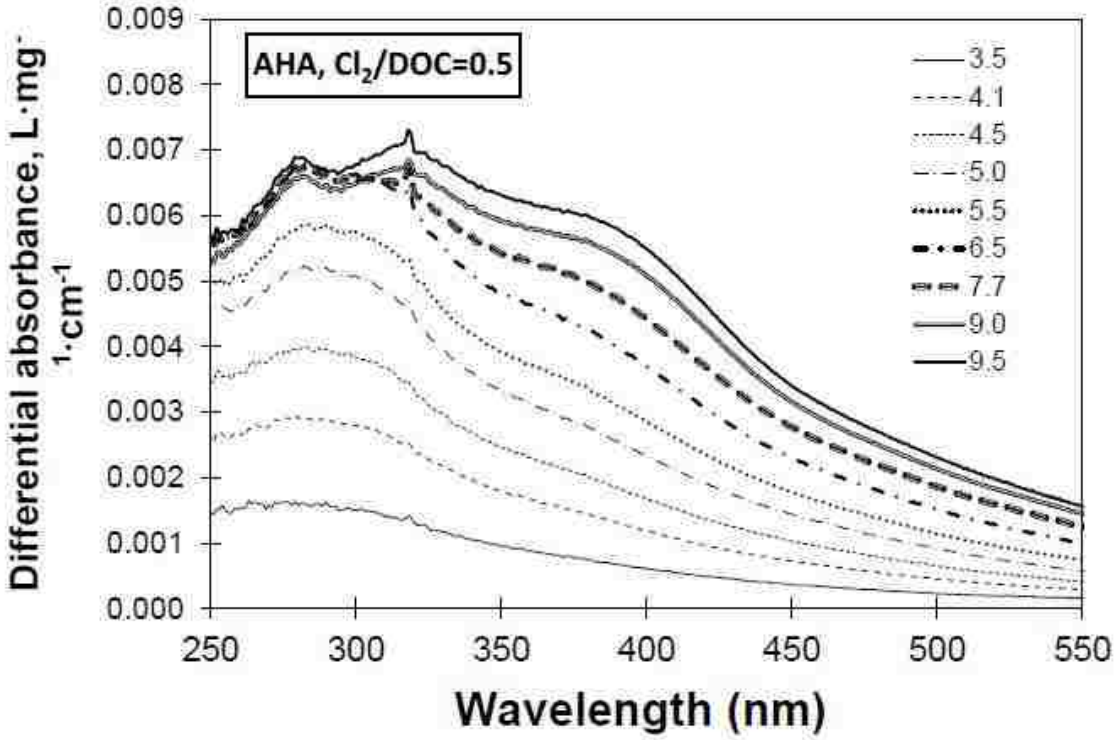
AHA, Cl2/DOC=0.5
3.5
4.1
4.5
5.0
5.5
6.5
7.7
9.0
9.5
Differential absorbance, L·mg-1·cm-1
Wavelength (nm)
0.000
0.001
0.002
0.003
0.004
0.005
0.006
0.007
0.008
0.009
250
300
350
400
450
500
550

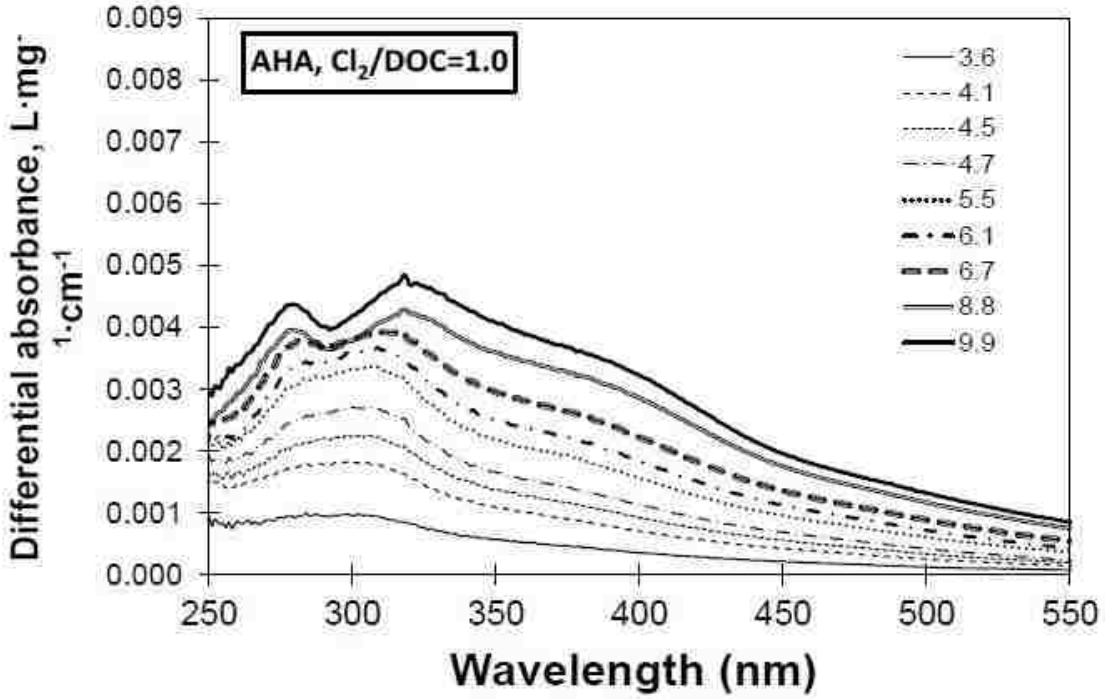
AHA, Cl2/DOC=1.0
3.6
4.1
4.5
4.7
5.5
6.1
6.7
8.8
9.9
Differential absorbance, L·mg-1·cm-1
0.009
0.008
0.007
0.006
0.005
0.004
0.003
0.002
0.001
0.000
250
300
350
400
450
500
550
Wavelength (nm)

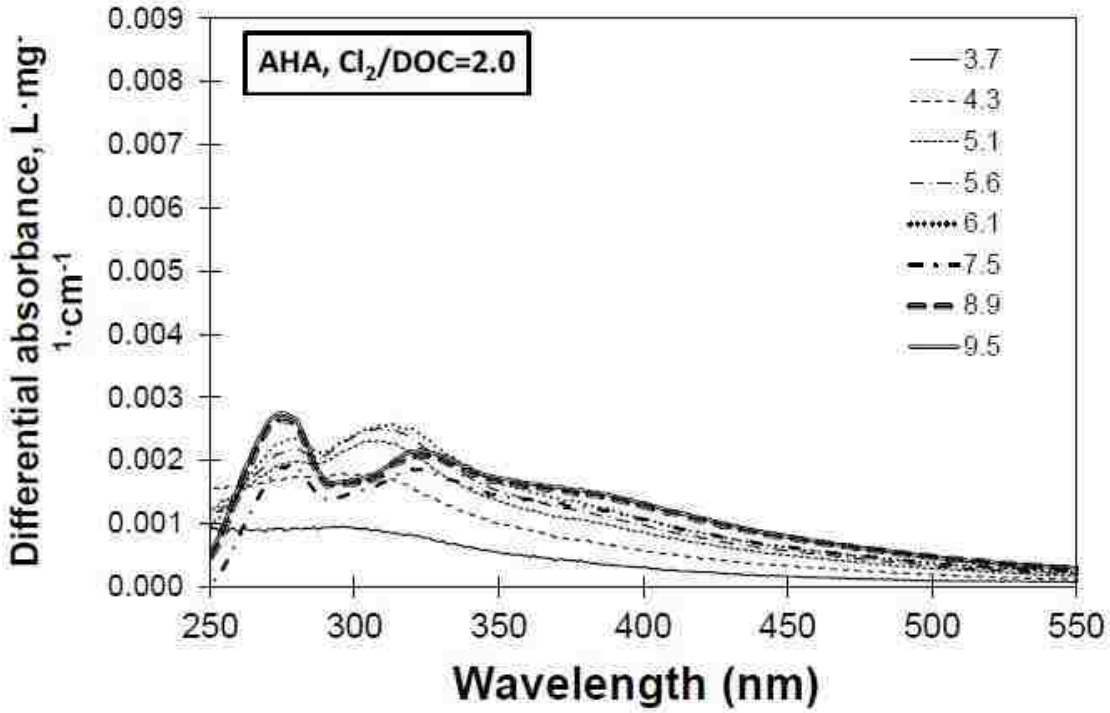
AHA, Cl2/DOC=2.0
3.7
4.3
5.1
5.6
6.1
7.5
8.9
9.5
Differential absorbance, L·mg-1·cm-1
0.009
0.008
0.007
0.006
0.005
0.004
0.003
0.002
0.001
0.000
250
300
350
400
450
500
550
Wavelength (nm)

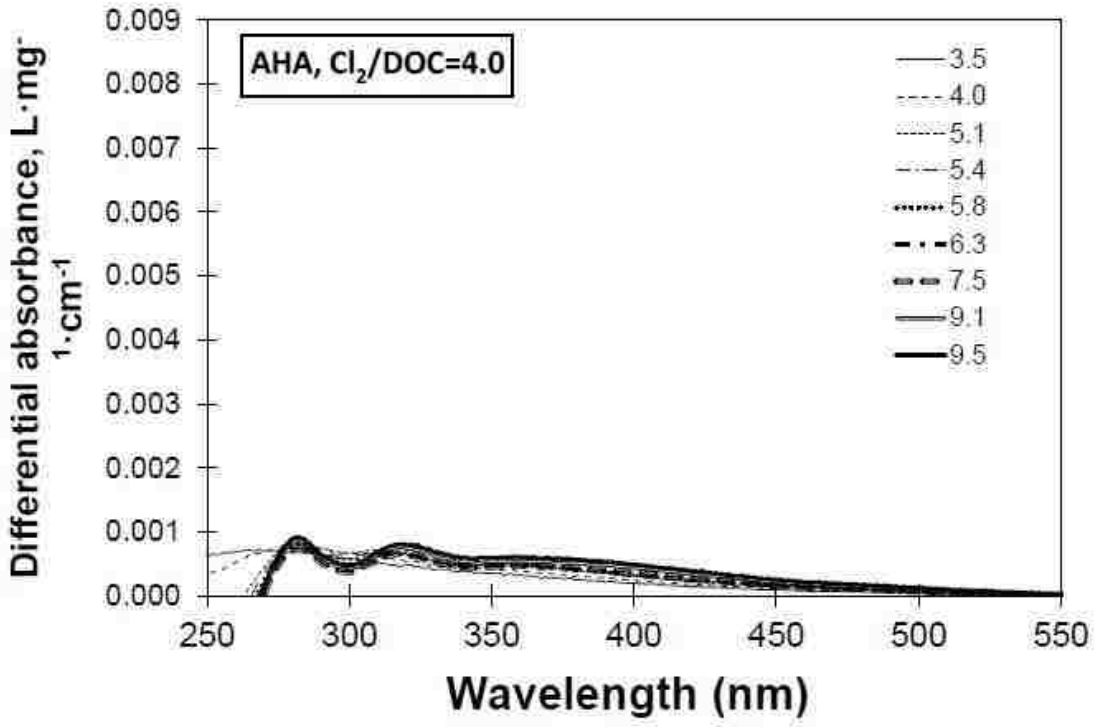

Figure 3.8 DOC-normalized pH-differential spectra for Aldrich humic acid altered by chlorination at varying Cl_2/DOC ratios. The reference spectrum was recorded at pH 3.3.

Determinations of $SUVA_{254}$ values for the examined DOM samples (Table 3-1) show that in parallel with changes of the DAS spectra indicating the degradation of the phenolic chromophores by chlorine and ozone, $SUVA_{254}$ values of AHA decreased from 7.83 to 0.60 $L \cdot mg^{-1} \cdot m^{-1}$ for Cl_2/DOC ratios of 0 and 4 respectively; while for SRFA $SUVA_{254}$ values decreased from 4.36 for unaltered SRFA to 2.57 for a 2.0 Cl_2/DOC ratio and 1.07 for a 2.0 O_3/DOC ratio.

Table 3-1 Apparent molecular weights and $SUVA_{254}$ values for AHA and SRFA altered by chlorine and ozone.

AHA	Cl_2/DOC = 0	Cl_2/DOC = 0.1	Cl_2/DOC = 0.5	Cl_2/DOC = 1	Cl_2/DOC = 2	Cl_2/DOC = 4
Weight averaged molecular weight (Da)	N/A	2120	1965	1932	1880	1517
$SUVA_{254}$ (L mg^{-1} m^{-1})	7.83	4.17	3.37	2.26	0.88	0.60
SRFA	Cl_2/DOC = 0	Cl_2/DOC = 1	Cl_2/DOC = 2	O_3/DOC = 1	O_3/DOC = 2	
Weight averaged molecular weight (Da)	1466	1315	1201	1125	1053	
$SUVA_{254}$ (L mg^{-1} m^{-1})	4.36	3.27	2.57	1.45	1.07	

HPSEC results also show the existence of pronounced changes of SRFA and AHA properties after its alteration. Chlorination caused a strong decrease of the intensities of HPSEC profiles acquired using a 254 nm observation wavelength. The position of the maxima in these profiles shifted to higher elution times indicting a decrease of the apparent weight-average molecular weight (AMW) as the chlorine or ozone dose increased (data not shown). This result agrees with the data of prior research showing that chlorine and ozone tend to preferentially react with higher AMW fractions of DOM and also created breakdown products with smaller AMW values [116]. Table 3-1 shows estimated weight averaged AMW values for AHA that decreased from 2121 Da of AHA treated using a 0.1 Cl_2/DOC ratio to 1517 Da for 4.0 Cl_2/DOC ratio. For SRFA the decrease was from 1466 Da for the initial sample to 1201 Da and 1053 Da for 2.0 Cl_2/DOC and O_3/DOC ratios, respectively.

To explore in more detail the significance of DOM properties determined based on its spectroscopic characteristics, the slopes of natural logarithms of absorbance in the range of 250 nm to 300 nm were calculated and compared with the corresponding values of apparent molecular weights determined using HPSEC [97,117]. Figure 3.9 shows that for all types of chlorinated AHA, the absolute values of the spectral slope decreased (more negative) with an increase of chlorine dose, and increased as pH increased from 3 to 10.

The pH effects may be a result of the changes of DOM molecular conformations (e.g., uncoiling at higher pH values) [20,118] that are not detected by the HPSEC measurements. To correlate the AMW data and the slope, the values of the latter parameters were averaged in the range of pHs 5 to 9. As expected, the values of the spectral slopes determined for chlorinated AHA and chlorinated and ozonated SRFA were strongly correlated with their respective AMW values, as demonstrated in Figure 3.10.

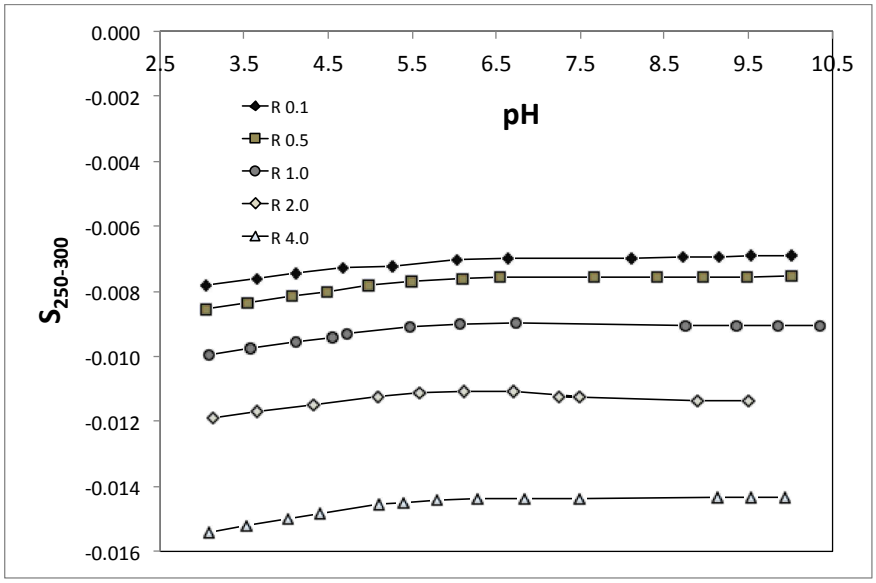

Figure 3.9 Slopes of natural logarithms of DOM absorbance in the range 250 to 300 nm versus pH. Data for chlorinated AHA (R stands for the ratio of chlorine to DOC of AHA by mass).

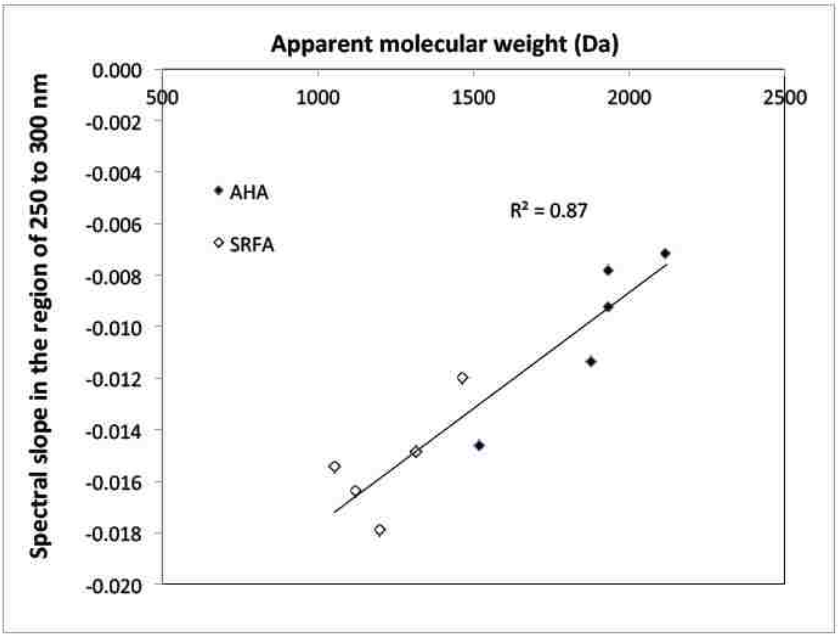

Figure 3.10 Correlation between spectral slopes of the DOM absorbance and the corresponding apparent molecular weight (AMW).

3.3 Mechanisms of DOM effects on copper release

Prior studies suggest the importance of colloidal interactions between the representative metal solid phases (such as Pb and Sn) and DOM [21]. The data in our study (Figure 3.2, 3.5 and Table 3-1) indicate that DOM fractions with high AMW values and aromaticities play the most important role in the copper release. However, the oxidation of DOM by chlorine or ozone accompanied by the decrease of its AMW and aromaticity can weaken the DOM-associated promotion of copper release.

To ascertain the occurrence of preferential sorption of high-AMW fractions of DOM on the copper solids, we examined changes of DOC concentrations and HPSEC profiles of

AHA remaining in solution in contact with malachite and CuO. The results of the experiments compiled in Table 3-2 show that the amount of AHA adsorbed on malachite increased as malachite dose increased. The percent of DOC removed from the solution via adsorption increased from 8% in the presence 100 mg/L malachite to 48% for a 1000 mg/L malachite dose. Relatively little AHA was adsorbed on CuO, and < 5% of DOC was removed for a 1000 mg/L CuO dose. Given a much smaller surface area of CuO (2.02 vs. 44.42 m^2/g for malachite), this was not surprising. However, the trends seen in the removal of DOC by sorption on CuO were similar to those for malachite.

Table 3-2 DOC and $SUVA_{254}$ values for AHA remaining in solution after adsorption on malachite and CuO.

Solid dose (mg/L)	100	200	500	1000	100	200	500	1000
DOC adsorbed (%)	8.1	18.7	33.2	47.9	2.1	3.7	4.8	4.7
$SUVA_{254}$, $L \cdot mg^{-1} \cdot m^{-1}$	7.14	7.03	7.06	4.79	7.76	7.85	7.47	7.33

Changes of HPSEC chromatograms of AHA and SFRA remaining in solution in the presence of varying amounts of malachite were in agreement with the changes of DOC concentrations (Figure 3.12 and Figure 3.12). As the dose of malachite increased, a decrease of peak intensity and a pronounced shift of the maxima position took place. That shift was clearly indicative of the preferential removal of high AMW fractions of DOM adsorbed by the model phase. This is consistent with the $SUVA_{254}$ values of AHA remaining in solution after contacting with suspended malachite, which decreased from

7.14 to 4.19 as malachite dose increased from 100 to 1000 mg/L. These results and the HPSEC data suggest that DOM molecules with relatively higher AMW and aromaticity were preferentially adsorbed on malachite. Similar but less pronounced effects were observed for CuO.

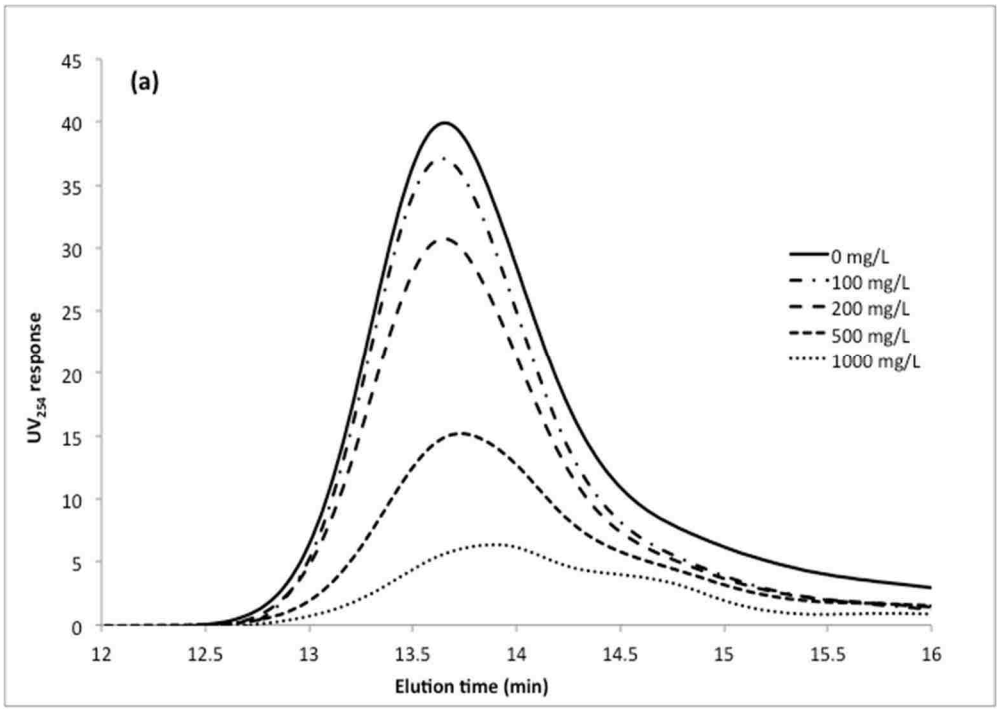

Figure 3.11 HPSEC chromatograms of SRFA remaining in solution after adsorption on malachite at its varying concentrations.

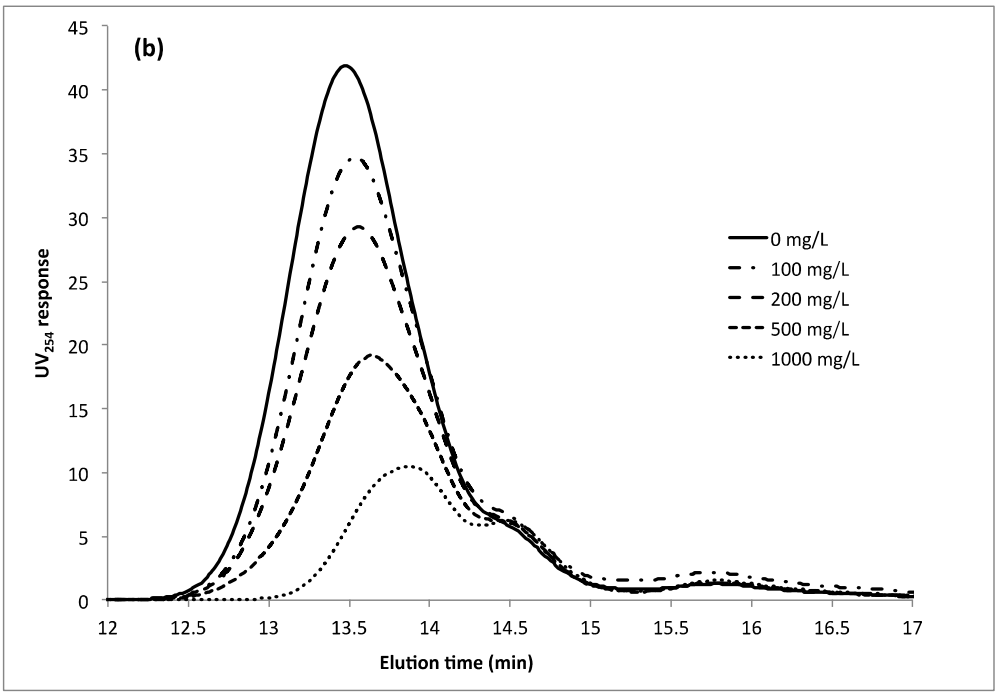

Figure 3.12 HPSEC chromatograms of AHA remaining in solution after adsorption on malachite at its varying concentrations.

The preferential removal of DOM fractions with higher AMW as a result of DOM interactions with malachite or CuO is in agreement with the data from previous studies that examined DOM adsorption on metal oxides such as goethite and kaolinite [41]. This trend agrees with the behavior of ζ-potentials on the model phases in the presence of DOM. For instance, measurements of ζ-potentials on malachite in the presence of varying concentrations of AHA chlorinated using 0.1 Cl_2/DOC ratio shows the accumulation of negative charge on the surface, with ζ-potential decreasing from -10 to -40.5 mV when DOC concentration increased from 0 to 10 mg/L (Figure 3.13). For AHA altered using higher doses of chlorine, the surface charge on malachite decreased to only -16 mV even the DOC concentration increased to 10 mg/L (for AHA Cl_2/DOC ratio=4). Similar effects were observed for CuO in which case the ζ-potential in the absence of DOM was ca. -5

mV and decreased to -44 mV in the presence of slightly chlorinated AHA at its concentration larger than 5 mg/L (the unchlorinated AHA was from another batch as mentioned in the methodology part and therefore was not compared here).

However, chlorination of AHA caused this effect to subside and largely disappear similarly to what was observed for malachite. Therefore, although the ozonation by-products might be more likely to form complexation with copper solids and thus led to more copper release, such an effect on promoting copper release could be counter-balanced by the changes in other DOM properties (e.g., its aromaticity, AMW, hydrophobicity) by ozonation or chlorination. This effect by ozone would eventually lead to less sorption of DOM onto the solid phases with less attendant colloidal dispersion and metal release. This view is consistent with studies of DOM effects on Pb and Sn solids [21] while an opposite trend was observed for Al and Fe solids [6,119]. We can speculate that the extent and type of effects of ozonation or chlorination of DOM on its influence of metal release can depend on both the nature of the exposed solids and site-specific DOM properties.

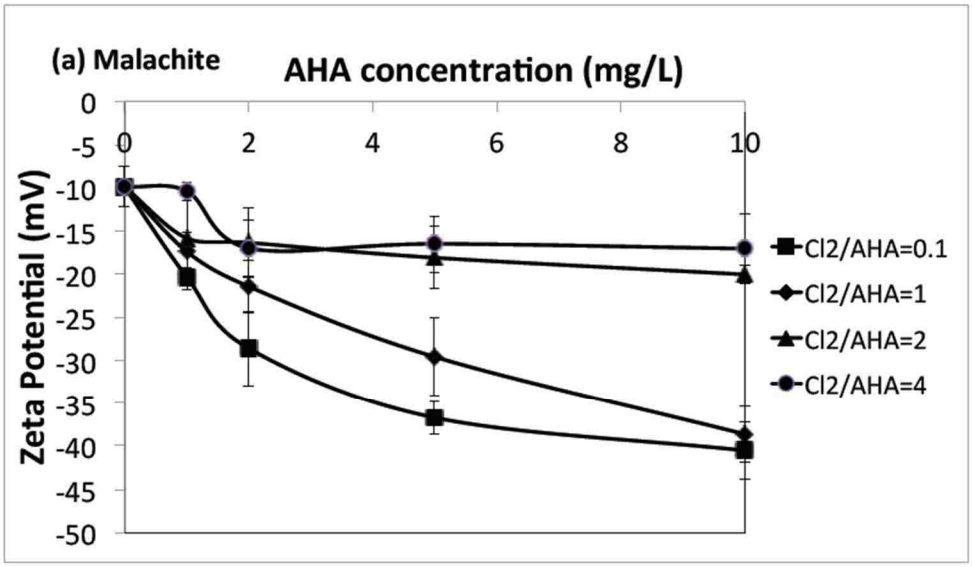
(a) Malachite
AHA concentration (mg/L)
Zeta Potential (mV)
0
-5
-10
-15
-20
-25
-30
-35
-40
-45
-50
0
2
4
6
8
10
Cl2/AHA=0.1
Cl2/AHA=1
Cl2/AHA=2
Cl2/AHA=4

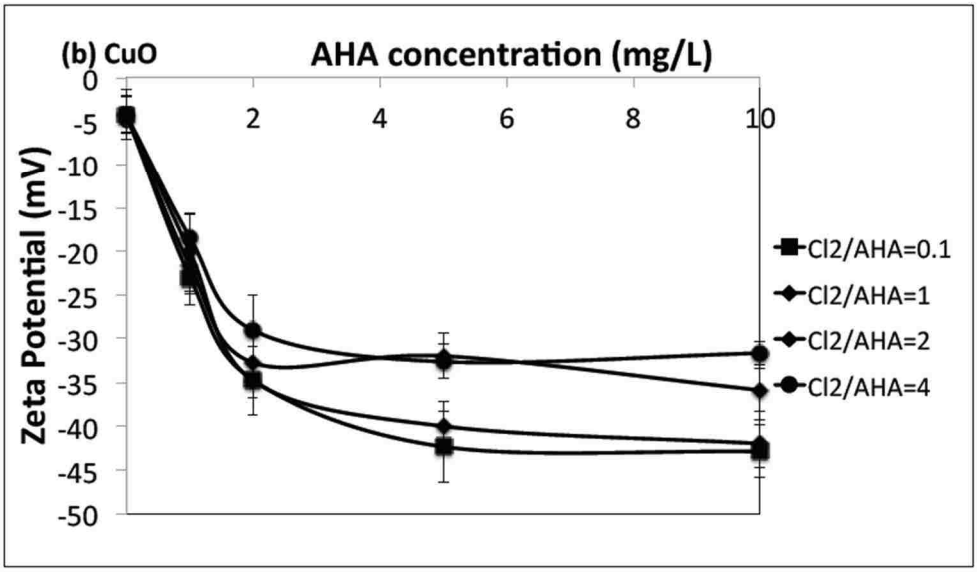
(b) CuO
AHA concentration (mg/L)
Zeta Potential (mV)
0
-5
-10
-15
-20
-25
-30
-35
-40
-45
-50
2
4
6
8
10
Cl2/AHA=0.1
Cl2/AHA=1
Cl2/AHA=2
Cl2/AHA=4

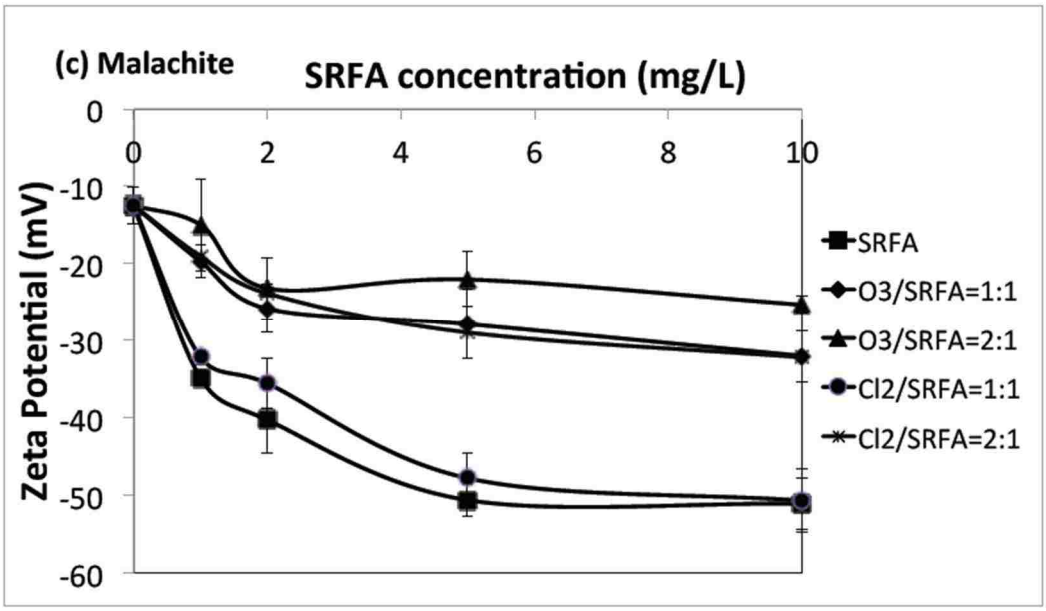

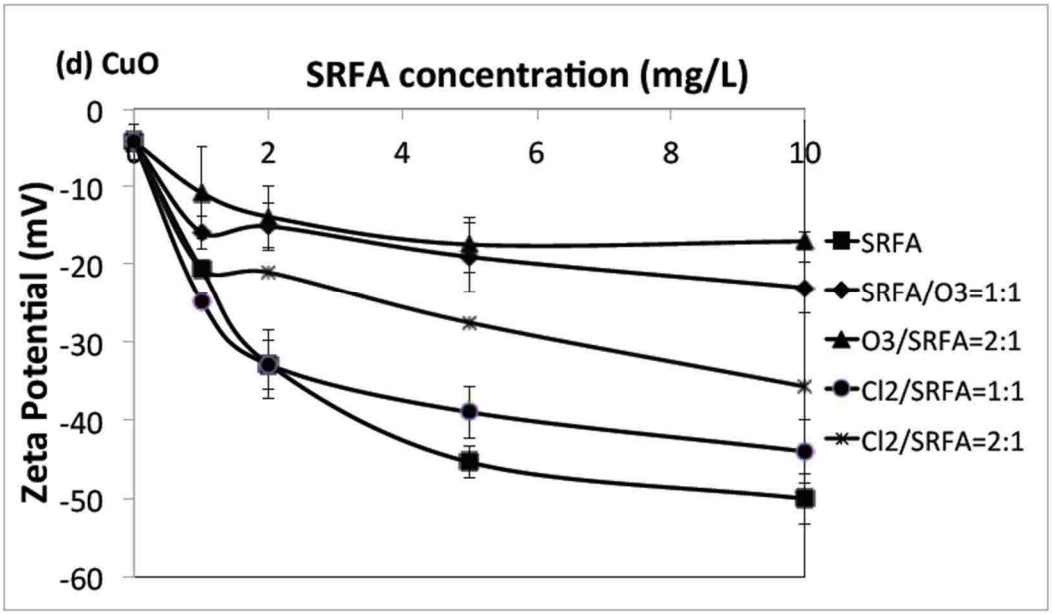

Figure 3.13 Effects of DOM concentration and alteration on ζ-potentials of model phases: (a) Malachite, with AHA; (b) CuO with AHA, (c) Malachite with SRFA and (d) CuO with SRFA.

In accord with the finding that DOM molecules with higher AMW and aromaticities play a key role in copper release from the model phases typical for corroding copper surfaces, we examined correlations between $SUVA_{254}$ and other parameters (spectral slope, specific DAS) characterizing DOM chemistry and copper concentrations released at a given DOM concentration (e.g., DOC=2 ppm). As expected, a strong correlation was observed between $SUVA_{254}$ and metal concentrations for AHA (Figure 3.14) and a similar trend was observed for SRFA (data not shown). However, the data for AHA and SRFA show the presence of distinct groupings, most likely due to the presence of considerable difference between these DOM samples.

These differences show that while the correlations observed in this study are robust, they may be strongly site-specific and more research is needed to explore the effects of DOM site specificity and water treatment processes other than alteration (e.g., coagulation, possibly in combination with chlorination or ozonation) on copper release from corroding surfaces.

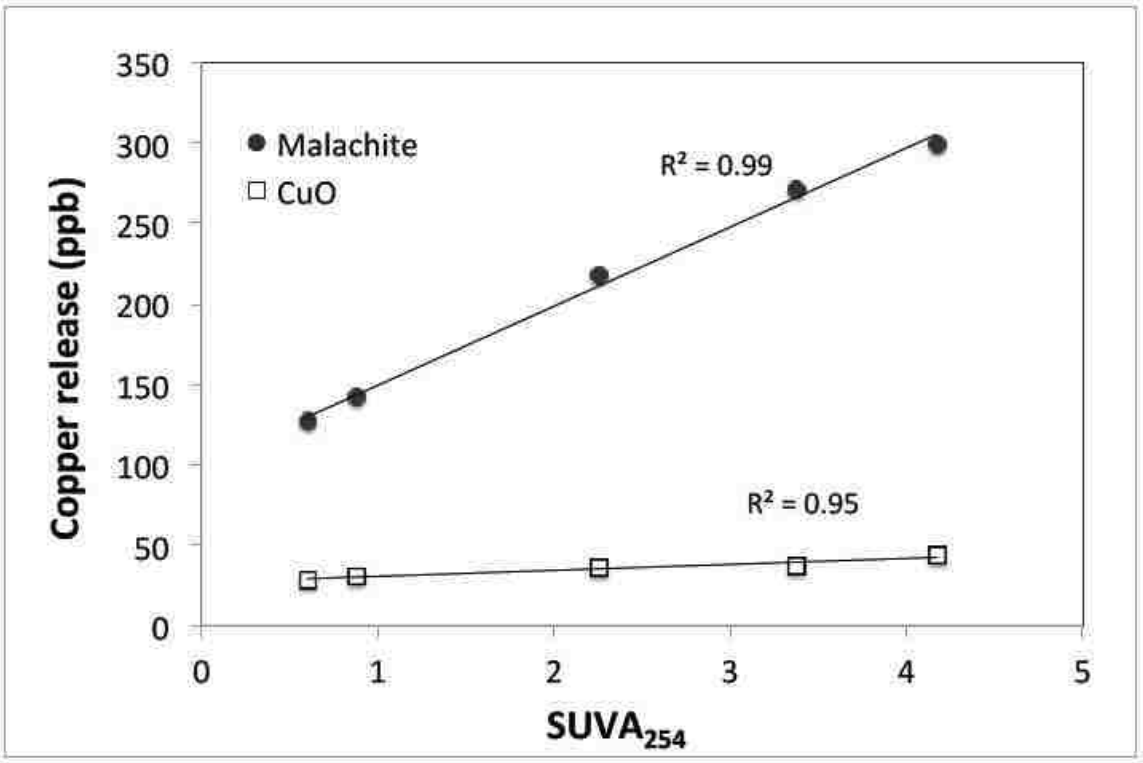

Figure 3.14 Correlation between SUVA254 of chlorinated AHA and copper release from malachite and CuO (DOC=2 mg/L).

Error! Reference source not found., Figure 3.14 and Figure 3.15 show the correlation between the values of the spectral slope, AMW, ζ-potential and, on the other hand, copper release. **Error! Reference source not found.** demonstrates a strong linear dependence between the values of spectral slope and AMW: a less negative spectral slope is related to larger AMW; and this relationship applies to both types of DOM investigated in this study. Furthermore, as shown in Figure 3.16, the spectral slope parameter is also closely related to ζ-potential at varied DOM level, that is, a less negative spectral slope is correlated with greater zeta potential and thus greater surface charge. This is in agreement with our previous discussion that molecules with larger AMW are preferentially adsorbed onto the

model phase surface and thus play a more important role in colloidal mobilization, and consequently result in greater copper release.

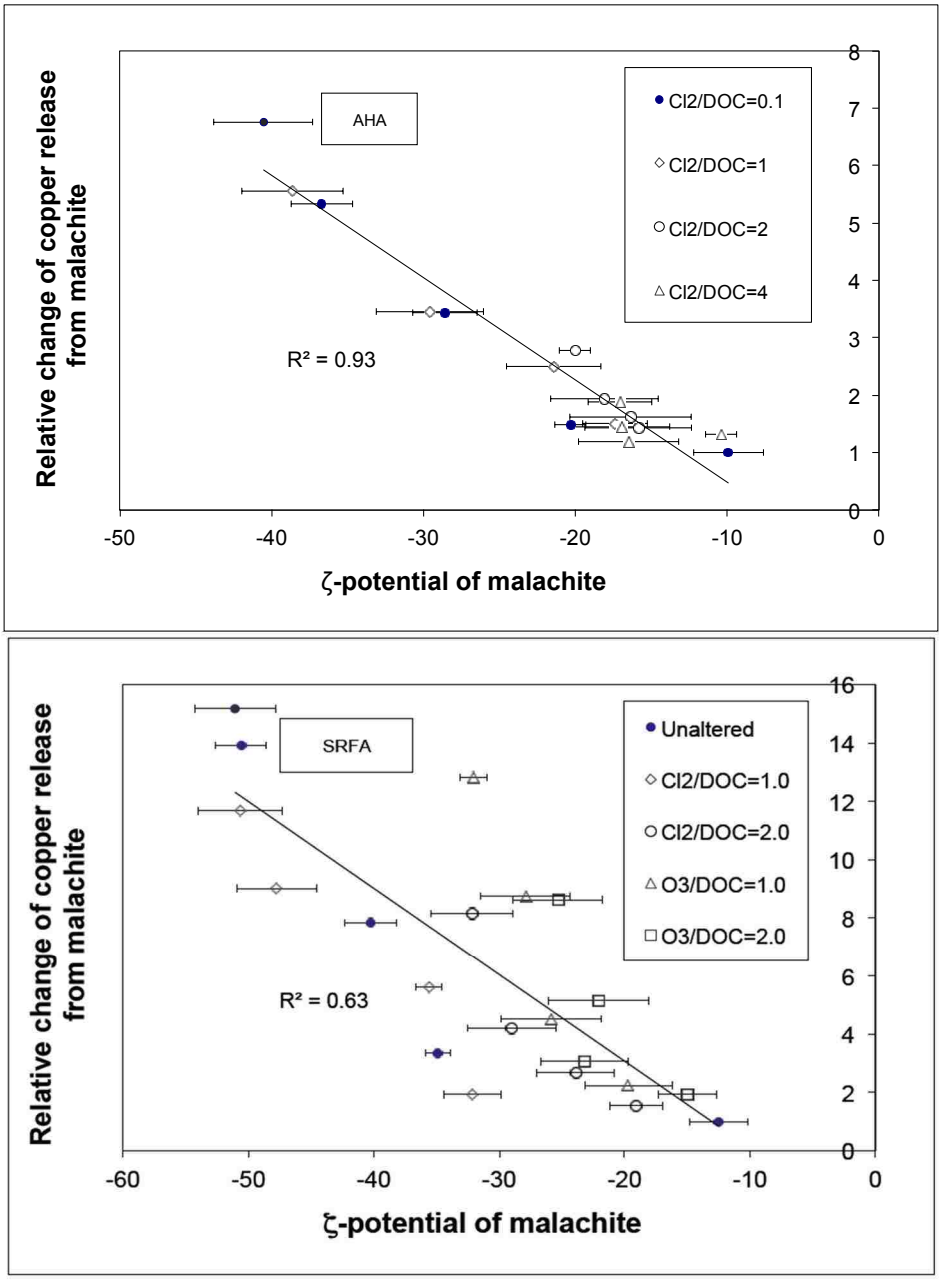

Figure 3.15 Correlation between ζ-potential of malachite and relative change of copper release in the presence of AHA and SRFA.

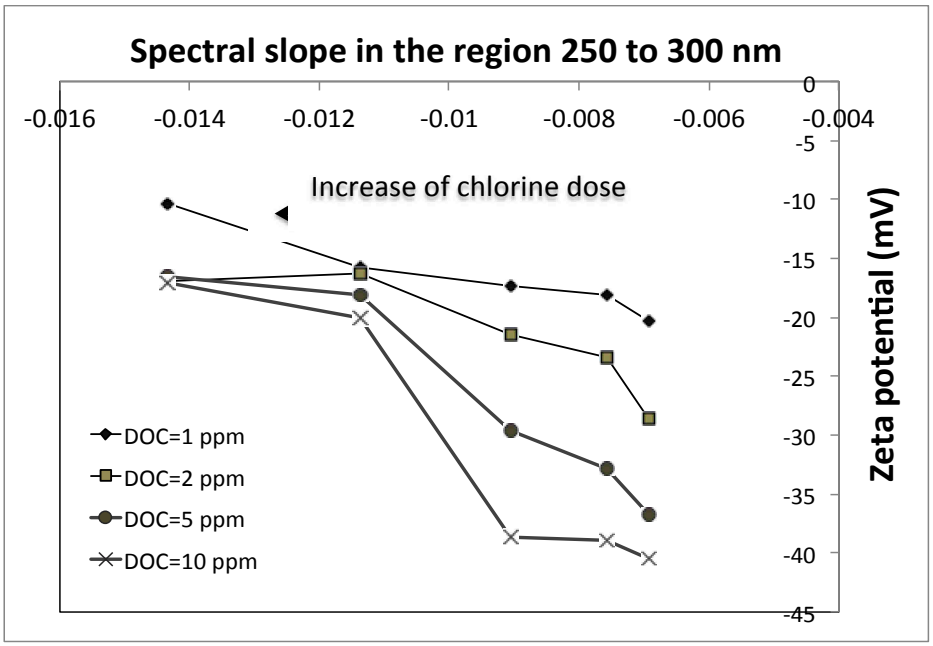

Figure 3.16 Correlation between ζ-potentials and spectral slopes for AHA chlorinated using varying chlorine/DOC ratios.

3.4 Conclusions of DOM properties affecting copper release from model phases

The experiments discussed above show that DOM can strongly promote copper release from the solid phases (malachite and CuO) typical for corroding copper surfaces. Alteration of DOM properties by chlorine and ozone strongly affects DOM properties which play a key role in copper mobilization. Both chlorination and ozonation decrease the aromaticity of DOM and also the abundance of carboxylic and phenolic groups in its molecules. These processes also decrease AMW values of DOM. The data of this study show that DOM molecules with higher AMW and aromaticities sorb preferentially on the surface of malachite and CuO and are critically important for metal release associated with colloidal dispersion. These observations were supported by strong linear correlations between

$SUVA_{254}$ values and metal release. The data indicate the presence of strong correlations between ζ-potentials of the suspended particles and the extent of metal mobilization from these model phases.

The results also demonstrate that DOM alteration by chlorine, ozone and other relevant water treatment operation is likely to suppress copper release, especially when SUVA values or alternative DOM characterization parameters such as the spectral slopes, intensity of differential absorbance or shifts of the ζ-potentials of the representative solid phases are below certain threshold levels. In terms of practical implications, the data for DOM examined in our study (SRFA and AHA) indicate that *per se*, DOM with $SUVA_{254}$ values < ca. 2 $L \cdot mg^{-1} \cdot m^{-1}$ are not likely to cause pronounced changes of copper release, especially for systems controlled by CuO rather than by a more commonly occurring malachite. Alternatively, negative shifts of the ζ-potential of CuO and/or malachite less than ca. 5 mV compared with the ζ-potentials of these phases in organic-free water at the same pH and alkalinity can also be indicative of a low likelihood of increases of copper release attributable to DOM in drinking water. These estimates can provide additional guidance for surface water treatment in situations when copper release needs to be controlled.

4 Effects of ionic strength on the chromophores of autochthonous and allochthonous DOM

Ionic strength (IS) is highly important for understanding of the behavior of DOM because IS affects practically all aspects of DOM interactions with heavy metals and organic compounds, as well as DOM properties themselves, for instance its protonation and conformation. In this chapter, we employed the *in situ* method of differential absorbance spectroscopy that allows using environmentally relevant DOM concentrations and yields feature-rich spectra that, as we show, can be interpreted based on a well-established approach (e.g., NICA-Donnan model). Once the changes of DOM functionalities induced by IS variations can be characterized or quantified, this approach can further help to understand interactions between DOM and many other metal ions.

4.1 Ionic strength (IS) effects on differential spectra of DOM

Examination of effects of varying IS values on the absorbance of SRFA, SRHA and PLFA showed that the increases of IS at a constant pH caused the intensity of DOM absorbance to increase monotonically at practically all wavelengths but the extent of this effect depends on the observation wavelength, type of DOM and pH.

Important aspects of this trend can be discerned via the comparison of differential absorbance spectra (DAS) obtained for SRFA, SRHA and PLFA at incrementally changing IS (Figure 4.1-3). Figure 4.1 demonstrates that in the case of SRFA, IS-differential spectra (calculated vs. a 0.001 mol/L sodium perchlorate concentration as reference) have bands with maxima at ca. 230 nm, 330 nm and > 370 nm. The first of these bands has a negative

sign at pH 5 but at higher pH its sign become positive. The structures in the range of wavelengths > 370 nm become increasingly prominent as the pH and ionic strength increases.

The intensity of the differential spectra of SRFA calculated for IS changes increased markedly with the pH. For example, at pH=5 and IS change from 0.001 mol/L to 0.2 mol/L, the intensity of the peak at wavelength 330 nm in the spectra is 0.00024 (L •mg^{-1} •cm^{-1}) while at pH=9, the intensity of this peak is almost an order of magnitude higher (0.0017 L •mg^{-1} •cm^{-1}).

Results for SRHA (Figure 4.2) demonstrate the presence of both strong similarities and differences compared with the data for SRFA. As was the case with SRFA, the intensity of the differential spectra of SRHA increased with the pH. For instance, at pH 5, there are no prominent peaks and the intensity at all wavelength are below 0.0006 (L •mg^{-1} •cm^{-1}) for all ionic strength levels. At higher pHs, for instance at pH 9, peaks located at ~245 nm and a band with maximum centered around 390 nm are prominent, and the band (~390 nm) reaches around 0.0025 (L •mg^{-1} •cm^{-1}) at the highest ionic strength level, which is about 4.5 times of the intensity when pH 5.

Figure 4.3 shows the DAS data for PLFA. In contrast with allochthonously generated SRFA and SRHA, PLFA generated autochthonously via the degradation of microbial biomass, is reportedly rich in nitrogen and has a relatively low hydrophobicity and aromaticity [120–123]. The $SUVA_{254}$ value of PLFA is approximately 1.9 L/m-mg C compared to SRFA and SRHA measured in our experiments and reported from prior studies as 5.8 and 7.2 L/m-mg C, respectively [124–126].

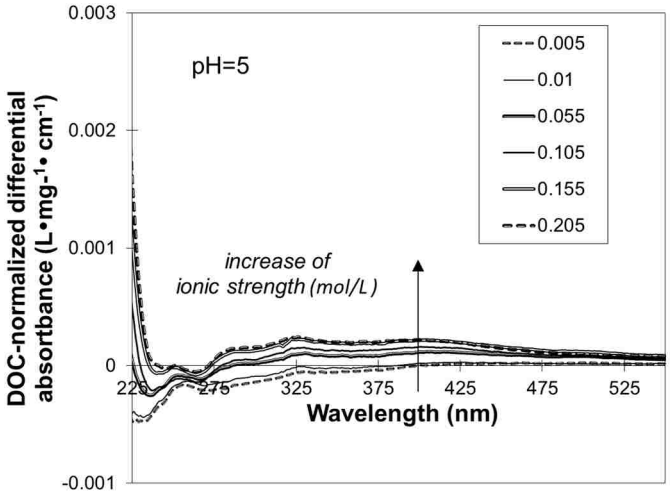
pH=5
0.005
0.01
0.055
0.105
0.155
0.205
increase of
ionic strength (mol/L)
DOC-normalized differential
absorbance (L•mg-1• cm-1)
0.003
0.002
0.001
0
-0.001
225
275
325
375
425
475
525
Wavelength (nm)

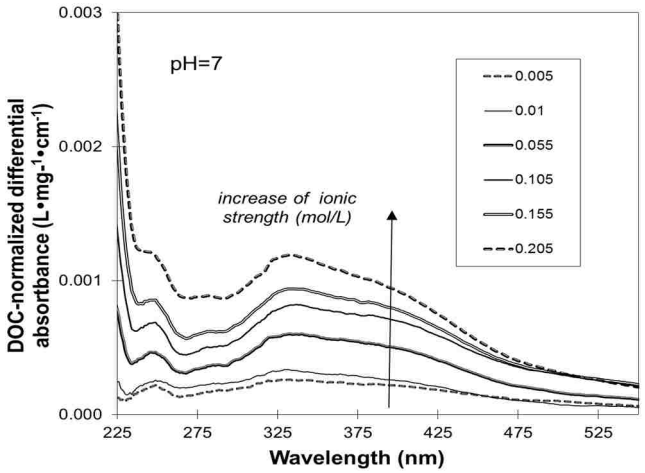
pH=7
0.005
0.01
0.055
0.105
0.155
0.205
increase of ionic
strength (mol/L)
DOC-normalized differential
absorbance (L•mg-1•cm-1)
0.003
0.002
0.001
0.000
225
275
325
375
425
475
525
Wavelength (nm)

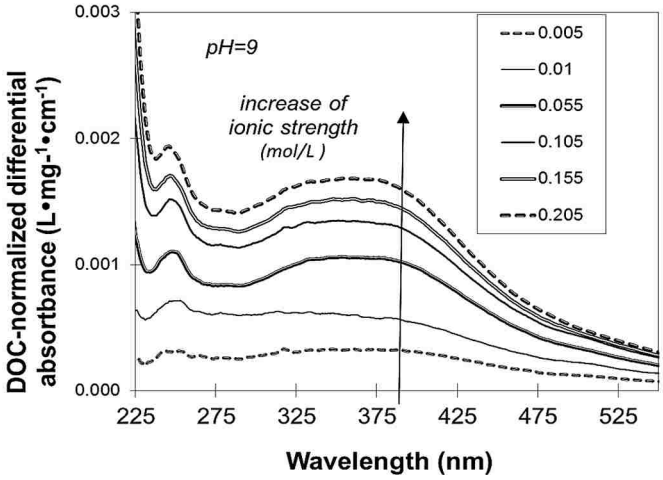
pH=9
0.005
0.01
0.055
0.105
0.155
0.205
increase of
ionic strength
(mol/L)
DOC-normalized differential
absorbance (L•mg-1•cm-1)
0.003
0.002
0.001
0.000
225
275
325
375
425
475
525
Wavelength (nm)

Figure 4.1 Differential absorbance spectra of SRFA at varying $NaClO_4$ concentrations (in mol/L) at pH=5, pH=7, and pH=9.

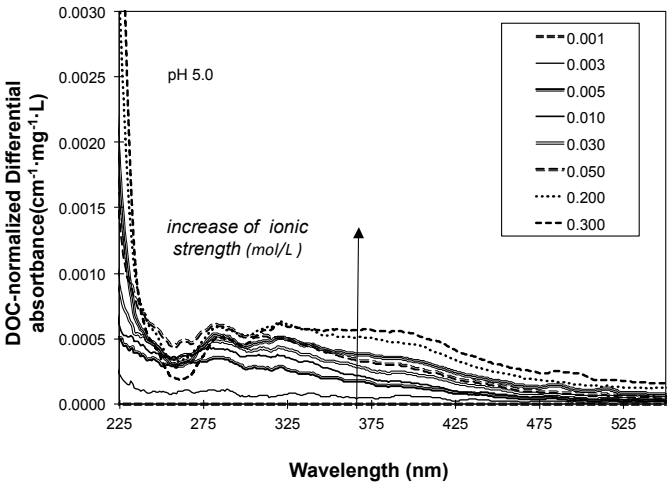

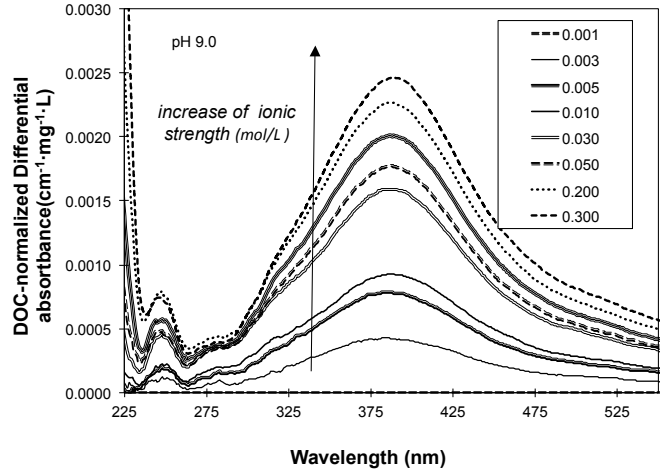

Figure 4.2 Differential absorbance spectra (DAS) of SRHA for varying ionic strength (in mol/L) at pH=5.0 and 9.0.

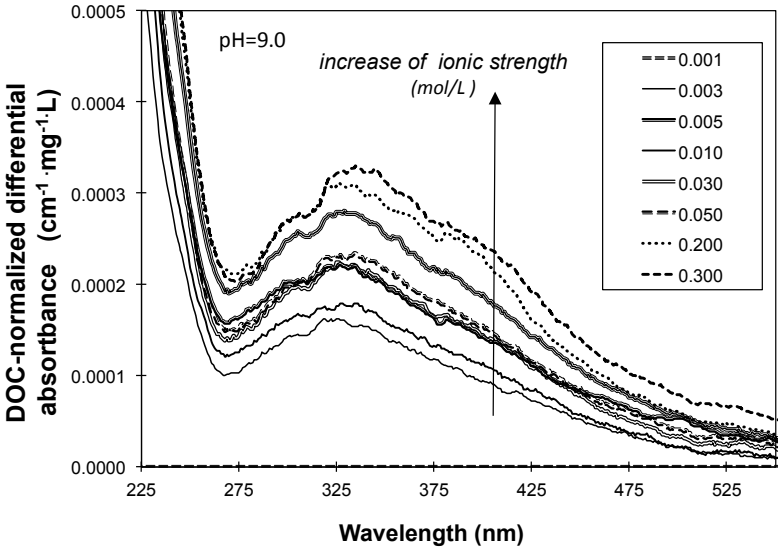

Figure 4.3 Differential absorbance spectra (DAS) of PLFA for varying NaClO4 concentrations (in mol/L) at pH=9.

As expected based on the lower aromaticity of PLFA, the magnitude of the response of the absorbance of this DOM to changes of the ionic strength was several times lower than that observed for SRFA and SRHA. Contributions of specific features in the differential absorbance of PLFA were also different from those of SRFA and SRHA. For instance, while the band or a shoulder with a maximum at 330 nm was observed for PLFA as well as for SRFA and SRHA, the band at wavelengths > 370 nm that was highly prominent for SRFA and especially SRHA had a low intensity or nearly absent in the case of PLFA. The low intensity of this characteristic band (> 370 nm) in the case of PLFA is likely to be a manifestation of the lower aromaticity of this DOM and hence lower susceptibility of its aromatic chromophores to changes induced by IS variations. This effect can also be associated with the lower molecular weight of PLFA (number-averaged molecular weight <1000 Dalton,[127]) compared with that of SRFA or SRHA (1390 and 1810 Dalton, respectively [128]).

To summarize these observations, the magnitude of changes induced by variations of IS was observed to increase in the order PLFA < SRFA < SRHA, that is, in the order of the increase of the aromaticity or molecular weight of DOM. For all examined DOM, differential spectra calculated vs. an *a priori* selected reference condition (a 0.001 mol/L ionic strength) show the presence of two major bands with maxima at ca. 330 nm and > 370 nm albeit the latter band is very weak in the case of PLFA. These bands are similar to those observed when the solutions pH was varied at a constant ionic strength and they are likely to reflect the occurrence of the deprotonation of operationally defined DOM carboxylic and phenolic groups at increasing IS values, as discussed in the sections that follow.

4.2 Effects of ionic strength of the spectral slopes of DOM

Prior research indicates that the absorbance of DOM at wavelengths exceeding ca. 300 nm is strongly affected by inter-chromophore interactions that depend the conformations of DOM molecules and are increasingly prominent for DOM with higher aromaticity and molecular weights [129–132]. Because IS variations can affect the Donnan volume as well as the protonation of DOM molecules, this may lead to changes of conformations of DOM molecules and concurrent changes of inter-chromophore interactions in them.

To quantify such changes, calculations of log-processed absorbance spectra of DOM were carried out. They showed that the logarithms of absorbance of all examined DOM samples underwent an increase with IS for practically all wavelengths but these increases were especially prominently for wavelengths > 300 nm, as shown for SRFA exposed to

varying ionic strengths at pH values 5, 7 and 9 in (Figure 4.4). Similar data for SRHA and PLFA exposed to IS variations at pH 9 are shown in Figure 4.5.

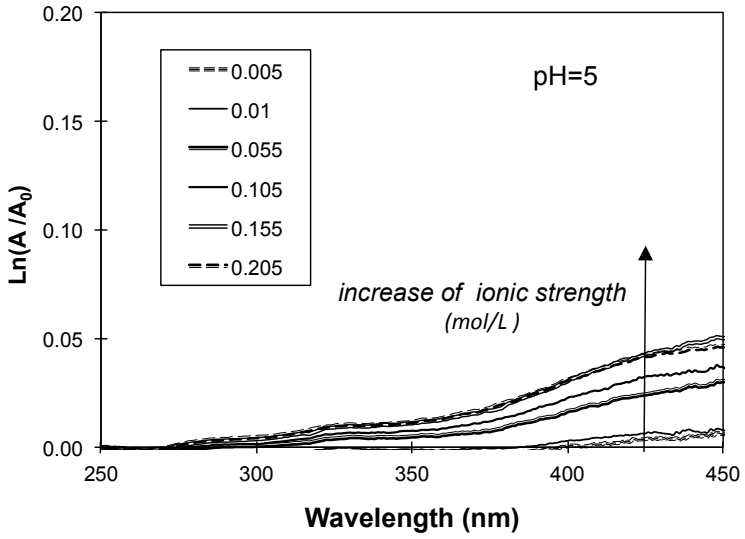

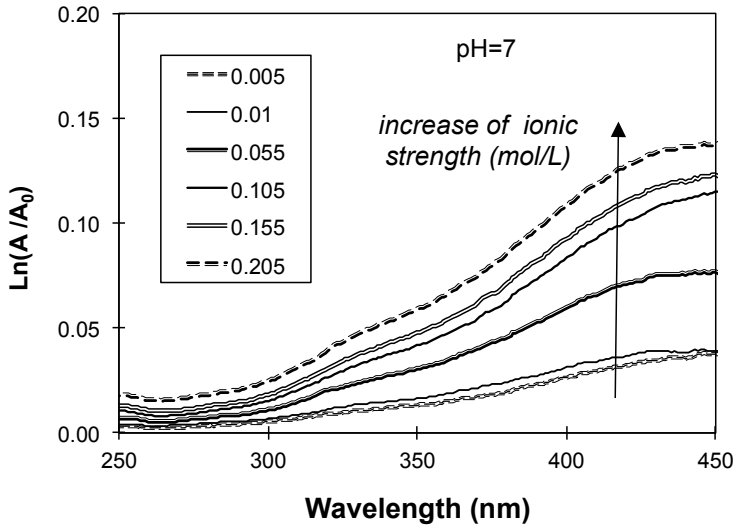

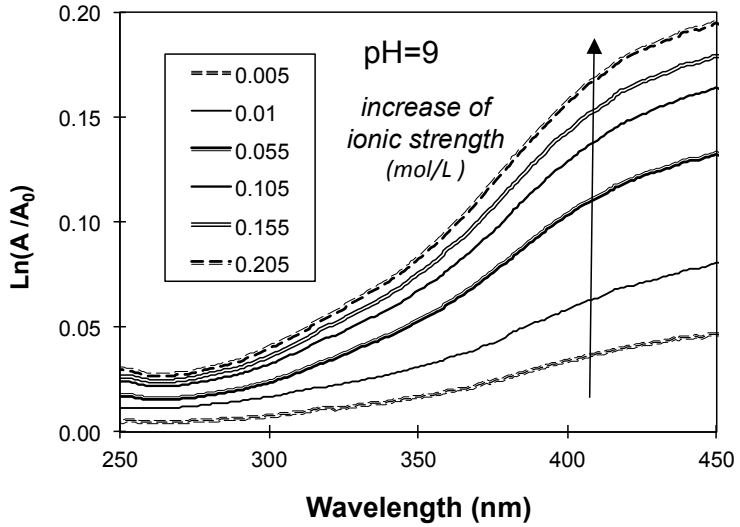

Figure 4.4 Log-transformed absorbance of SRFA at increasing ionic strength at pH 5, 7, and 9.

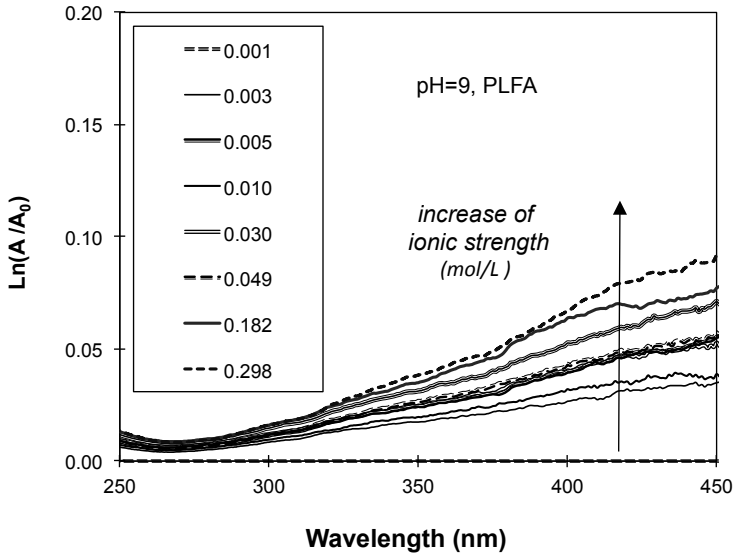

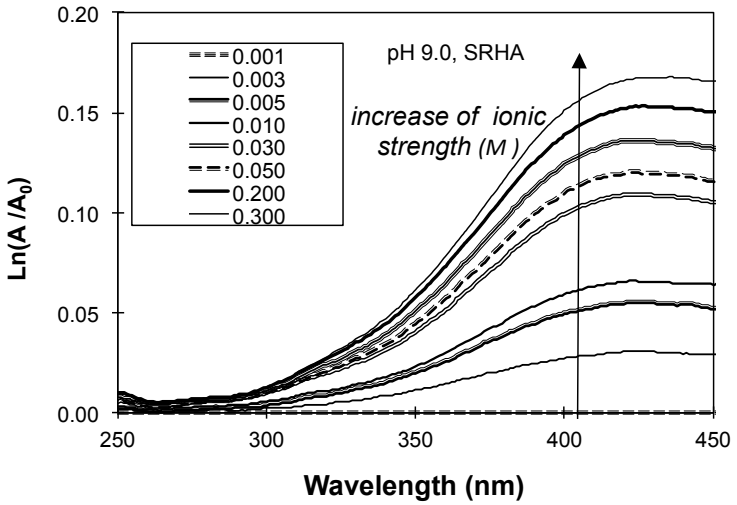

Figure 4.5 Log-transformed differential absorbance spectra of PLFA and SRHA calculated for increasing ionic strength.

To quantify effects of IS variations using a single index, slopes of the log-processed DOM absorbance spectra in the range of wavelengths 350-400 nm (denoted as $S_{350\text{-}400}$) were determined as well. The $S_{350\text{-}400}$ parameter was introduced based on the results of prior studies that have shown that for humic substances, spectral slope values tend to be correlated with apparent molecular weights of DOM found in a broad range of natural waters [97,133,134]. The degradation of DOM by photolysis or chlorination causes the absolute values of the spectral slope to increase [135,136]. In contrast, DOM deprotonation or DOM-metal complexation cause the absolute values of the spectral slopes to decrease [101]. The dependence of $S_{350\text{-}400}$ values vs. IS logarithms is shown in Figure 4.6. This figure demonstrates that the absolute values of the slopes of the log-processed absorbance spectra underwent a consistent decrease at higher IS values.

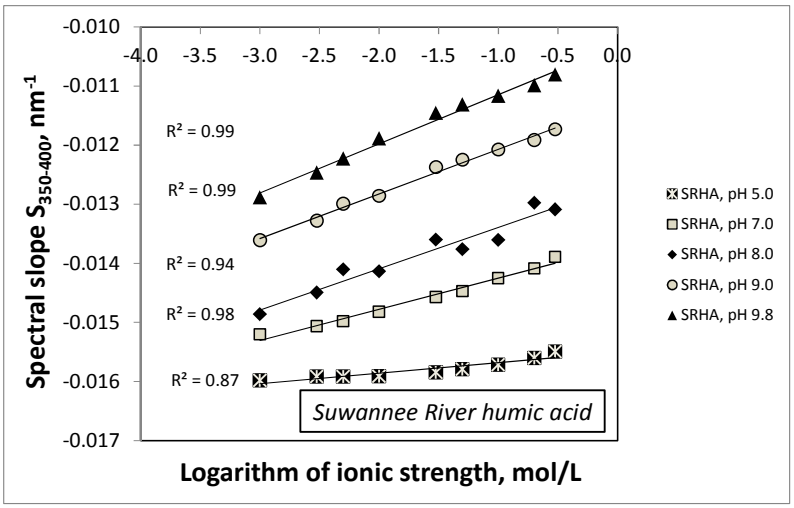

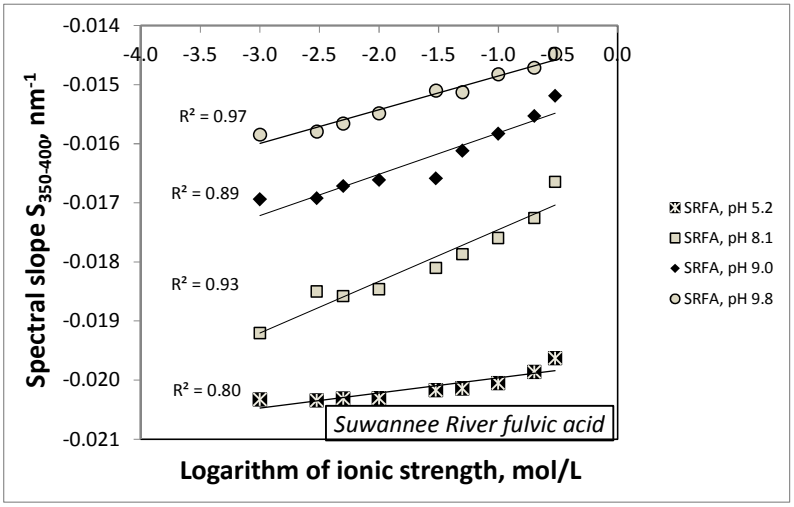

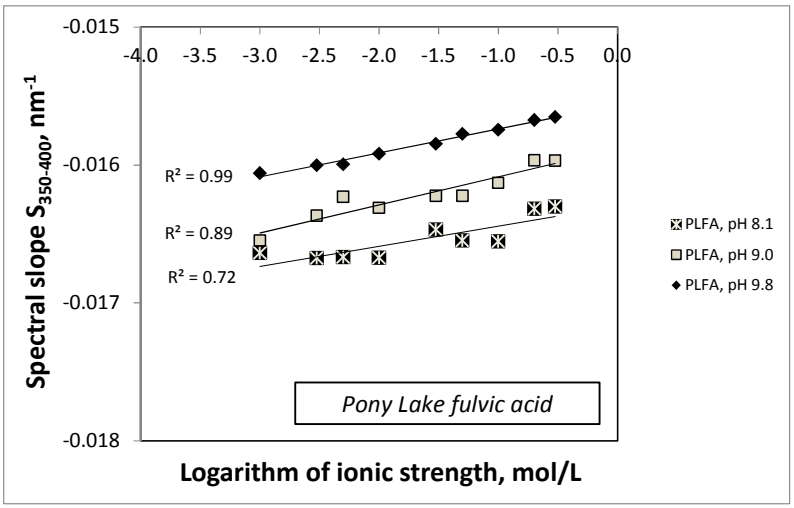

Figure 4.6 Correlations between logarithms of ionic strength and spectral slopes $S_{350\sim400}$ measured for SRHA, SRFA and PLFA.

The notion that IS variations affect DOM chromophores in a way similar to that induced by their deprotonation caused by intentional increases of pH values was also suggested by the close resemblance of the shapes and intensities of the linear differential spectra of all examined DOM samples when either the IS values were varied at a constant pH, or the pH was varied at a constant IS (Figure 4.7).

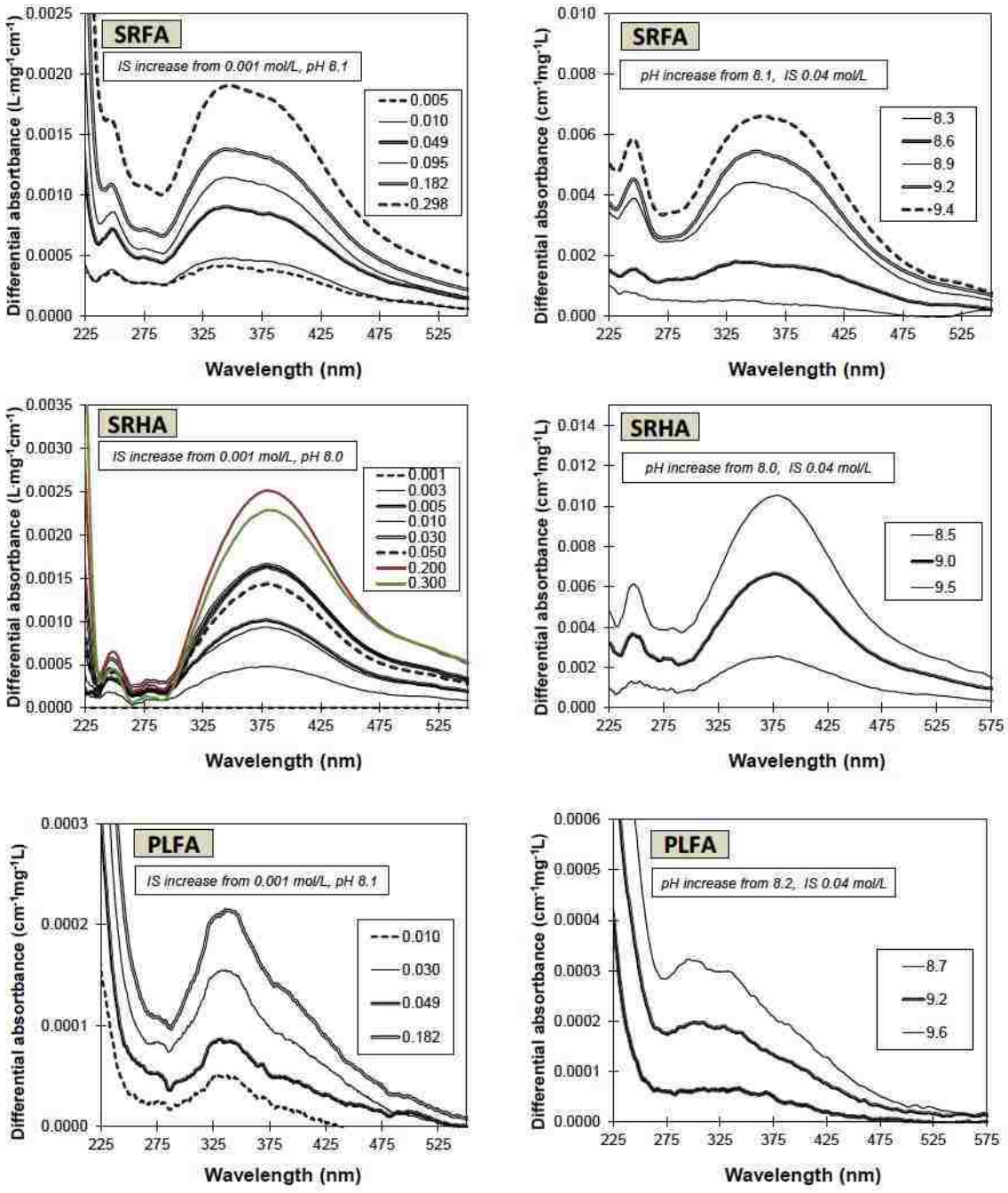

Figure 4.7 Comparison of differential spectra for SRHA varying ionic strengths (vs. 0.001 mol/L reference ionic strength) at a constant 8.0 pH and varying pHs (vs. 8.1 reference pH) at a constant 0.04 mol/L ionic strength.

4.3 Data interpretation based on the NICA-Donnan model

Because the observed IS effect on DOM properties appears to be similar to that expected to take place as a result of the deprotonation of DOM molecules, Visual MINTEQ calculations were carried out to determine whether the observed changes of the spectral slopes induced by IS variations are correlated with the theoretically predicted changes of the deprotonation of the phenolic (or high-affinity site (HAS)) and carboxylic (or low affinity site (LAS)) in SRFA and SRHA in such conditions. NICA-Donnan model parameters that were used in our calculations are compiled in Table 4-1. Model calculations for PLFA were not performed because the intrinsic properties of this DOM are clearly different from those of SRFA and SRHA while the required protonation constants for PLFA are not included in the MINTEQ database. The model calculations showed that the $S_{350\text{-}400}$ values determined for SRHA and SRFA for the entire range of pHs and IS values used in the experiments were correlated with the charges of the phenolic sites in these DOM samples (Figure 4.8 (a)). The correlation was nearly perfectly linear for SRHA but for SRFA it deviated from linearity for low charges of the phenolic groups for pH 5.

Table 4-1 Potentiometric and spectrophotometric NICA-Donnan parameters for protonation-active groups in SRHA and SRFA.

	SRHA	**SRFA**
Potentiometric parameters from MINTEQ database		
$\tilde{K}_{LAS}$	2.93	2.34
$\tilde{K}_{HAS}$	8.00	8.60
Q_{LAS}, meq/g	3.15	5.88

$Q_{HAS,}$ meq/g	2.55	1.86
m_{LAS}	0.81	0.66
m_{HAS}	0.63	0.76
b	0.49	0.57
Spectrophotometric parameters deduced from Figure 4.9		
$\tilde{K}_{LAS}$	4.50	4.60
$\tilde{K}_{HAS}$	9.85	9.03
$DSlope_{LAS}$ (350-400 nm)	0.000936	0.00356
$DSlope_{HAS}$ (350-400 nm)	0.00774	0.00592
m_{LAS}	0.30	0.20
m_{HAS}	0.20	0.39

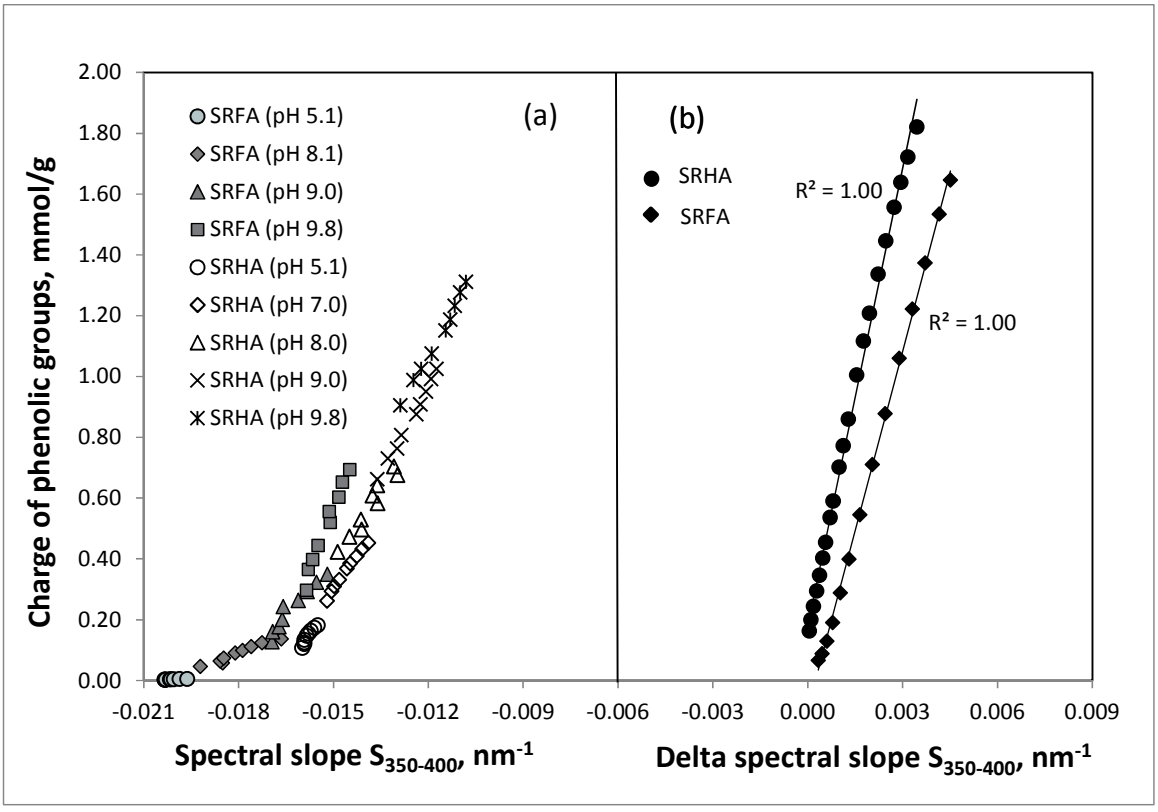

Figure 4.8 Correlations between spectral slopes and NICA-Donnan model calculations of charges associated with the phenolic groups in DOM: (a) correlations between absolute

values of spectral slopes measured for SRFA and SRHA at varying ionic strengths and fixed pHs; (b) correlations between differential of spectral slopes and phenolic charges at a constant ionic strength and pH variation.

To further examine similarities in effects of variations of IS or pH values on DOM chromophores, changes of the spectral slopes vs. pH at a constant ionic strength were also interpreted based on the NICA-Donnan model [58]. In accord with the approach presented in prior research [65,101,137], we used the differential spectral slope in the range of wavelengths 350 to 400 nm ($DSlope_{350\text{-}400}$) measured at varying pHs to examine effects of pH on the protonation of SRHA and SRHA. The results were interpreted based on the NICA-Donnan theory and expressions presented in prior literature [49,96,114,137,138]:

Equation 4-1

$$DSlope_{pH}(\lambda)=\left[\frac{DSlope_{LAS}(\lambda)}{1+\left(\tilde{K}_{LAS}\left[H^{+}\right]\right)^{m_{LAS}}}+\frac{DSlope_{HAS}(\lambda)}{1+\left(\tilde{K}_{HAS}\left[H^{+}\right]\right)^{m_{HAS}}}\right]-\left[\frac{DSlope_{LAS}(\lambda)}{1+\left(\tilde{K}_{LAS}\left[H^{+}\right]_{ref}\right)^{m_{LAS}}}+\frac{DSlope_{HAS}(\lambda)}{1+\left(\tilde{K}_{HAS}\left[H^{+}\right]_{ref}\right)^{m_{HAS}}}\right]$$

In the above equation, $DSlope_{LAS}(\lambda)$ and $DSlope_{HAS}(\lambda)$ correspond to the maximum change of absorbance associated with the deprotonation of the low-affinity site (LAS, mostly carboxylic) and high-affinity site (HAS, mostly phenolic) groups, respectively, $DSlope_{LAS}(\lambda)$ and $DSlope_{HAS}(\lambda)$ referred to DSlope value in the range of wavelengths 350 to 400 nm. $\tilde{K}_{LAS}$ and $\tilde{K}_{HAS}$ are the median values of the protons affinity distributions for

these groups, m_{LAS} and m_{HAS} define the width of these distributions and are measures of the heterogeneity of DOM [76].

Results of these calculations are presented in Figure 4.9 while Table 4-1 contains a compilation of the fitting parameters used in these calculations. The correlation between the differential spectral slopes and charges of DOM phenolic groups calculated for a constant IS and varying pHs are shown in Figure 4.8(b). Comparison of the data presented in Figure 4.8(a) and Figure 4.8(b) demonstrates that changes of the protonation of the phenolic groups in SRFA and SRHA induced by either variations of IS (Figure 4.8 (a)) or pH result (Figure 4.8 (b)) in similar slopes. This result provides additional support to the point that the influence of IS on the chromophores in DOM can be formally ascribed to the changes of the protonation status of these groups.

The data presented above appear to strongly support the fundamental assumptions incorporated in the NICA-Donnan model. However, further work needs to be done with DOM of varying provenance to examine in more detail whether the differences in the responses of SRFA, SRHA and PLFA to IS variations are defined by their different molecular weights, charges and/or conformations, or other mechanisms, for instance differences in the intrinsic chemistry of DOM chromophores.

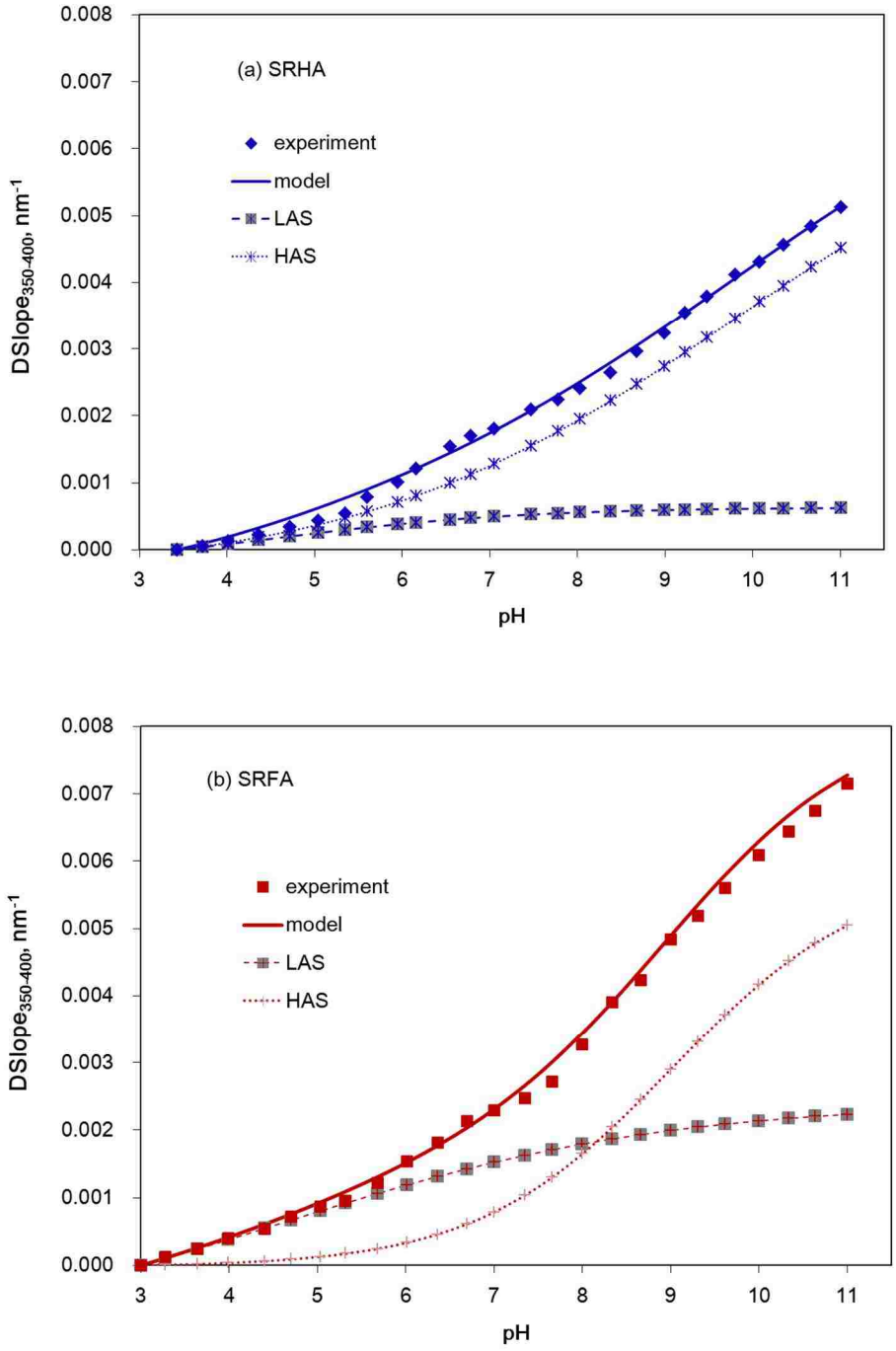

Figure 4.9 Effects of pH on the differential spectral slope determined for the range of wavelengths 350 to 400 nm ($DSlope_{350-400}$) and its NICA-based fitting for SRHA (a) and SRFA (b).

4.4 Conclusions regarding the effects of ionic strength on the chromophores in DOM

This chapter presented experimental and model data examining effects of variations of the ionic strength on the absorbance of DOM. These measurements were carried out for DOM of both allochthonous (SRFA and SRHA) and autochthonous (PLFA) provenance, pH values ranging from ca. 5 to ca. 10 and ionic strengths from 0.001 to 0.3 mol/L. Major results of this study can be summarized as follows:

1. Increases of ionic strength are accompanied by consistent increases of the absorbance of DOM at practically all wavelengths. The magnitude of these changes depends on the solution pH. Specifically, changes of DOM absorbance at low pHs (e.g., pH 5) are much less prominent than those at pH>9. The magnitude of changes induced by variations of IS increases in the order PLFA < SRFA < SRHA, that is to say in the order of the increase of the aromaticity or molecular weight of DOM.

2. For all examined DOM, differential spectra calculated vs. an *a priori* selected reference condition (0.001 mol/L ionic strength) show the presence of two major bands with maxima at ca. 330 nm and > 370 nm. The latter band is very weak in the case of PLFA but it is prominent for SRFA and even more so for SRHA. These bands are similar to those observed when the solutions pH was varied at a constant ionic strength. They are suggested to reflect the occurrence of the deprotonation of operationally defined DOM carboxylic and phenolic groups at increasing ionic strengths.

3. The absolute values of the spectral slopes of the log-processed absorbance spectra of DOM calculated for a 350 to 400 nm wavelength range decreased proportionally to the

logarithm of IS values. This decrease is linearly correlated with the logarithm of ionic strength. This trend can be suggested to correspond to the deprotonation of its functional groups at increasing IS values. Model calculations carried out for SRFA and SRHA indicate that values of the spectral slopes measured at varying pHs and ionic strengths are strongly and largely linearly correlated with the changes of the operationally defined phenolic groups in DOM.

4. The presented data show that effects of ionic strength on DOM can be quantified for DOM at its environmentally relevant concentrations. More experiments need to be carried with DOM of varying provenance to explore in more detail effects of the ionic strength on the spectroscopic properties of DOM and establish methods to incorporate these data into formal models of DOM interactions with protons, metals cations and other solution components.

5 Interactions between major hardness cation and DOM and competitive binding of calcium and copper: *in situ* differential spectroscopic approach and NICA-Donnan modeling

In this chapter, differential absorbance spectroscopy (DAS) is combined with the NICA-Donnan speciation model to carry an in-depth examination of the effects of two typical hardness major cations (i.e., calcium and magnesium) on the chomorphores in standard aquatic DOM. These experiments were performed for a wide range of pHs, ionic strengths and total metal concentrations. The data demonstrate the presence of several features associated with Me^{2+}-DOM interactions and strong relationships between the intensity of these features and the extent of Me^{2+}-DOM binding. Furthermore, competition between these hardness cation and trace-level heavy metals (e.g., copper) is also investigated by this spectroscopic approach to reveal how major background cations with relatively weak affinity to DOM but great abundance in natural system can affect the binding behavior of trace-level heavy metals with strong affinity to DOM functional groups.

5.1 Effect of calcium binding on SRHA chromophores

In accord with observations made in previous studies of metal-DOM interactions [108,139,107], the intensity of SRHA absorbance decreased quasi-exponentially with the observation wavelength. *Per se,* changes of SRHA absorbance induced by gradually increasing concentrations of Ca^{2+} were inconspicuous in the zero-order spectra but they were well discernible in the differential absorbance spectra calculated using Equation 2-1, as shown in Figure 5.1.

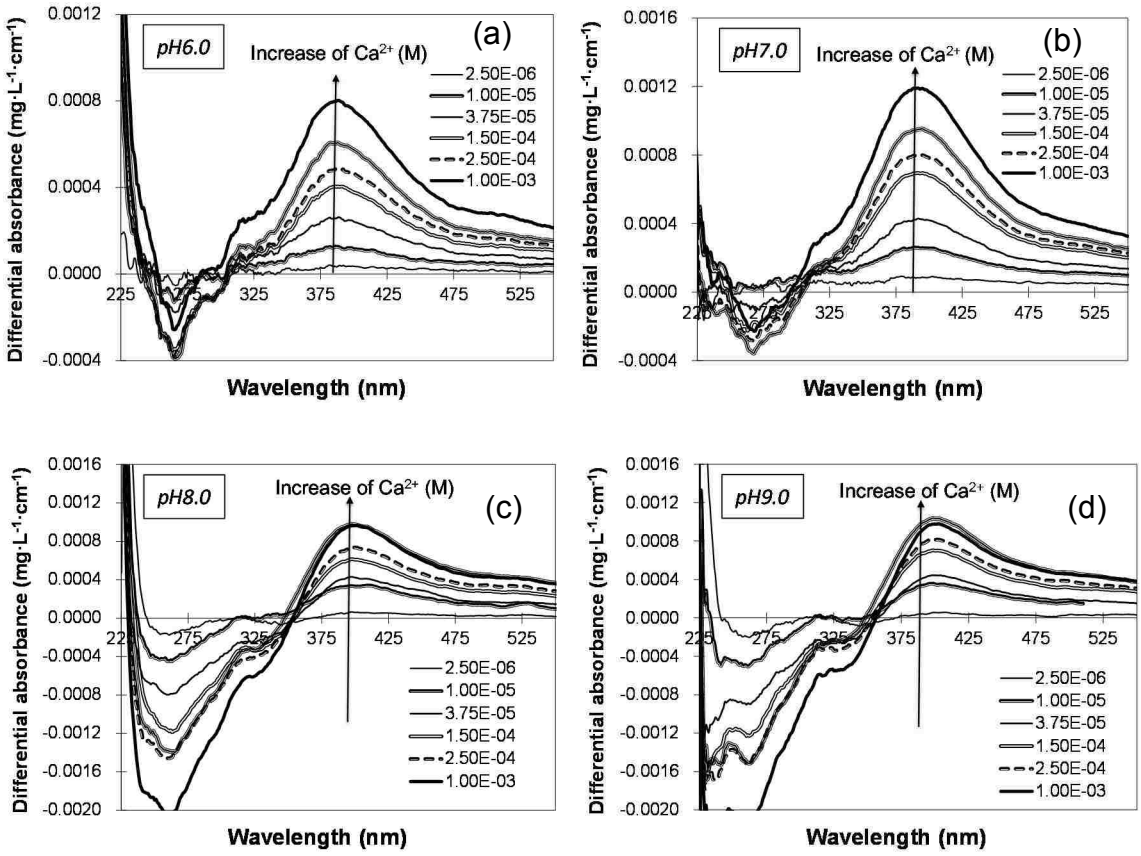

Figure 5.1 Differential spectra of the Ca-SRHA system generated at varying total calcium concentrations and pHs: (a) pH 6.0, (b) pH 7.0, (c) pH 8.0 and (d) pH 9.0. Ionic strength 0.01 mol L^{-1}, DOC concentration 5.0 mg L^{-1}, and with total calcium concentration varied from 2.5 to 1000 μ mol/L

The differential spectra shown at higher pHs (pH 8 and 9) have two bands with maxima at 280 and 380 nm, and an additional weaker band with a maximum at 320 nm. The sign of the band with the 280 nm maximum is negative while that at 380 is positive corresponding to decreasing and increasing, respectively, absorbance of SRHA chromophores in these regions. Results reported in earlier studies [113,140] indicate that the band at 250 nm is more likely to be associated with the deprotonation of carboxylic groups in DOM while the bands located in the 300-390 nm region reflect the engagement of phenolic functional group in

DOM. Alternatively, these bands have been hypothesized to be a results of a bathochromic shift of DOM absorbance sub-bands caused by the presence a ligand-to-metal charge transfer transition observed for a number of model compounds [141,142]. Changes of pH affected the intensity of the differential spectra SRHA but their shape remained largely the same. This indicates that the nature of the SRHA sites involved in Ca binding did not change for the 6.0 to 9.0 pH range.

Effects of Ca^{2+} on SRHA chromophores contributing to relatively low intensity yet potentially sensitive features that tend to be located at wavelengths > 350 nm were examined via the logarithmic transformation of DOM absorbance spectra[139,143,144]. These calculations show that, as mentioned above, logarithms of SRHA absorbance decreased quasi-linearly with the wavelength although the slopes of $\ln A_{\square}$ vs. wavelength dependence are somewhat different in wavelength regions <250 nm, 250 to ca. 350 nm, 350 to ca. 450 nm and > 450 nm.

Increasing total Ca^{2+} concentrations caused consistent changes of the slopes of the log-transformed spectra, especially for wavelengths >350 nm. This trend can be clearly demonstrated using differential log-transformed absorbance spectra calculated using Equation 2-2. Results of these calculations for the Ca^{2+}/SRHA system at pHs from 6 to 9 and a 0.01 mol L^{-1} ionic strength are shown in Figure 5.2

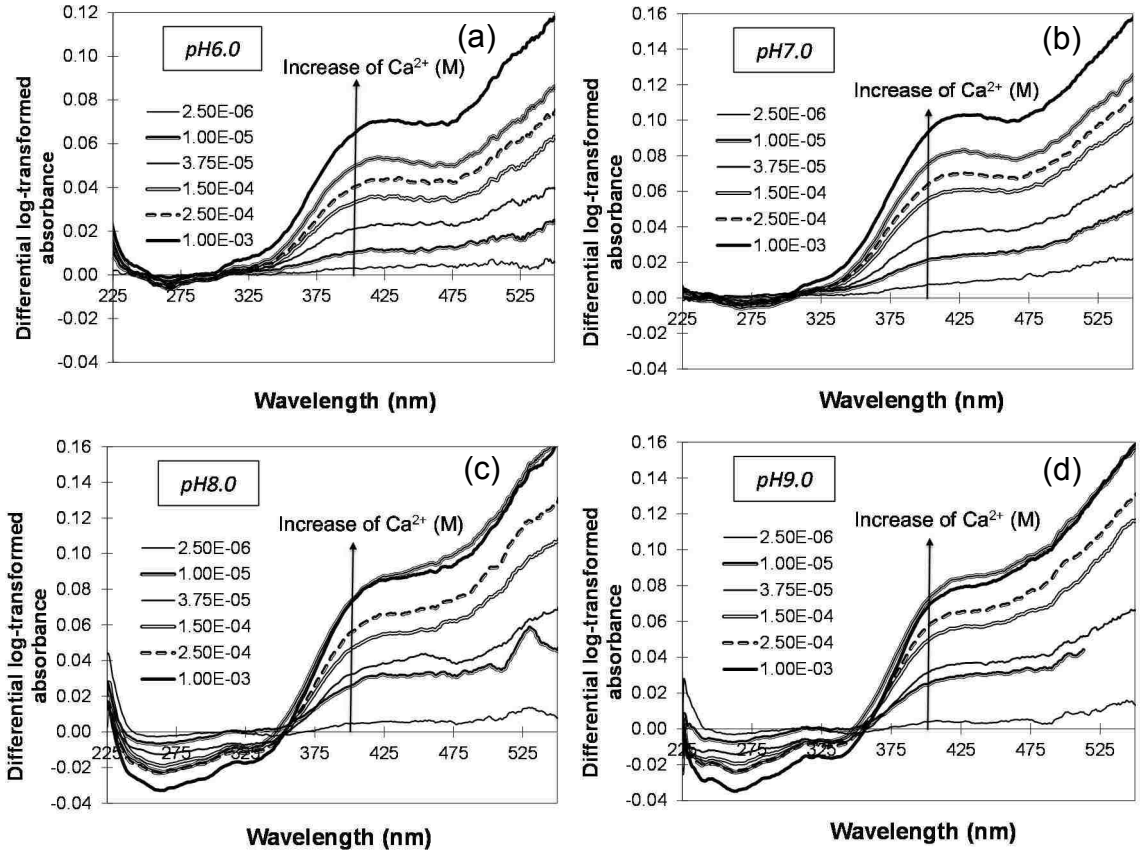

Figure 5.2 Differential log-transformed spectra of the Ca^{2+}-SRHA system at varying total calcium concentrations and pHs: (a) pH 6.0, (b) pH 7.0, (c) pH 8.0 and (d) pH 9.0. Ionic strength 0.01 mol L^{-1}, DOC concentration 5.0 mg L^{-1}, and with total calcium concentration varied from 2.5 to 1000 μmol/L.

This figure shows that, in agreement with the results seen for other metal cations [139,143,144], the differential log-transformed spectra are especially sensitive to the presence of Ca^{2+} in the 350 to 400 nm wavelength region. Accordingly, we used both the absolute values of the slopes of the log-transformed absorbance spectra in this range of wavelengths and their differentials (denoted as $S_{350-400}$ and $DS_{350-400}$, respectively) calculated vs. applicable reference conditions to estimate the extent of the binding of Ca^{2+} by SRHA.

Values of the differential slopes $DS_{350\text{-}400}$ increased monotonically at increasing total Ca^{2+} concentrations and pH, as demonstrated in Figure 5.3 (a). The datasets of $DS_{350\text{-}400}$ values obtained in these conditions were then compared with the concentrations of Ca^{2+} ions bound by SRHA at various pHs and total Ca^{2+} levels. The concentrations of Ca^{2+}-SRHA-bound complexes were determined using the NICA-Donnan approach [145–148] and the complexation constants compiled in Table 4-1. Relationships between the concentrations of Ca^{2+} bound by DOM and corresponding $DS_{350\text{-}400}$ values are shown in Figure 5.3 (b). It demonstrates that $DS_{350\text{-}400}$ values measured in a wide range of pH values are strongly correlated with the concentration of DOM-bound Ca^{2+} ions. The correlations are nearly linear and have similar slopes (0.0103 $mol \cdot L^{-1} \cdot nm$) for all examined pH values and total Ca^{2+} concentrations.

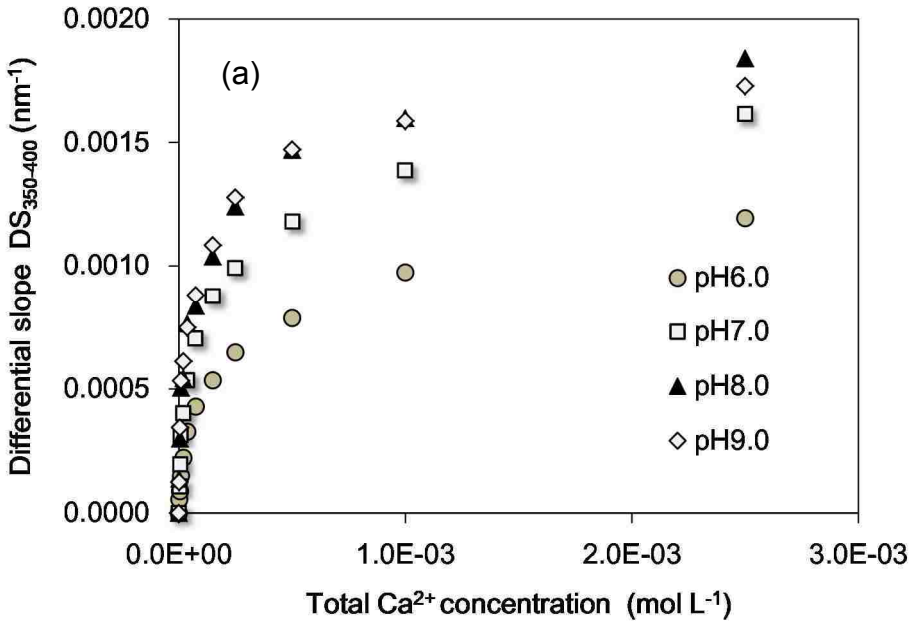

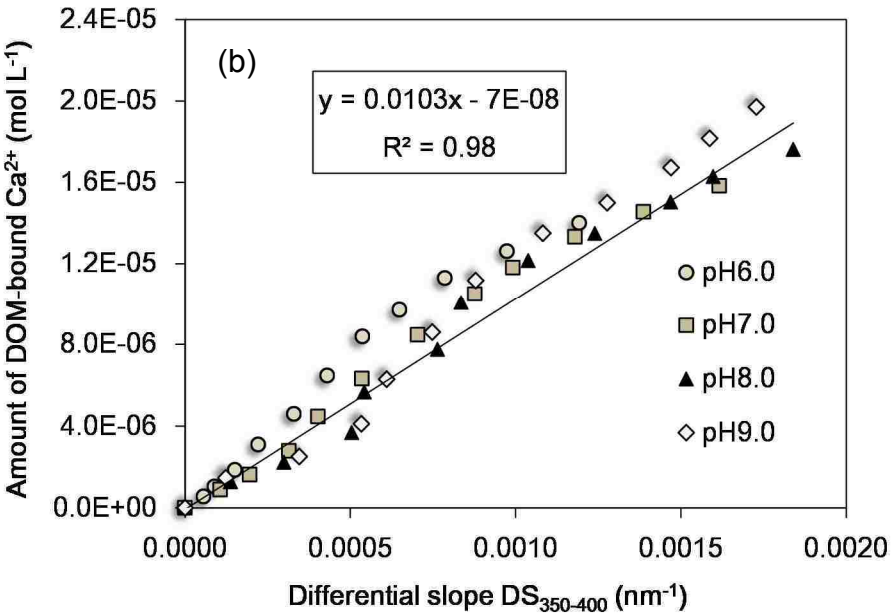

Figure 5.3 Correlation between changes of the spectral slope in the range of 350 to 400 nm and (a) total Ca^{2+} concentration and (b) the amount of SRHA-bound Ca^{2+} ions predicted for varying total Ca^{2+} concentrations.

5.2 Effect of magnesium binding on DOM chromophores

Another major hardness cation, magnesium, is also studied by this *in situ* spectroscopic approach and the effects of magnesium on DOM ultra-visible absorbance spectra are shown in Figure 5.4. The presence of increasing magnesium concentration resulted in subtle but consistent changes of DOM absorbance for all examined pH values and ionic strengths (IS), as illustrated in in Figure 5.4 (a) for SRHA at pH 7.0 and ionic strength 0.01 mol L^{-1}. This was consistent with observations for calcium and in previous studies of other metal-DOM interactions [107,113].

To discern effects of magnesium on NOM chromophores in more detail, differential absorbance spectra (DAS) were calculated using Equation 2-1. Results of this data

processing are presented in Figure 5.4(b). The shown spectra have three distinct bands with peaks at wavelength 250, 310 and 390 nm. The band with the 250 nm maximum is relatively less intense and its sign is negative indicating a decrease rather than increase of DOM absorbance in this range. The sign of the other two bands is positive and they are more intense, especially the band with the 390 nm maximum. Similar features were observed in practically all conditions at which the Mg^{2+}/DOM system was examined. The similarities of the shape and the location of the peaks (e.g., around 310~320 nm and 390~390 nm) between calcium and magnesium suggest the two divalent cations share some common features in the interactions or binding to DOM functional groups.

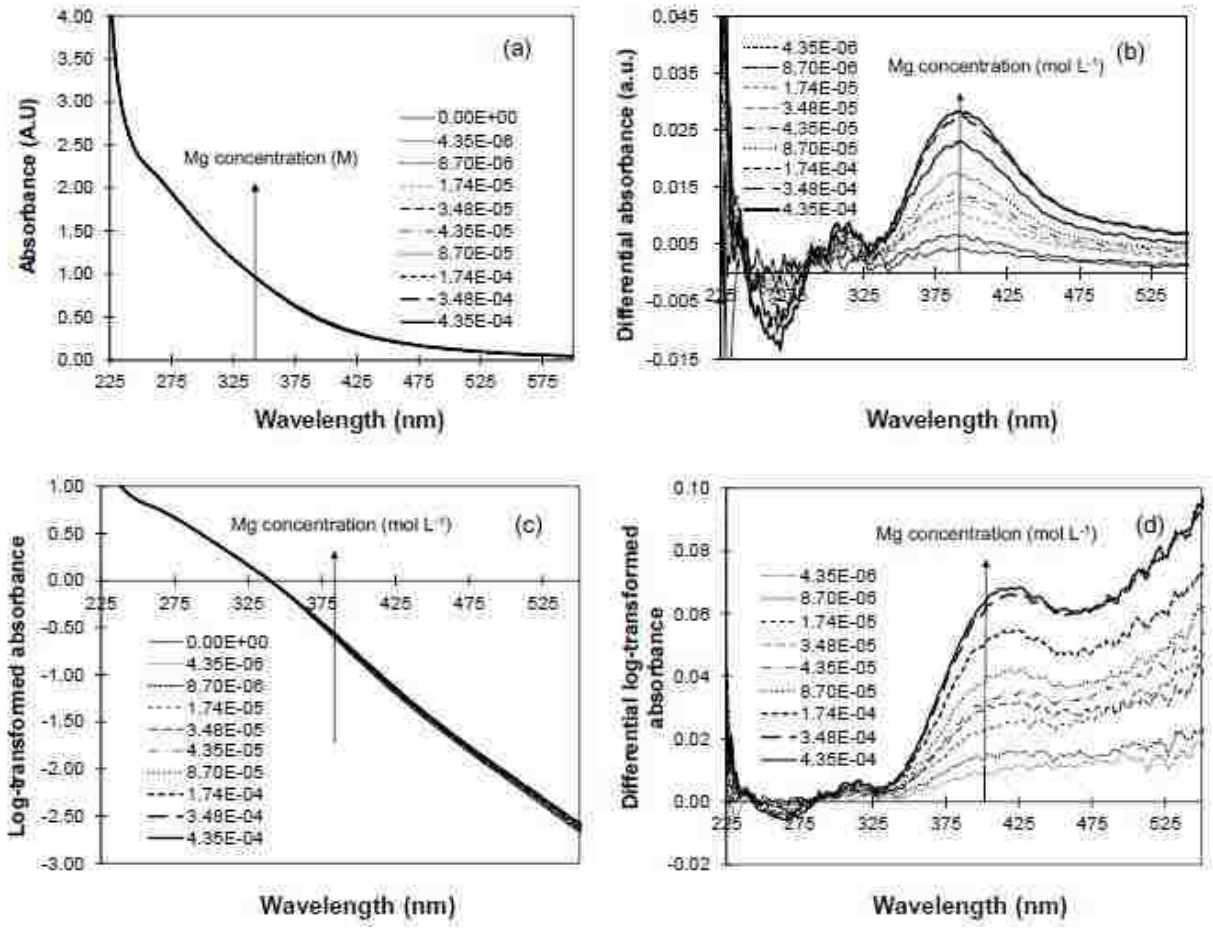

Figure 5.4 Absorbance spectra of SRHA recorded at varying concentrations of magnesium at pH 7.0 and ionic strength 0.01 mol L^{-1}. (a) zero-order spectra; (b) differential spectra; (c) log-transformed spectra; and (d) differential log-transformed spectra. DOC concentration 5.0 mg L^{-1}; cell length 5 cm, spectra are not normalized by DOC or cell length.

Figure 5.4(c) demonstrates that the logarithms of DOM absorbance decrease linearly with the wavelength but the log-transformed spectra have several regions (e.g., <250 nm, 250 to ca. 350 nm, 350 to ca. 450 nm, and > 450 nm) with somewhat different slopes. Increasing magnesium concentrations caused consistent changes of the slopes of the log-transformed spectra, especially for wavelengths > 350 nm (Figure 5.4(d)). Because the slope of log-transformed absorbance of DOM in the range of wavelengths 350-400 nm is most sensitive to variations of Mg^{2+} concentrations, the absolute values of the slopes of log-transformed

spectra in this wavelength range and their changes (denoted as $S_{350\text{-}400}$ and $DS_{350\text{-}400}$, respectively) were used to estimate Mg^{2+}-DOM binding.

For calcium, we have demonstrated that $DS_{350\text{-}400}$ values measured in a wide range of pH values are strongly and nearly linearly correlated with the concentration of DOM-bound Ca^{2+} ions. Our next question is whether this linear correlation also applies to other cations, especially divalent hardness cations that have similar interactions with DOM. Therefore, the dataset of $DS_{350\text{-}400}$ values for magnesium were compared with the concentrations of Mg^{2+}-SRHA or Mg^{2+}-SRFA complexes estimated using the NICA-Donnan model, with the complexation constants included in the Visual MINTEQ database [147]. Relationships between the MINTEQ-based estimates of the concentrations of magnesium bound by DOM and corresponding changes of the parameter $DS_{350\text{-}400}$ are shown in Figure 5.5. It demonstrates that for all examined conditions including SRHA and SRFA, $DS_{350\text{-}400}$ values determined are linearly correlated with the concentrations of DOM-bound Mg^{2+} ions.

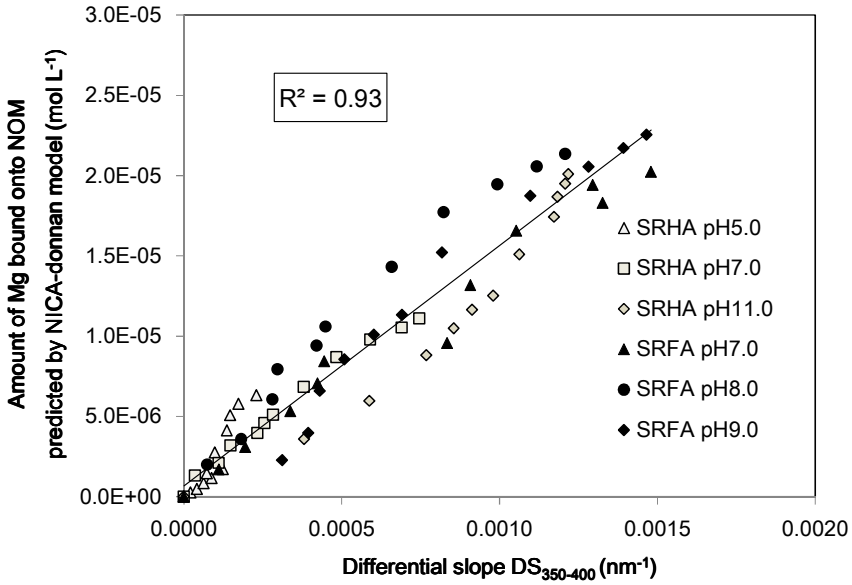

Figure 5.5 Correlation between $DS_{350\text{-}400}$ values and concentrations of Mg^{2+}-DOM complexes calculated using the NICA-Donnan model (parameters shown in Table 2-1). Results for varying pHs, total magnesium concentrations and a 0.01 mol L^{-1} ionic strength.

5.3 Competitive binding of copper by SRHA in the presence of varying concentrations of calcium

Given the success of the approach described above to quantify the binding of hardness cation by DOM, the competitive binding of Cu^{2+} and Ca^{2+} by SRHA was examined in this section. The pH was maintained at 6 for competition study because it allowed a wide enough range of copper concentrations for which the formation of solid phases such as malachite was not expected. In these experiments, the background concentrations of Ca^{2+} was set at 0, 0.00025 and 0.0025 mol/L levels while the total concentration of copper added to the solution varied incrementally from 0 to $5 \cdot 10^{-5}$ mol/L. Differential spectra for this system were calculated vs. each of the reference states that corresponded to the same pH, ionic strength and respective Ca concentration in the absence of copper.

Representative differential spectra generated for the Cu^{2+}/Ca^{2+}/SRHA system for the selected fixed Ca^{2+} background levels and varying total copper concentrations are shown in Figure 5.6. Their shape is notably different from those obtained for SRHA at varying total calcium concentrations, especially for wavelengths < 350 nm (Figure 5.1). Specifically, while contributions of the bands located at 250, 280, 320 and 380 nm can be detected in the Cu^{2+}-differential spectra, all these bands have a positive sign. This indicates that for all SRHA chromophores engaged in Cu^{2+} binding, the latter process causes their absorbance to increase, most likely, as discussed below, due to the deprotonation of these chromophores caused by the displacement of the bound protons by the copper ions. In addition, the magnitude of the response of SRHA absorbance to the variations of total copper concentration is considerably higher than that for Ca^{2+} at the same pH and ionic strength.

The differences of the shapes and intensities of the differential spectra shown in Figure 5.1 and Figure 5.6 are indicative of the differences in the mode of binding and natures of SRHA sites involved in interactions with Cu^{2+} and Ca^{2+}. This is consistent with the results of our previous study which correlated contributions of Gaussian bands present in the differential spectra of DOM and the covalent-bonding index ($(\chi_m)^2 r_c$) of metal ions [107].

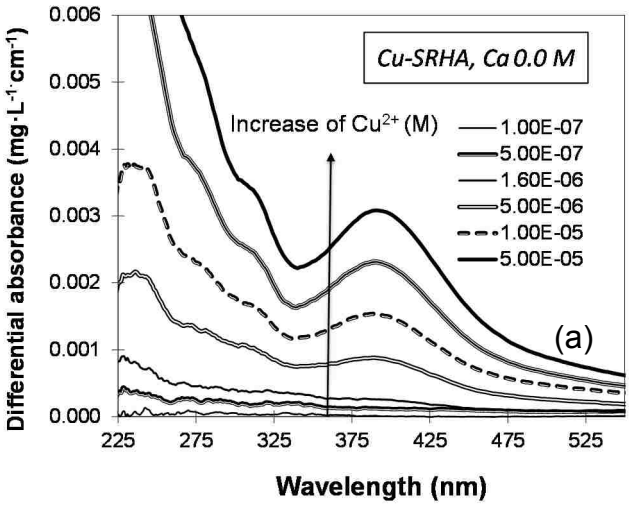
Cu-SRHA, Ca 0.0 M
Increase of Cu2+ (M)
1.00E-07
5.00E-07
1.60E-06
5.00E-06
1.00E-05
5.00E-05
(a)
Differential absorbance (mg·L-1·cm-1)
Wavelength (nm)
0.000
0.001
0.002
0.003
0.004
0.005
0.006
225
275
325
375
425
475
525

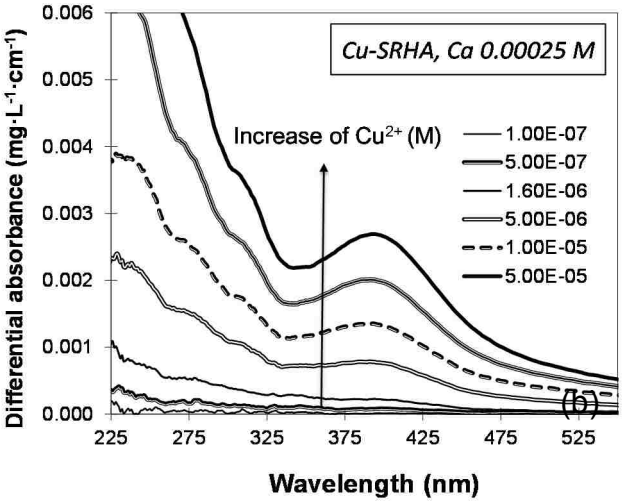
Cu-SRHA, Ca 0.00025 M
Increase of Cu2+ (M)
1.00E-07
5.00E-07
1.60E-06
5.00E-06
1.00E-05
5.00E-05
(b)
Differential absorbance (mg·L-1·cm-1)
Wavelength (nm)
0.000
0.001
0.002
0.003
0.004
0.005
0.006
225
275
325
375
425
475
525

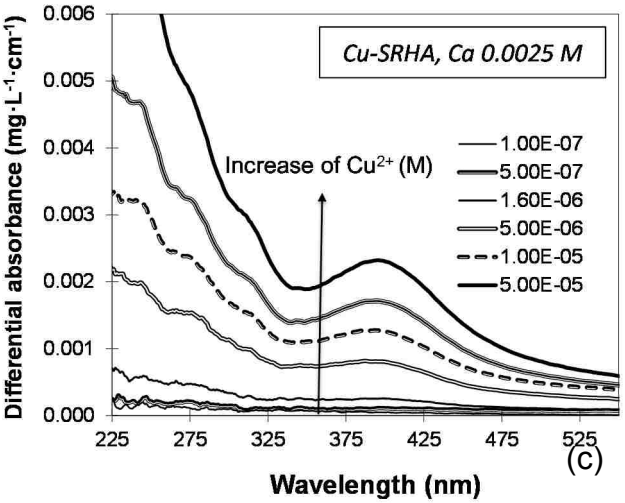
Cu-SRHA, Ca 0.0025 M
Increase of Cu2+ (M)
1.00E-07
5.00E-07
1.60E-06
5.00E-06
1.00E-05
5.00E-05
(c)
Differential absorbance (mg·L-1·cm-1)
Wavelength (nm)
0.000
0.001
0.002
0.003
0.004
0.005
0.006
225
275
325
375
425
475
525

Figure 5.6 Comparison of differential spectra of SRHA generated at varying total concentrations of copper and in the presence of 0, 0.00025 and 0.0025 mol L^{-1} total calcium concentration, respectively. pH 6.0, ionic strength 0.01 mol L^{-1}.

The differential log-transformed absorbance spectra of SRHA measured in the same conditions are shown in Figure 5.7. Results shown in this figure are consistent with those for calcium only in Figure 5.2. In both cases, the intensity of the log-transformed absorbance spectra changes nearly linearly vs. the observation wavelength, and changes induced by interactions between SRHA and Cu^{2+} are most prominent in the 350 to 500 nm wavelength region. In accord with this observation, the parameters quantifying the spectral slope in this region and its differential ($S_{350\text{-}400}$ and $DS_{350\text{-}400}$) were employed to estimate Cu^{2+}-DOM binding at varying system conditions.

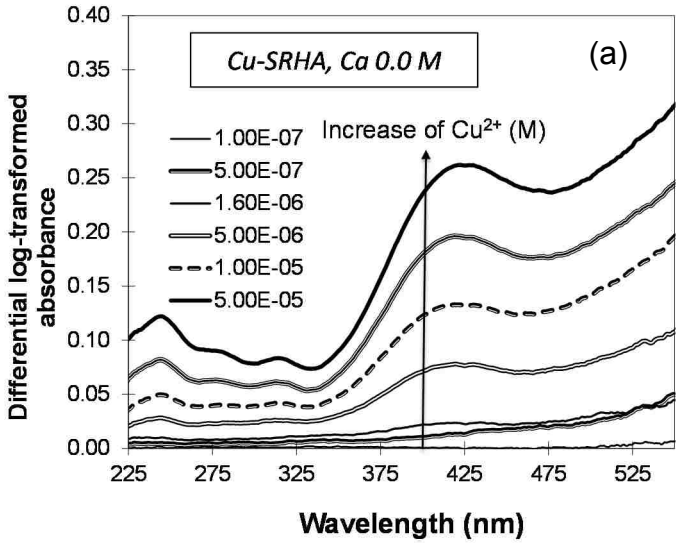

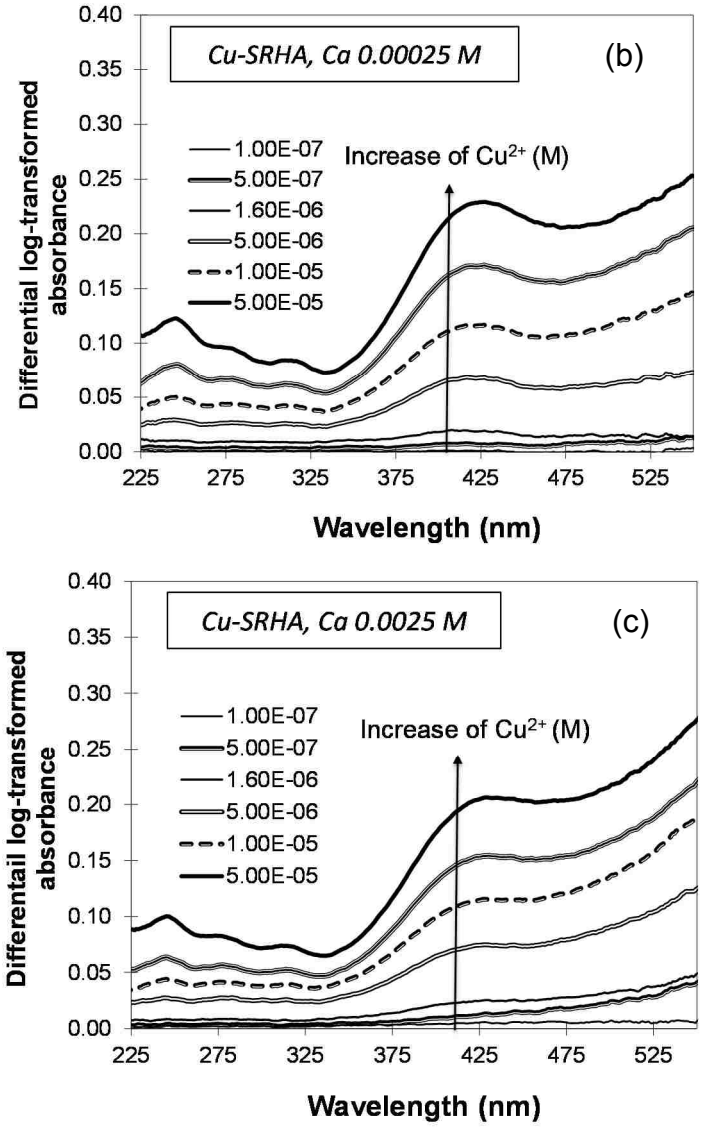

Figure 5.7 Comparison of differential log-transformed spectra of SRHA calculated for varying total concentrations of copper in the absence of calcium, in the presence of 0.00025 mol L^{-1} and 0.0025 mol L^{-1} calcium concentration, respectively. pH 6.0, ionic strength 0.01 mol L^{-1}.

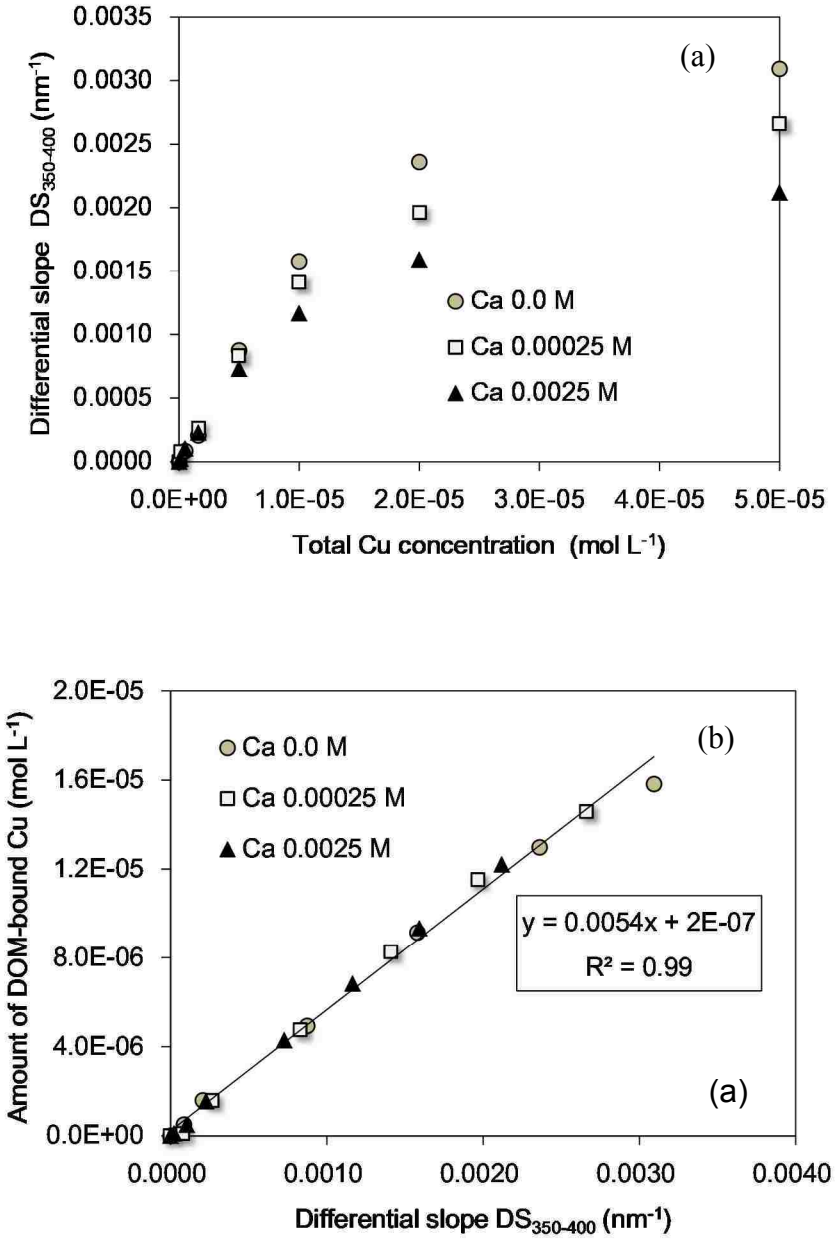

Figure 5.8 Correlation between changes of the spectral slope in the range of 350 to 400 nm and (a) total Cu concentration and (b) the amount of SRHA-bound copper ions predicted for varying background calcium concentrations.

These calculations showed that $DS_{350\text{-}400}$ increased gradually with total Cu^{2+} concentrations but increasing levels of background Ca^{2+} ions suppressed that effect in some extent, as

(b)

shown in Figure 5.8 (a). Similarly to how it was done for Ca^{2+}-SRHA complexation, the datasets of $DS_{350-400}$ values were compared with the concentrations of Cu^{2+} ions bound by SRHA in the presence of varying background Ca^{2+} levels. Relevant calculations were done using the Nica-Donnan model and complexation constants presented in Table 2-1.

Relationships between the concentrations of Cu^{2+}-SRHA complexes and corresponding $DS_{350-400}$ values are shown in Figure 5.8 (b). It demonstrates that $DS_{350-400}$ measured in a wide range of copper concentrations is strongly correlated with the concentration of DOM-bound Cu^{2+} ions irrespective of the background calcium concentrations. The correlations are nearly linear and have similar slopes in the all range of copper in absence and presence of calcium.

5.4 Further interpretation of effects of competitive binding of Ca^{2+} and Cu^{2+} on SRHA chromophores

Despite the existence of linear correlations between the concentrations of Ca^{2+}-SRHA or Cu^{2+}-SRHA complexes and $DS_{350-400}$ values (Figure 5.3 and Figure 5.8, respectively), the slope of that correlation for Cu^{2+} (0.0054 mol L^{-1} nm) was notably different from that for Ca^{2+}, in which case it was about twice, 0.0103 mol·L^{-1}·nm.

This confirms the notion that the response of SRHA chromophores contributing to the absorbance at wavelengths > 350 nm and quantified using the spectral slope $S_{350-400}$ to binding of Ca^{2+} or Cu^{2+} is different. This is consistent with the results of prior research [107]

that compared the response of differential absorbance at 400 nm to binding of metals with different covalent and/or ionic indexes.

On the other hand, the observed differences in the responses of SRHA chromophores to binding of calcium and copper can be related not only to the changes of differential spectral slopes but also to their absolute values $S_{350\text{-}400}$ measured at varying total copper and calcium concentrations (Figure 5.9 (a)). This figure demonstrates that the $S_{350\text{-}400}$ values increased with both concentrations of Ca^{2+} and Cu^{2+}, but the magnitude of response the $S_{350\text{-}400}$ values to increases of Cu^{2+} concentration was less at higher calcium concentrations, as also demonstrated for the $DS_{350\text{-}400}$ values in Figure 5.8.

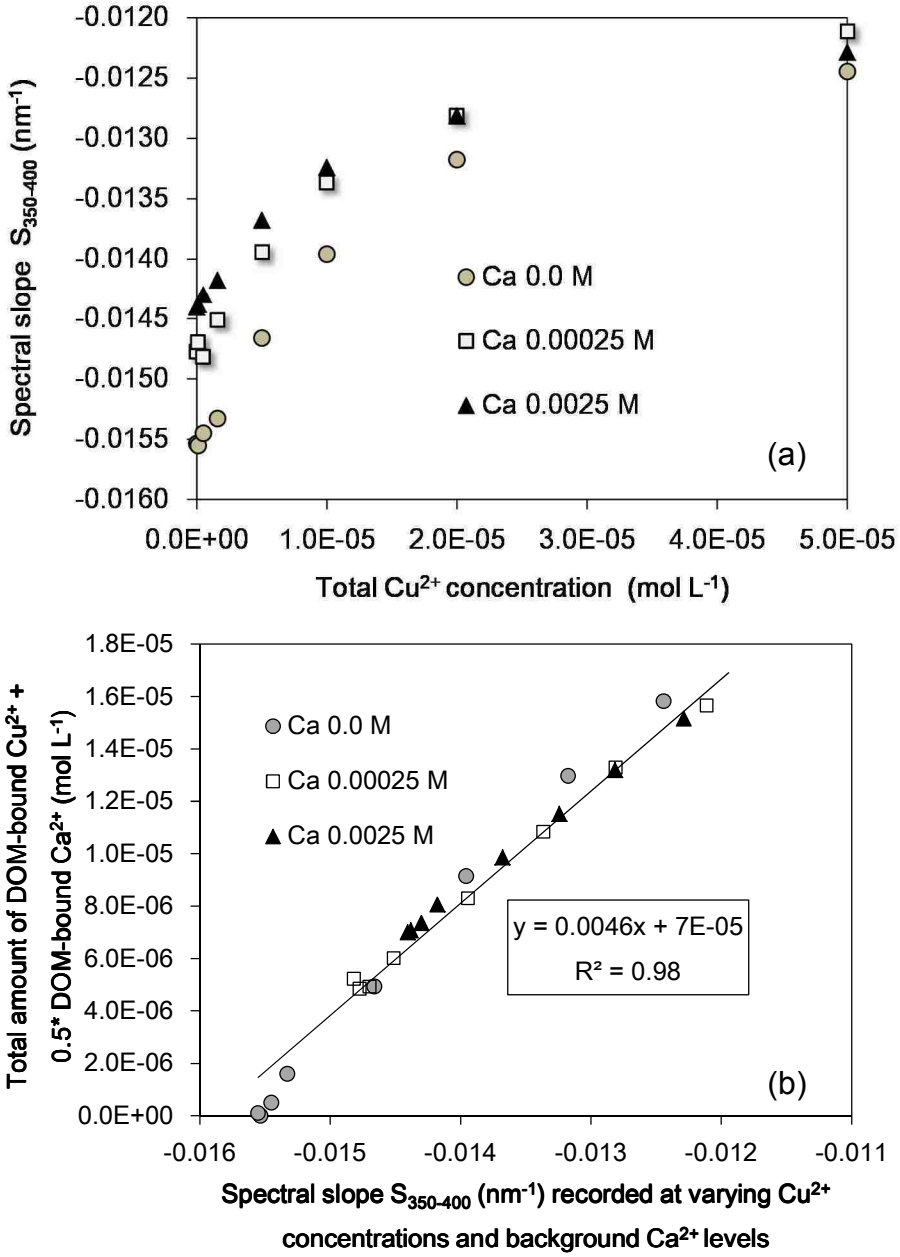

Figure 5.9 (a) Effects of total copper concentrations on the absolute values of spectral slopes measured at varying background concentrations of calcium; (b) correlation between the spectral slopes and corrected sums of the concentrations of SRHA-bound copper and calcium ions.

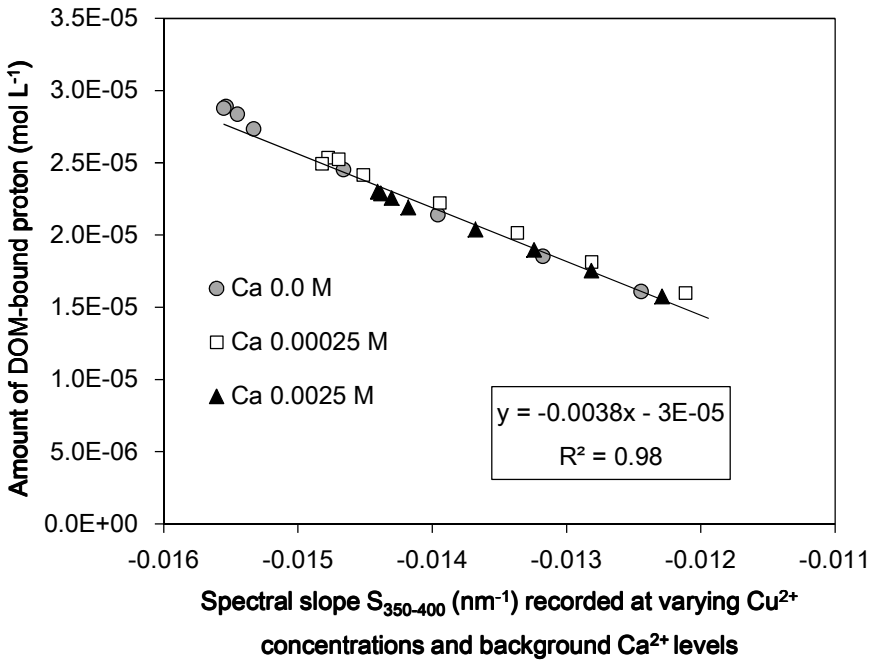

Figure 5.10 Correlation between absolute values of the spectral slopes and concentrations of SRHA-bound protons at varying copper concentrations and background calcium levels.

As opposed to the existence of highly linear correlations between the amounts of either Ca^{2+} or Cu^{2+} bound by SRHA and corresponding $DS_{350-400}$ values, absolute $S_{350-400}$ values did not form a single dataset when compared with the sums of molar concentrations of Ca^{2+}-SRHA and Cu^{2+}-SRHA complexes (data not shown). However, instead of using the sum of [Cu^{2+}-SRHA] and [Ca^{2+}-SRHA] concentrations predicted based on the NICA-Donnan model, a corrected sum of [Cu^{2+}-SRHA] and α[Ca^{2+}-SRHA] was used where the coefficient α was assigned a 0.5 value. The corrected sum of the concentrations of calcium and copper complexes with SRHA has a strong linear correlation with the $S_{350-400}$ values (Figure 5.9(b)).

This was interpreted to indicate that in the context of changes of the spectral slopes, the need to introduced the corrected sum $[Cu^{2+}\text{-SRHA}]+\alpha[Ca^{2+}\text{-SRHA}]$ signifies that the binding of one Cu^{2+} ion is accompanied by the replacement of *n* of protons (where *n* can vary depending on the mode of binding from 0 to 2) from the protonation- and complexation-active functional groups in SRHA, while the binding of one Ca^{2+} causes only *n/2* proton to be replaced.

This observation was confirmed by comparing the amounts of protons that remain to be bound by SRHA molecules at varying calcium and copper concentrations and corresponding changes of the spectral slopes. Figure 5.10 demonstrates that the $S_{350\text{-}400}$ values obtained for these measurements are strongly correlated with the amount of protons bound onto carboxylic and phenolic functional groups of DOM predicted by NICA-Donnan Model.

Given that the strong linear correlation exists between $DS_{350\text{-}400}$ and the concentrations of DOM-bound Ca and Cu, it can be suggested that the binding of Cu^{2+} and Ca^{2+} by SRHA is accompanied by the replacement of the protons bound by carboxylic and phenolic functional groups. Further analysis of the data shown in Figure 5.3, Figure 5.8, Figure 5.9 and Figure 5.10 demonstrates that at pH 6.0, the actual number of protons released as a result of binding of either Cu^{2+} and Ca^{2+} was close to 0.8 and 0.4, respectively. These values are somewhat lower than those hypothesized to take place in prior research which suggested that the number of protons released per a bound Cu^{2+} ion was close to 1 [149,150]. The significance of this difference needs be further examined to determine whether it is

caused by limitations of the precision of the complexation constants used to model Ca^{2+}- and Cu^{2+}-SRHA interactions, or other factors need to be accounted for.

5.5 Conclusions of tracking hardness cations interacting with DOM as well as the competitive binding to DOM between hardness cation and copper using in situ spectroscopic approach

This study addressed quantified hardness cation-DOM interactions using differential absorbance spectroscopy (DAS) in combination with the NICA-Donnan speciation model. DAS results demonstrated the existence of strong interactions between calcium/ magnesium and DOM at all examined conditions and demonstrated that the binding of Me^{2+} by DOM was accompanied by the replacement of protons in the protonation-active phenolic and carboxylic groups. The slope of the log-transformed absorbance spectra of DOM in the range of wavelength 350-400 nm was found to be indicative of the extent of Me^{2+}-DOM binding. The differential and absolute values of the spectral slopes were strongly correlated with the amount of DOM-bound hardness ions.

This study also demonstrated that effects of the competitive binding of calcium ion, one of the most ubiquitous and environmentally important ions, and Cu^{2+}, a typical environmental contaminant, by DOM could be elucidated by the method of absorbance spectroscopy for a wide range of pHs, total Ca and Cu concentrations. In addition of the capacity of this approach to provide detailed information about the microscopic nature of the functional groups involved in these interactions, it also can quantify the amount of metal bound on DOM. The data confirm the strong performance of the NICA-Donnan Model for the

Cu^{2+}/Ca^{2+}/SRHA system. In that latter case, the complexation constants used in the NICA-Donnan modeling has been obtained primarily via ISE measurements. However, the presented approach that utilizes *in situ* spectroscopic measurements can be employed to quantify and ultimately yield complexation parameters for any combination of competing ions interacting with DOM irrespective of whether data of ISE measurements or related methods are available for such systems. This capability of the approach developed in our research will be examined in future studies.

6 Conclusions

In this dissertation, the ultimate goal was to provide insights into the nature of DOM interactions with metals and metal solid phases which representative of corrosion in drinking water distribution systems. Experiments to achieve this goal also lead to the necessity of probing DOM interactions with selected metal cations as well as the competition between different metal ions.

In the metal solid phase study, we selected Aldrich humic acid (AHA) and standard Suwannee River fulvic acid (SRFA), as well as their chlorinated and ozonated form to gain more insight on how water treatment can affect DOM properties and so how it affects copper release. The data generated in our experiments show clearly that DOM with relatively high apparent molecular weight (AMW), aromaticities and contributions of protonation-active phenolic and carboxylic groups can play a key role in adsorption and colloidal dispersion of the solids that are deemed to define the extent of copper release in

drinking water. We also found that copper release is well correlated with a number of spectroscopic parameters characterizing DOM properties, notably $SUVA_{254}$, spectral slopes of DOM absorbance, and differential absorbance at wavelength of 280 nm and 350 nm that is indicative of the contributions of carboxylic and phenolic functional groups. Some alternative parameters, such as $SUVA_{254}$ of DOM, changes of the ζ–potential of the solid phases that is indicative of the surface activity of DOM, are also strong predictors of the enhancement of copper release in drinking water conditions.

The results also demonstrate that DOM alteration by chlorine, ozone and other relevant water treatment operation is likely to suppress copper release, especially when SUVA values or alternative DOM characterization parameters such as the spectral slopes, intensity of differential absorbance or shifts of the ζ-potentials of the representative solid phases are below certain threshold levels. In terms of practical implications, the data for DOM examined in our study (SRFA and AHA) indicate that *per se*, DOM with $SUVA_{254}$ values < ca. 2 $L \cdot mg^{-1} \cdot m^{-1}$ are not likely to cause pronounced changes of copper release, especially for systems controlled by CuO rather than by a more commonly occurring malachite. Alternatively, negative shifts of the ζ-potential of CuO and/or malachite less than ca. 5 mV compared with the ζ-potentials of these phases in organic-free water at the same pH and alkalinity can also be indicative of a low likelihood of increases of copper release attributable to DOM in any specific drinking water. These estimates can provide additional guidance for surface water treatment in situations when copper release needs to be controlled.

The next goals that ensued from the initial phase of the study were to probe changes of chromophores in DOM when interacting with background singly charged cations (as reflected by ionic strength), major hardness cations and competitive binding between trace-level heavy metals and hardness cations. To examine the effects of ionic strength (IS) on DOM chromophores, allochthonous (Suwannee River humic and fulvic acids) and one example of autochthonous (Pony Lake fulvic acid) provenance were studied and the results showed that increases of IS from 0.001 to 0.3 mol/L were accompanied by relatively small but consistent increases of the absorbance of DOM. The extent of these changes increased with the solution pH and in the order PLFA < SRFA < SRHA. The absolute values of spectral slopes of the absorbance spectra of DOM calculated for a 350 to 400 nm wavelength range decreased with increasing ionic strength and this decrease was linearly correlated with the logarithm of ionic strength. This trend appears to correspond to the deprotonation of its functional groups at increasing IS values, which was indicated by model calculations showing that values of the spectral slopes are strongly and largely linearly correlated with the extent of IS-induced deprotonation of the operationally defined phenolic groups in DOM.

Following the study of ionic strength (IS) effects on DOM, changes of chromophores caused by their interactions with major divalent hardness cations (Me^{2+}) were further investigated by the spectroscopic approach. Me^{2+}-DOM interactions were quantified using linear and log-transformed DOM absorbance spectra acquired at varying pHs, ionic strengths, total Ca^{2+} and Mg^{2+} concentrations. The similarities of DAS peaks in both shape and locations of calcium and magnesium suggested the similar mechanisms of Mg and Ca interacting with functional groups in DOM. The existence of strong linear correlations

between Me^{2+}-DOM concentrations and $DS_{350-400}$ values indicates that interactions between Me^{2+} and DOM can be ascertained based on highly precise *in situ* methods and their data can be used to check the performance and ultimately optimize parameters of the NICA-Donnan or related models.

The competitive binding of Ca^{2+} and Cu^{2+} by DOM exemplified by Suwannee River Humic Acid (SRHA) was examined as well. The data show that the differential spectra associated with the binding of the metal cations by DOM exhibit specific features that have consistent differences for Ca^{2+}/Mg^{2+} and Cu^{2+}. The competition between Ca^{2+} and Cu^{2+} for the binding sites in DOM was tracked by examining the intensity and shapes of the differential spectra generated for the Ca^{2+}/Cu^{2+}/DOM system. The extent of metal binding by DOM was quantified by calculating the slopes of log-transformed absorbance spectra in the range of wavelength 350 to 400 nm (denoted as $S_{350-400}$) and comparing the data with predictions made using the NICA-Donnan model. The data showed the presence of unambiguous correlations between the amounts of Ca^{2+} and Cu^{2+} by DOM and change of the spectral slope. The observed effects were interpreted based on the assumption that the binding of Ca^{2+} and Cu^{2+} by SRHA was accompanied by the replacement of protons bound by carboxylic and phenolic functional groups of DOM. The equivalent number of protons replaced by Cu^{2+} and Ca^{2+} ions was estimated to be ca. 0.8 and 0.4, respectively. The presented results confirm both the strong performance of the NICA-Donnan approach and the performance of the presented *in situ* method in quantifying metal-DOM interactions for ultimately any combination of competing ions.

References

(1) Thurman, E. M. *Organic geochemistry of natural waters*; Springer, 1985.
(2) Murray, A. G.; Eldridge, P. M. Marine viral ecology: incorporation of bacteriophage into the microbial planktonic food web paradigm. *J. Plankton Res.* **1994**, *16*, 627–641.
(3) Findlay, S.; Sinsabaugh, R. L. *Aquatic ecosystems: interactivity of dissolved organic matter*; Academic Press: San Diego, Calif., 2003.
(4) Leenheer, J. A.; Croué, J.-P. Peer Reviewed: Characterizing Aquatic Dissolved Organic Matter. *Environ. Sci. Technol.* **2003**, *37*, 18A – 26A.
(5) Fimmen, R. L.; Cory, R. M.; Chin, Y. P.; Trouts, T. D.; McKnight, D. M. Probing the oxidation–reduction properties of terrestrially and microbially derived dissolved organic matter. *Geochim. Cosmochim. Acta* **2007**, *71*, 3003–3015.
(6) Edwards, M.; Benjamin, M. M. Transformation of NOM by Ozone and its Effect on Iron and Aluminum Solubility. *J. Am. Water Works Assoc.* **1992**, *84*, 56–66.
(7) Gao, Y.; Korshin, G. Effects of NOM properties on copper release from model solid phases. *Water Res.* **2013**.
(8) Thurman, E. M.; Malcolm, R. L. Preparative isolation of aquatic humic substances. *Environ. Sci. Technol.* **1981**, *15*, 463–466.
(9) Leenheer, J. A. Comprehensive approach to preparative isolation and fractionation of dissolved organic carbon from natural waters and wastewaters. *Environ. Sci. Technol.* **1981**, *15*, 578–587.
(10) Dryer, D. J. *Development of differential absorbance spectroscopy for the study of metal complexation behavior of natural organic matter*; University of Washington, 2010.
(11) Tan, K. H. *Humic matter in soil and the environment: principles and controversies*; CRC Press, 2014.
(12) Aiken, G. R.; McKnight, D. M.; Thorn, K. A.; Thurman, E. M. Isolation of hydrophilic organic acids from water using nonionic macroporous resins. *Org. Geochem.* **1992**, *18*, 567–573.
(13) *Humic substances: structures, models and functions*; Humic Substances Seminar, G., Elham A; Davies, G.; Royal Society of Chemistry (Great Britain), Eds.; Royal Society of Chemistry: Cambridge, 2001.
(14) Leenheer, J. A.; Rostad, C. E.; Gates, P. M.; Furlong, E. T.; Ferrer, I. Molecular resolution and fragmentation of fulvic acid by electrospray ionization/multistage tandem mass spectrometry. *Anal. Chem.* **2001**, *73*, 1461–1471.
(15) MacCarthy, P. The principles of humic substances: An introduction to the first principle. *Spec. Publ.-R. Soc. Chem.* **2001**, *273*, 19–30.

(16) Sutton, R.; Sposito, G. Molecular Structure in Soil Humic Substances: The New View. *Environ. Sci. Technol.* **2005**, *39*, 9009–9015.
(17) Kelleher, B. P.; Simpson, A. J. Humic substances in soils: are they really chemically distinct? *Environ. Sci. Technol.* **2006**, *40*, 4605–4611.
(18) Abbt-Braun, G.; Lankes, U.; Frimmel, F. H. Structural characterization of aquatic humic substances–The need for a multiple method approach. *Aquat. Sci.* **2004**, *66*, 151–170.
(19) McDonald, S.; Bishop, A. G.; Prenzler, P. D.; Robards, K. Analytical chemistry of freshwater humic substances. *Anal. Chim. Acta* **2004**, *527*, 105–124.
(20) Gao, Y.; Chen, D.; Weavers, L. K.; Walker, H. W. Ultrasonic control of UF membrane fouling by natural waters: Effects of calcium, pH, and fractionated natural organic matter. *J. Membr. Sci.* **2012**, *401–402*, 232–240.
(21) Korshin, G. V.; Ferguson, J. F.; Lancaster, A. N. Influence of natural organic matter on the morphology of corroding lead surfaces and behavior of lead-containing particles. *Water Res.* **2005**, *39*, 811–818.
(22) Korshin, G. V.; Ferguson, J. F.; Lancaster, A. N. Influence of natural organic matter on the corrosion of leaded brass in potable water. *Corros. Sci.* **2000**, *42*, 53–66.
(23) Schulten, H.-R.; Schnitzer, M. Chemical Model Structures for Soil Organic Matter and Soils. *Soil Sci. Febr. 1997* **1997**, *162*, 115–130.
(24) Schwarzenbach, R. P.; Gschwend, P. M.; Imboden, D. M. *Environmental organic chemistry*; John Wiley & Sons, 2005.
(25) Leenheer, J. A.; Wershaw, R. L.; Reddy, M. M. Strong-acid, carboxyl-group structures in fulvic acid from the Suwannee River, Georgia. 2. Major structures. *Environ. Sci. Technol.* **1995**, *29*, 399–405.
(26) Edwards, M.; Sprague, N. Organic matter and copper corrosion by-product release: a mechanistic study. *Corros. Sci.* **2001**, *43*, 1–18.
(27) Croué, J.-P.; Benedetti, M. F.; Violleau, D.; Leenheer, J. A. Characterization and copper binding of humic and nonhumic organic matter isolated from the South Platte River: Evidence for the presence of nitrogenous binding site. *Environ. Sci. Technol.* **2003**, *37*, 328–336.
(28) Broo, A. E.; Berghult, B.; Hedberg, T. Copper corrosion in water distribution systems—the influence of natural organic matter (nom) on the solubility of copper corrosion products. *Corros. Sci.* **1998**, *40*, 1479–1489.
(29) Broo, A. E.; Berghult, B.; Hedberg, T. Copper corrosion in drinking water distribution systems — the influence of water quality. *Corros. Sci.* **1997**, *39*, 1119–1132.
(30) Calle, G. R.; Vargas, I. T.; Alsina, M. A.; Pastén, P. A.; Pizarro, G. E. Enhanced Copper Release from Pipes by Alternating Stagnation and Flow Events. *Environ. Sci. Technol.* **2007**, *41*, 7430–7436.
(31) D'Antonio, L.; Fabbricino, M.; Nasso, M.; Trifuoggi, M. Copper release in low and high alkaline water. *Environ. Technol.* **2008**, *29*, 473–478.
(32) Hong, P. K.; Macauley, Y. Y. Corrosion and leaching of copper tubing exposed to chlorinated drinking water. *Water. Air. Soil Pollut.* **1998**, *108*, 457–471.
(33) Ni, L.; Li, S. Effects of organic matter coming from Chinese tea on soluble copper release from copper teapot. *Sci. Total Environ.* **2008**, *389*, 202–207.

(34) Reiber, S. H. Copper plumbing surfaces: an electrochemical study. *J. Am. Water Works Assoc.* **1989**, 114–122.
(35) Rehring, J. P.; Edwards, M. Copper corrosion in potable water systems: Impacts of natural organic matter and water treatment processes. *Corrosion* **1996**, *52*, 307–317.
(36) Korshin, G. V.; Perry, S. A. L.; Ferguson, J. F. Influence of natural organic matter on corrosion of copper in potable waters. *J. Am. Water Works Assoc.* **1996**, *88*, 36–47.
(37) Frenkel, A. I.; Korshin, G. V.; Ankudinov, A. L. XANES study of Cu2+-binding sites in aquatic humic substances. *Environ. Sci. Technol.* **2000**, *34*, 2138–2142.
(38) Gamble, D. S.; Langford, C. H.; Underdown, A. W. Light scattering measurements of Cu(II)-fulvic acid complexing: The interdependence of apparent complexing capacity and aggregation. *Org. Geochem. Org. Geochem.* **1985**, *8*, 35–39.
(39) Yan, M.; Dryer, D.; Korshin, G.; Benedetti, M. F. In Situ Study of Binding of Copper by Fulvic Acid: Comparison of Differential Absorbance Data and Model Predictions. *Water Res.* **2012**.
(40) Zhan, W.; Sathasivan, A.; Joll, C.; Wai, G.; Heitz, A.; Kristiana, I. Impact of NOM character on copper adsorption by trace ferric hydroxide from iron corrosion in water supply system. *Chem. Eng. J.* **2012**, *200–202*, 122–132.
(41) Gu, B.; Schmitt, J.; Chen, Z.; Liang, L.; McCarthy, J. F. Adsorption and desorption of natural organic matter on iron oxide: mechanisms and models. *Environ. Sci. Technol.* **1994**, *28*, 38–46.
(42) Kaiser, K.; Zech, W. Release of Natural Organic Matter Sorbed to Oxides and a Subsoil. *Soil Sci. Soc. Am. J.* **1999**, *63*, 1157–1166.
(43) Vargas, I. T.; Pavissich, J. P.; Olivares, T. E.; Jeria, G. A.; Cienfuegos, R. A.; Pastén, P. A.; Pizarro, G. E. Increase of the concentration of dissolved copper in drinking water systems due to flow-induced nanoparticle release from surface corrosion by-products. *Corros. Sci.* **2010**, *52*, 3492–3503.
(44) Taxén, C.; Letelier, M. V.; Lagos, G. Model for estimation of copper release to drinking water from copper pipes. *Corros. Sci.* **2012**.
(45) Hidmi, L.; Edwards, M. Role of Temperature and pH in Cu(OH)2 Solubility. *Environ. Sci. Technol.* **1999**, *33*, 2607–2610.
(46) Nguyen, C. K.; Powers, K. A.; Raetz, M. A.; Parks, J. L.; Edwards, M. A. Rapid free chlorine decay in the presence of Cu(OH)2: Chemistry and practical implications. *Water Res.* **2011**, *45*, 5302–5312.
(47) Palit, A.; Pehkonen, S. O. Copper corrosion in distribution systems: evaluation of a homogeneous Cu< sub> 2</sub> O film and a natural corrosion scale as corrosion inhibitors. *Corros. Sci.* **2000**, *42*, 1801–1822.
(48) Leenheer, J. A.; Brown, G. K.; MacCarthy, P.; Cabaniss, S. E. Models of Metal Binding Structures in Fulvic Acid from the Suwannee River, Georgia. *Environ. Sci. Technol.* **1998**, *32*, 2410–2416.
(49) Kinniburgh, D. G.; van Riemsdijk, W. H.; Koopal, L. K.; Borkovec, M.; Benedetti, M. F.; Avena, M. J. Ion binding to natural organic matter: competition, heterogeneity, stoichiometry and thermodynamic consistency. *Colloids Surf. Physicochem. Eng. Asp.* **1999**, *151*, 147–166.

(50) Dryer, D. J.; Korshin, G. V. Investigation of the Reduction of Lead Dioxide by Natural Organic Matter. *Environ. Sci. Technol.* **2007**, *41*, 5510–5514.
(51) Peng, C.-Y.; Korshin, G. V. Speciation of trace inorganic contaminants in corrosion scales and deposits formed in drinking water distribution systems. *Water Res.* **2011**, *45*, 5553–5563.
(52) Baalousha, M.; Motelica-Heino, M.; Coustumer, P. L. Conformation and size of humic substances: Effects of major cation concentration and type, pH, salinity, and residence time. *Colloids Surf. Physicochem. Eng. Asp.* **2006**, *272*, 48–55.
(53) Iskrenova-Tchoukova, E.; Kalinichev, A. G.; Kirkpatrick, R. J. Metal cation complexation with natural organic matter in aqueous solutions: molecular dynamics simulations and potentials of mean force. *Langmuir* **2010**, *26*, 15909–15919.
(54) Leenheer, J. A. Systematic approaches to comprehensive analyses of natural organic matter. *Ann. Environ. Sci.* **2009**, *3*, 1–130.
(55) Wall, N. A.; Choppin, G. R. Humic acids coagulation: influence of divalent cations. *Appl. Geochem.* **2003**, *18*, 1573–1582.
(56) Yang, R.; van den Berg, C. M. Metal complexation by humic substances in seawater. *Environ. Sci. Technol.* **2009**, *43*, 7192–7197.
(57) Feng, X.; Simpson, A. J.; Simpson, M. J. Chemical and mineralogical controls on humic acid sorption to clay mineral surfaces. *Org. Geochem.* **2005**, *36*, 1553–1566.
(58) Iskrenova-Tchoukova, E.; Kalinichev, A. G.; Kirkpatrick, R. J. Metal cation complexation with natural organic matter in aqueous solutions: molecular dynamics simulations and potentials of mean force. *Langmuir* **2010**, *26*, 15909–15919.
(59) Majzik, A.; Tombácz, E. Interaction between humic acid and montmorillonite in the presence of calcium ions II. Colloidal interactions: Charge state, dispersing and/or aggregation of particles in suspension. *Org. Geochem.* **2007**, *38*, 1330–1340.
(60) Pinheiro, J. P.; Mota, A. M.; Benedetti, M. F. Lead and calcium binding to fulvic acids: salt effect and competition. *Environ. Sci. Technol.* **1999**, *33*, 3398–3404.
(61) Mantoura, R. F. C.; Dickson, A.; Riley, J. P. The complexation of metals with humic materials in natural waters. *Estuar. Coast. Mar. Sci.* **1978**, *6*, 387–408.
(62) Davis, J. A. Adsorption of natural dissolved organic matter at the oxide/water interface. *Geochim. Cosmochim. Acta* **1982**, *46*, 2381–2393.
(63) Tipping, E. The adsorption of aquatic humic substances by iron oxides. *Geochim. Cosmochim. Acta* **1981**, *45*, 191–199.
(64) Römkens, P. F.; Bril, J.; Salomons, W. Interaction between Ca2+ and dissolved organic carbon: implications for metal mobilization. *Appl. Geochem.* **1996**, *11*, 109–115.
(65) Yan, M.; Benedetti, M. F.; Korshin, G. V. Study of Iron and Aluminum Binding to Suwannee River Fulvic Acid Using Absorbance and Fluorescence Spectroscopy: Comparison of Data Interpretation based on NICA-Donnan and Stockholm Humic Models. *Water Res.* **2013**.
(66) O'Shea, T. A.; Mancy, K. H. The effect of pH and hardness metal ions on the competitive interaction between trace metal ions and inorganic and organic complexing agents found in natural waters. *Water Res.* **1978**, *12*, 703–711.

(67) Gao, Y. Ultrasonic Control of Ultrafiltration Membrane Fouling by Surface Water: Effects of Calcium, pH, Ionic Strength and Natural Organic Matter (NOM) Fractions, The Ohio State University, 2010.
(68) Bolan, N. S.; Syers, J. K.; Sumner, M. E. Calcium-Induced Sulfate Adsorption by Soils. *Soil Sci. Soc. Am. J.* **1993**, *57*, 691.
(69) Lee, Y. J.; Elzinga, E. J.; Reeder, R. J. Cu(II) adsorption at the calcite–water interface in the presence of natural organic matter: Kinetic studies and molecular-scale characterization. *Geochim. Cosmochim. Acta* **2005**, *69*, 49–61.
(70) Frenkel, A. I.; Korshin, G. V. Studies of Cu(II) in soil by X-ray absorption spectroscopy. *Can. J. Soil Sci.* **2001**, *81*, 271–276.
(71) Korshin, G. V.; Frenkel, A. I.; Stern, E. A. EXAFS Study of the Inner Shell Structure in Copper(II) Complexes with Humic Substances. *Environ. Sci. Technol.* **1998**, *32*, 2699–2705.
(72) Karlsson T, P. P., Skyllberg U. Complexation of copper(ll) in organic soils and in dissolved organic matter--EXAFS evidence for chelate ring structures. *Environ. Sci. Technol.* **2006**, *40*, 2623–2628.
(73) Koopal, L. K.; Saito, T.; Pinheiro, J. P.; Van Riemsdijk, W. H. Ion binding to natural organic matter: General considerations and the NICA–Donnan model. *Colloids Surf. Physicochem. Eng. Asp.* **2005**, *265*, 40–54.
(74) Montenegro, A. C.; Orsetti, S.; Molina, F. V. Modelling proton and metal binding to humic substances with the NICA–EPN model. *Environ. Chem.* **2014**, *11*, 318–332.
(75) Benedetti, M. F.; Van Riemsdijk, W. H.; Koopal, L. K. Humic Substances Considered as a Heterogeneous Donnan Gel Phase. *Environ. Sci. Technol.* **1996**, *30*, 1805–1813.
(76) Milne, C. J.; Kinniburgh, D. G.; Van Riemsdijk, W. H.; Tipping, E. Generic NICA-Donnan model parameters for metal-ion binding by humic substances. *Environ. Sci. Technol.* **2003**, *37*, 958–971.
(77) Pinheiro, J. P.; Mota, A. M.; Benedetti, M. F. Lead and Calcium Binding to Fulvic Acids: Salt Effect and Competition. *Environ. Sci. Technol.* **1999**, *33*, 3398–3404.
(78) Christl, I.; Kretzschmar, R. Relating Ion Binding by Fulvic and Humic Acids to Chemical Composition and Molecular Size. 1. Proton Binding. *Environ. Sci. Technol.* **2001**, *35*, 2505–2511.
(79) Christl, I.; Metzger, A.; Heidmann, I.; Kretzschmar, R. Effect of Humic and Fulvic Acid Concentrations and Ionic Strength on Copper and Lead Binding. *Environ. Sci. Technol.* **2005**, *39*, 5319–5326.
(80) Christl, I. Ionic strength-and pH-dependence of calcium binding by terrestrial humic acids. *Environ. Chem.* **2012**, *9*, 89–96.
(81) Cabaniss, S. E.; Shuman, M. S. Copper binding by dissolved organic matter: I. Suwannee River fulvic acid equilibria. *Geochim. Cosmochim. Acta* **1988**, *52*, 185–193.
(82) Buffle, J.; Greter, F. L.; Haerdi, W. Measurement of complexation properties of humic and fulvic acids in natural waters with lead and copper ion-selective electrodes. *Anal. Chem.* **1977**, *49*, 216–222.

(83) Breault, R. F.; Colman, J. A.; Aiken, G. R.; McKnight, D. Copper speciation and binding by organic matter in copper-contaminated streamwater. *Environ. Sci. Technol.* **1996**, *30*, 3477–3486.
(84) Christl, I.; Kretzschmar, R. C-1s NEXAFS spectroscopy reveals chemical fractionation of humic acid by cation-induced coagulation. *Environ. Sci. Technol.* **2007**, *41*, 1915–1920.
(85) Frenkel, A. I.; Korshin, G. V.; Ankudinov, A. L. XANES Study of Cu2+-Binding Sites in Aquatic Humic Substances. *Environ. Sci. Technol.* **2000**, *34*, 2138–2142.
(86) Manceau, A.; Matynia, A. The nature of Cu bonding to natural organic matter. *Geochim. Cosmochim. Acta* **2010**, *74*, 2556–2580.
(87) Ankudinov, A. L.; Nesvizhskii, A. I.; Rehr, J. J. Dynamic screening effects in x-ray absorption spectra. *Phys. Rev. B* **2003**, *67*, 115120.
(88) Ankudinov, A. L.; Ravel, B.; Rehr, J. J.; Conradson, S. D. Real-space multiple-scattering calculation and interpretation of x-ray-absorption near-edge structure. *Phys. Rev. B* **1998**, *58*, 7565.
(89) Gordon, M. L.; Cooper, G.; Morin, C.; Araki, T.; Turci, C. C.; Kaznatcheev, K.; Hitchcock, A. P. Inner-shell excitation spectroscopy of the peptide bond: Comparison of the C 1s, N 1s, and O 1s spectra of glycine, glycyl-glycine, and glycyl-glycyl-glycine. *J. Phys. Chem. A* **2003**, *107*, 6144–6159.
(90) Stöhr, J. *NEXAFS spectroscopy*; Springer, 1992; Vol. 25.
(91) Hu, W.-G.; Mao, J.; Schmidt-Rohr, K.; Xing, B.; Ghabbour, E. A.; Davies, G. NMR evidence for crystalline domains in humic substances. *Underst. Humic Subst. Adv. Methods Prop. Appl.* **1999**, 63–68.
(92) Mao, J.-D.; Hu, W.-G.; Schmidt-Rohr, K.; Davies, G.; Ghabbour, E. A.; Xing, B. Quantitative Characterization of Humic Substances by Solid-State Carbon-13 Nuclear Magnetic Resonance. *Soil Sci. Soc. Am. J.* **2000**, *64*, 873.
(93) Mao, J.; Chen, N.; Cao, X. Characterization of humic substances by advanced solid state NMR spectroscopy: Demonstration of a systematic approach. *Org. Geochem.* **2011**, *42*, 891–902.
(94) Smernik, R. J.; Olk, D. C.; Mahieu, N. Quantitative solid-state 13C NMR spectroscopy of organic matter fractions in lowland rice soils. *Eur. J. Soil Sci.* **2004**, *55*, 367–379.
(95) Mopper, K.; Stubbins, A.; Ritchie, J. D.; Bialk, H. M.; Hatcher, P. G. Advanced instrumental approaches for characterization of marine dissolved organic matter: extraction techniques, mass spectrometry, and nuclear magnetic resonance spectroscopy. *Chem. Rev.* **2007**, *107*, 419–442.
(96) Dryer, D. J.; Korshin, G. V.; Fabbricino, M. In Situ Examination of the Protonation Behavior of Fulvic Acids Using Differential Absorbance Spectroscopy. *Environ. Sci. Technol.* **2008**, *42*, 6644–6649.
(97) Helms, J. R.; Stubbins, A.; Ritchie, J. D.; Minor, E. C.; Kieber, D. J.; Mopper, K. Absorption spectral slopes and slope ratios as indicators of molecular weight, source, and photobleaching of chromophoric dissolved organic matter. *Limnol. Oceanogr.* **2008**, 955–969.
(98) Chin, Y.-P.; Aiken, G.; O'Loughlin, E. Molecular weight, polydispersity, and spectroscopic properties of aquatic humic substances. *Environ. Sci. Technol.* **1994**, *28*, 1853–1858.

(99) Korshin, G. V.; Wu, W. W.; Benjamin, M. M.; Hemingway, O. Correlations between differential absorbance and the formation of individual DBPs. *Water Res.* **2002**, *36*, 3273–3282.
(100) Korshin, G. V.; Benjamin, M. M.; Chang, H. S.; Gallard, H. Examination of NOM chlorination reactions by conventional and stop-flow differential absorbance spectroscopy. *Environ. Sci. Technol.* **2007**, *41*, 2776–2781.
(101) Yan, M.; Wang, D.; Korshin, G. V.; Benedetti, M. F. Quantifying metal ions binding onto dissolved organic matter using log-transformed absorbance spectra. *Water Res.* **2013**, *47*, 2603–2611.
(102) Dempsey, B. A.; O'Melia, C. R. Proton and calcium complexation of four fulvic acid fractions. *Aquat. Terr. Humic Mater.* **1983**, *239*.
(103) Chin, Y. P.; Gschwend, P. M. The abundance, distribution, and configuration of porewater organic colloids in recent sediments. *Geochim. Cosmochim. Acta* **1991**, *55*, 1309–1317.
(104) Clesceri, L. .; Eaton, A. .; Greenberg, A. E.; Franson, M. A. . *Standard methods for the examination of water and wastewater*; 19th edition supplement.; American Public Health Association: Washington, DC, 1996.
(105) Standard Methods for the Examination of Water and Wastewater. 20 ed. 1998, Washington: APHA, AWWA, WPCF.
(106) Liu, C.; Nanaboina, V.; Korshin, G. Spectroscopic study of the degradation of antibiotics and the generation of representative EfOM oxidation products in ozonated wastewater. *Chemosphere* **2012**, *86*, 774–782.
(107) Yan, M.; Korshin, G. V. Comparative Examination of Effects of Binding of Different Metals on Chromophores of Dissolved Organic Matter. *Environ. Sci. Technol.* **2014**, *48*, 3177–3185.
(108) Yan, M.; Dryer, D.; Korshin, G. V.; Benedetti, M. F. In situ study of binding of copper by fulvic acid: Comparison of differential absorbance data and model predictions. *Water Res.* **2013**, *47*, 588–596.
(109) Benedetti, M. F.; Van Riemsdijk, W. H.; Koopal, L. K. Humic Substances Considered as a Heterogeneous Donnan Gel Phase. *Environ. Sci. Technol.* **1996**, *30*, 1805–1813.
(110) Kinniburgh, D. G.; van Riemsdijk, W. H.; Koopal, L. K.; Borkovec, M.; Benedetti, M. F.; Avena, M. J. Ion binding to natural organic matter: competition, heterogeneity, stoichiometry and thermodynamic consistency. *Colloids Surf. Physicochem. Eng. Asp.* **1999**, *151*, 147–166.
(111) Milne, C. J.; Kinniburgh, D. G.; Van Riemsdijk, W. H.; Tipping, E. Generic NICA-Donnan model parameters for metal-ion binding by humic substances. *Environ. Sci. Technol.* **2003**, *37*, 958–971.
(112) Yan, M.; Korshin, G. V.; Chang, H.-S. Examination of disinfection by-product (DBP) formation in source waters: A study using log-transformed differential spectra. *Water Res.* **2014**, *50*, 179–188.
(113) Yan, M.; Korshin, G. V.; Claret, F.; Croué, J.-P.; Fabbricino, M.; Gallard, H.; Schäfer, T.; Benedetti, M. F. Effects of charging on the chromophores of dissolved organic matter from the Rio Negro basin. *Water Res.* **2014**, *59*, 154–164.

(114) Kinniburgh, D. G.; Milne, C. J.; Benedetti, M. F.; Pinheiro, J. P.; Filius, J.; Koopal, L. K.; Van Riemsdijk, W. H. Metal ion binding by humic acid: application of the NICA-Donnan model. *Environ. Sci. Technol.* **1996**, *30*, 1687–1698.
(115) Milne, C. J.; Kinniburgh, D. G.; Van Riemsdijk, W. H.; Tipping, E. Generic NICA-Donnan model parameters for metal-ion binding by humic substances. *Environ. Sci. Technol.* **2003**, *37*, 958–971.
(116) Sarathy, S. R.; Mohseni, M. The Impact of UV/H2O2 Advanced Oxidation on Molecular Size Distribution of Chromophoric Natural Organic Matter. *Environ. Sci. Technol.* **2007**, *41*, 8315–8320.
(117) Green, S. .; Blough, N. . Optical absorption and fluorescence properties of chromophoric dissolved organic matter in natural waters. **1994**.
(118) Hong, S.; Elimelech, M. Chemical and physical aspects of natural organic matter (NOM) fouling of nanofiltration membranes. *J. Membr. Sci.* **1997**, *132*, 159–181.
(119) Edwards, M.; Benjamin, M. M. Effect of preozonation on coagulant-NOM interactions. *J.-Am. Water Works Assoc.* **1992**, *84*, 63–72.
(120) Brown, A.; McKnight, D. M.; Chin, Y.-P.; Roberts, E. C.; Uhle, M. Chemical characterization of dissolved organic material in Pony Lake, a saline coastal pond in Antarctica. *Mar. Chem.* **2004**, *89*, 327–337.
(121) Mao, J.; Cory, R. M.; McKnight, D. M.; Schmidt-Rohr, K. Characterization of a nitrogen-rich fulvic acid and its precursor algae from solid state NMR. *Org. Geochem.* **2007**, *38*, 1277–1292.
(122) Mcknight, D. M.; Boyer, E. W.; Westerhoff, P. K.; Doran, P. T.; Kulbe, T.; Andersen, D. T. Spectrofluorometric characterization of dissolved organic matter for indication of precursor organic material and aromaticity. *Limnol. Oceanogr.* **2001**, *46*, 38–48.
(123) Mcknight, D. M.; Andrews, E. D.; Spaulding, S. A.; Aiken, G. R. Aquatic fulvic acids in algal-rich antarctic ponds. *Limnol. Oceanogr.* **1994**, *39*, 1972–1979.
(124) Benedetti, M.; Ranville, J. F.; Ponthieu, M.; Pinheiro, J. P. Field-flow fractionation characterization and binding properties of particulate and colloidal organic matter from the Rio Amazon and Rio Negro. *Org. Geochem.* **2002**, *33*, 269–279.
(125) Reszat, T. N.; Hendry, M. J. Characterizing dissolved organic carbon using asymmetrical flow field-flow fractionation with on-line UV and DOC detection. *Anal. Chem.* **2005**, *77*, 4194–4200.
(126) Weishaar, J. L.; Aiken, G. R.; Bergamaschi, B. A.; Fram, M. S.; Fujii, R.; Mopper, K. Evaluation of specific ultraviolet absorbance as an indicator of the chemical composition and reactivity of dissolved organic carbon. *Environ. Sci. Technol.* **2003**, *37*, 4702–4708.
(127) Schwede-Thomas, S. B.; Chin, Y.-P.; Dria, K. J.; Hatcher, P.; Kaiser, E.; Sulzberger, B. Characterizing the properties of dissolved organic matter isolated by XAD and C-18 solid phase extraction and ultrafiltration. *Aquat. Sci.* **2005**, *67*, 61–71.
(128) Chin, Y.-P.; Aiken, G. R.; Danielsen, K. M. Binding of pyrene to aquatic and commercial humic substances: The role of molecular weight and aromaticity. *Environ. Sci. Technol.* **1997**, *31*, 1630–1635.
(129) Andrew, A. A.; Del Vecchio, R.; Subramaniam, A.; Blough, N. V. Chromophoric dissolved organic matter (CDOM) in the Equatorial Atlantic Ocean: optical

properties and their relation to CDOM structure and source. *Mar. Chem.* **2013**, *148*, 33–43.
(130) Boyle, E. S.; Guerriero, N.; Thiallet, A.; Vecchio, R. D.; Blough, N. V. Optical properties of humic substances and CDOM: Relation to structure. *Environ. Sci. Technol.* **2009**, *43*, 2262–2268.
(131) Del Vecchio, R.; Blough, N. V. On the origin of the optical properties of humic substances. *Environ. Sci. Technol.* **2004**, *38*, 3885–3891.
(132) Green, S. A.; Blough, N. V. Optical absorption and fluorescence properties of chromophoric dissolved organic matter in natural waters. *Limnol. Oceanogr.* **1994**, *39*, 1903–1916.
(133) Carder, K. L.; Steward, R. G.; Harvey, G. R.; Ortner, P. B. Marine humic and fulvic acids: their effects on remote sensing of ocean chlorophyll. *Limnol. Oceanogr.* **1989**, *34*, 68–81.
(134) Loiselle, S. A.; Bracchini, L.; Dattilo, A. M.; Ricci, M.; Tognazzi, A.; Cozar, A.; Rossi, C. Optical characterization of chromophoric dissolved organic matter using wavelength distribution of absorption spectral slopes. *Limnol. Oceanogr.* **2009**, *54*, 590–597.
(135) Loiselle, S.; Vione, D.; Minero, C.; Maurino, V.; Tognazzi, A.; Dattilo, A. M.; Rossi, C.; Bracchini, L. Chemical and optical phototransformation of dissolved organic matter. *Water Res.* **2012**, *46*, 3197–3207.
(136) Yan, M.; Korshin, G. V.; Chang, H.-S. Examination of disinfection by-product (DBP) formation in source waters: A study using log-transformed differential spectra. *Water Res.* **2014**, *50*, 179–188.
(137) Yan, M.; Korshin, G. V.; Claret, F.; Croué, J.-P.; Fabbricino, M.; Gallard, H.; Schäfer, T.; Benedetti, M. F. Effects of charging on the chromophores of dissolved organic matter from the Rio Negro basin. *Water Res.* **2014**, *59*, 154–164.
(138) Janot, N.; Reiller, P. E.; Korshin, G. V.; Benedetti, M. F. Using spectrophotometric titrations to characterize humic acid reactivity at environmental concentrations. *Environ. Sci. Technol.* **2010**, *44*, 6782–6788.
(139) Yan M; Wang D; Korshin GV; Benedetti MF. Quantifying metal ions binding onto dissolved organic matter using log-transformed absorbance spectra. *Water Res.* **2013**, *47*, 2603–2611.
(140) Dryer, D. J.; Korshin, G. V.; Fabbricino, M. In Situ Examination of the Protonation Behavior of Fulvic Acids Using Differential Absorbance Spectroscopy. *Environ. Sci. Technol.* **2008**, *42*, 6644–6649.
(141) Cornard, J. P.; Dangleterre, L.; Lapouge, C. Computational and spectroscopic characterization of the molecular and electronic structure of the Pb (II)-quercetin complex. *J. Phys. Chem. A* **2005**, *109*, 10044–10051.
(142) Cornard, J. P.; Lapouge, C. Theoretical and spectroscopic investigations of a complex of Al (III) with caffeic acid. *J. Phys. Chem. A* **2004**, *108*, 4470–4478.
(143) Yan, M.; Li, D.; Gao, J.; Cheng, J. Influence of chlorination on metal binding by dissolved organic matter: A study using Log-transformed differential spectra. *Chemosphere* **2014**, *103*, 290–298.
(144) Yan, M.; Benedetti, M. F.; Korshin, G. V. Study of iron and aluminum binding to Suwannee River fulvic acid using absorbance and fluorescence spectroscopy:

Comparison of data interpretation based on NICA-Donnan and Stockholm humic models. *Water Res.* **2013**, *47*, 5439–5446.
(145) Benedetti, M. F.; Milne, C. J.; Kinniburgh, D. G.; Van Riemsdijk, W. H.; Koopal, L. K. Metal ion binding to humic substances: application of the non-ideal competitive adsorption model. *Environ. Sci. Technol.* **1995**, *29*, 446–457.
(146) Cabaniss, S. E. Forward Modeling of Metal Complexation by NOM: I. A priori Prediction of Conditional Constants and Speciation. *Environ. Sci. Technol.* **2009**, *43*, 2838.
(147) Milne CJ; Kinniburgh DG; van Riemsdijk WH; Tipping E. Generic NICA-Donnan model parameters for metal-ion binding by humic substances. *Environ. Sci. Technol.* **2003**, *37*, 958–971.
(148) Cabaniss, S. E. Forward Modeling of Metal Complexation by NOM: I. A priori Prediction of Conditional Constants and Speciation. *Environ. Sci. Technol.* **2009**, *43*, 2838–2844.
(149) Lu Y; Allen HE. Characterization of copper complexation with natural dissolved organic matter (DOM)--link to acidic moieties of DOM and competition by Ca and Mg. *Water Res.* **2002**, *36*, 5083–5101.
(150) Hansen, A. M.; Leckie, J. O.; Mandelli, E. F.; Altmann, R. S. Study of copper(II) association with dissolved organic matter in surface waters of three Mexican coastal lagoons. *Environ. Sci. Technol.* **1990**, *24*, 683–688.